2017 ANNUAL REPORT

HP-HT laboratory
EXPERIMENTAL VOLCANOLOGY AND GEOPHYSICS

laboratory
NEW TECHNOLOGIES

Department of Seismology and Tectonophysics
Istituto Nazionale di Geofisica e Vulcanologia
Via di Vigna Murata 605 I 00143 Roma - Italia I Tel +39-0651860437 I Fax +39-0651860507
www.ingv.it

Contents

HP-HT Laboratory of Experimental Volcanology and Geophysics
LNT Laboratory of New Technologies
2017 Annual Report

1 | ABSTRACT

In this annual report, we have summarized the most important research activities of the High Pressure High Temperature Laboratory of Experimental Volcanology and Geophysics and of the Laboratory of New Technologies that were conducted in 2017. The Labs hosted 24 full-time visiting scientists, 7 associated researchers, 25 PhD/Master students, and 9 visiting scientists. During this year, 37 national- to international-level projects/collaborations were active, involving more than 20 partner laboratories and institutions. The HPHT Lab continued its numerous research studies in petrology, mineralogy and volcanology (28 studies) and in rock physics (14 studies), whereas the LNTS Lab designed and developed new measuring systems, sensors and instrumentations (8 prototypes), with the agreement of a novel issued patent. Finally, the Lab personnel have organized and participated to 75 meetings, workshops and seminars in Italy and abroad, and have published 40 scientific articles in the most important international journals.

2I PERSONNEL

HPHT Laboratory

Piergiorgio Scarlato I Senior Researcher, Responsible of the HP-HT group

Carmela (Lilli) Freda I Senior Researcher

Gianfilippo De Astis I Contract Researcher

Elisabetta Del Bello I Contract Researcher

Pierdomenico Del Gaudio I Researcher

Valeria Misiti I Technologist

Tullio Ricci I Researcher

Elena Spagnuolo I Contract Researcher

Jacopo Taddeucci I Researcher

Telemaco Tesei I Contract Researcher

Pierre Yves Tournigand I Contract Researcher

Laboratory of New Technologies

Giovanni Romeo I Technical Director, Responsible of the Laboratory of New Technologies

Giuseppe Di Stefano I Senior Technologist

Alessandro Iarocci I Engineer Technologist

Massimo Mari I Technician

Francesco Pongetti I Engineer Technician

Giuseppe Spinelli I Technician

Mario Tozzi I Engineer Technologist

Giuseppe Urbini I Engineer Technologist

Associated researchers

Cristiano Collettini I Sapienza Università di Roma, Italy **I Associate Professor in Structural Geology**

Giancarlo Della Ventura I Università di Roma Tre, Italy **I Full Professor in Mineralogy**

Giulio Di Toro I Università degli Studi di Padova, Italy **I Full Professor in Structural Geology**

Gianluca Iezzi I Università di Chieti, Italy **I Associate Professor in Mineralogy**

Silvio Mollo I Sapienza Università di Roma, Italy **I Associate Professor in Petrology**

Collaborators

Matteo Masotta I Università di Pisa **I Researcher**

Marco M. Scuderi I Sapienza Università di Roma, Italy **I Marie Curie Fellow**

Vincenzo Stagno I Sapienza Università di Roma, Italy **I Researcher**

HPHT Laboratory

- Multiple press 840 ton | Voggenreiter

- Piston cylinder - 3/4" and 1" pressure plates | Voggenreiter

- Multianvil - Walker type 6/8 | Voggenreiter

- Quick Press - Piston Cylinder 3/4" and 1" pressure plates | Depth of the Earth

- Bi-Tri-Axial Press (BRAVA) | RMP - INGV

- Low to High Velocity rotary shear Apparatus (SHIVA) | RMP - INGV

- Electron microprobe equipped with 5 WDS and 1 EDS | JEOL JXA-8200

- Field Emission Scanning Electron Microscope equipped with EDS and BSE detectors | JEOL JSM-6500F

- Auto Carbon coater | JEOL JEC-530

- Fine coater | JEOL JFC-2300HR

- High and low temperature furnaces | Lenton

- Impedance analyser | Solartron SI1260

- Digital oscilloscope | Tektronix DPO4032

- Wave generator | Agilent 33250A

- H-Frame presses 10 ton | Enerpac

- Uniaxial testing machine with double load cell (15 and 250 kN) and LVDT controller | Tecnotest

- Precision balance | Sartorius

- Optical and stereo microscopes | Leica DMRXP and Euromex

- Ultra-high velocity, intensified, gated digital camera | Cordin 204-2

- High speed digital camcorder | Optronis and NAC 512 SC

- Stereomicroscopes | Leica MZ 9.5

- Semiautomatic polisher | Buehler Minimet 1000

- Power Supply | Agilent 6575A

- Helium Picnometer | AccuPyc II 1340

- Permeameter with double intensifier | Rock Physics

- Rheometer MCR 301 Physica | Anton Paar

- Vertical Furnace RHTV 120-300/18 | Nabertherm

- High Temperature Furnace LHT 04/18 | Nabertherm

- Cecchi data acquisition system **I** Applied Seismology

- Rock drilling, cutting, and grinding equipment for samples preparation

- Thermal High speed camera **I** FLIR SC 645

- Welder PUK U3 **I** Lampert

- Laser line generator **I** Edmund optics

- Precision test sieves **I** Endecotts

- Laser MGL-III, 532nm 200mW, PSU-III-LED/Unit **I** Changchun New Industries

- Multi-Wavelenght Analyser with Particle sizing according to ISO 13317 **I** LUMiReader@PSA

- Polarized Free-field Microphones 40AN 1/2", Low Frequency (0.5Hz - 20kHz) **I** G.R.A.S.

- Vacuometro Pirani PVG-500

- Petrographic microscope ECLIPSE E-50i POL **I** Nikon

- Drying oven UF 75 **I** Memmert

- 4K digital camcorders **I** Sony

- High speed digital camcorder **I** NAC Memrecam-HX6

- Shock-tube apparatus (Jet-Buster) **I** INGV

- High speed digital camcorders **I** NAC 512 SC, Optronis CR600x2, NAC HX6, NAC HX3

- Laser range finder **I** Vectronix VECTOR 21

Acquired in 2017

- Time Lapse Camera with 24-70 lens **I** Brinno TLC200 Pro

Laboratory of New Technologies

- Analog Oscilloscope **I HP**
- Analog Oscilloscope **I Iwatsu SS5710**
- Analog Oscilloscope **I Tektronix TDS220**
- Analog Oscilloscope **I Tektronix**
- Oscilloscope **I HP54201**
- Oscilloscope **I HP54602b**
- Power supply **I Elind HL series**
- Power supply **I Elind 6TD20**
- Power supply **I DC DF1731SB**
- Signal generator **I HP8656A**
- Function generator **I HP3325A**
- Multimeter **I HP3478A**
- Milling machine for printed circuit boards **I T-Tech**
- Logic state analyzer **I HP16500A**
- Superheterodyne spectrum analyzer **I Tektronix**
- Soldering-reworking station **I JBC advanced AM6500**
- Oscilloscope **I FLUKE 199C**
- Oscilloscope **I Tektronix DPO4000**
- Oscilloscope **I Tektronix MSO4034**
- Calibrator **I FLUKE 5700 (series II)**
- Function generator **I HP33120**
- Function generator **I AGILENT 33250 A**
- PXI Industrial computer with I/O boards **I National Instruments**
- Universal counter **I HP53131A**
- Waveform generator **I Agilent 33210 A**
- Oscilloscope W wave surfer **I LeCroy 44MXs-A**
- Drone Phantom2 vision plus
- Drone S800 with specialized payloads

Acquired in 2017

- Drone Phantom 3 pro with termination sysem

Machine shop

- Lathe **I** Grazioli Fortuna

- Small lathe **I** Ceriani

- Small milling machine **I** Schaublin

- Cutting machine **I** Ercoletta

- Bending machine **I** Ercoletta

- Drill press **I** Serrmac

- Small drill press **I** Webo

- Bandsaw **I** Femi

- Grinder **I** Femi

- Extractor hood **I** Filcar

- Inverter welding machine **I** Tecnica

- TIG welding machine **I** Cebora

- Miter saw

- Numerically controlled milling machine

4I LABORATORY ACTIVITIES

Experimental laboratory

Super press | Multi Anvil

17 experiments have been conducted in the frame of 3 projects. All projects are devoted to the study of **deep mantle**.

Super press | Piston cylinder

The 3/4 inch pressure plate has been used for 13 experiments related to one project: **synthesis of hydrous trachyte**.

Quick press | Piston cylinder

The 1 inch pressure plate has been used for 2 experiments related to one project: **trachyte experiments**.

The 3/4 inch pressure plate has been used for 45 experiments related to 5 projects.

The 1/2 inch pressure plate has been used for 6 experiments: 2 experiments were calibration at very high pressure and the other 4 experiments related to **hydrogenate olivine crystals**.

Furnaces

45 experiments have been performed in the frame of the following projects:

- Olivine-clinopyroxene-plagioclase-melt cation exchange reactions as a tool for understanding magma dynamics.

Slow to High Velocity rotary shear Apparatus (SHIVA)

The activity of SHIVA in 2017 has been mainly devoted to the investigation of frictional properties of cohesive (gabbro, Carrara marble, basalts, granite, peridotite and novaculites) and non-cohesive gouges (mainly smectites) under vacuum, room humidity and in the presence of fluids. The main motivation to test the role of smectites mixtures was for their wide distribution in the frontal prism of subduction zones and in the active fault system of the central Appenines (which, as an example, hosted the Amatrice-Norcia earthquake sequence 2016-2017). The experiments performed during 2017 aimed at retrieving constrains for tsunami earthquake numerical modeling and up-scale the experimental results to nature. Moreover, we tested mixture of calcite and smectites to investigate the role of smectites in producing and propagating earthquakes within carbonatic tectonic settings and to trace back the processes responsible for rock textures observed during field surveys. With SHIVA we investigated the nucleation, propagation and arrest of earthquakes resulting from crustal deformation conditions (pressure, temperature, presence of fluids, stress perturbations, etc.). We studied the physico-chemical processes related to the deformation (i.e. acoustic emission, slip patterns) which are considered precursory to rupture nucleation. We also studied the frictional properties of the gouge material recovered from the drilling (CRISP IODP Costa Rica) project to provide

information regarding the occurrence and the main causes of the "slip to the trench" responsible for, as an example, the great tsunami which followed the Tohoku-Oki 2011 M9.0 earthquake. To achieve these goals, we performed 148 experiments during year 2017.

Moreover we established two relevant collaborations in the field of induced and triggered seismicity with the Borehole Reasearch Center of Karrad (Pune, India) and the institute of Geology, Chinese Academy of Geological Sciences (Beijing, China). In the respect of triggered and induced seismicity we provided relevant advancements in testing the role of chemistry and viscosity of fluids during pressurized fluid injection in seismogenic pre-existing faults.

BRAVA

During the 2017 we performed about 120 experiments testing most of the capabilities of the apparatus. The experimental work has been focused on consolidating the research lines developed in the past years. In the following we summarize the main research themes:

1) Characterization of the frictional properties of carbonate-bearing faults during experiments at high strain and slow sliding velocities (Mercuri's PhD thesis).

2) Weakness of serpentine minerals revealed by friction experiments under room and hydrothermal conditions (Tesei et al.).

3) The role of anisotropy in fault mechanics tested via cylindrical samples of sandstone with a pre-imposed saw-cut filled with powdered weak marl (Giorgetti PhD thesis).

4) Laboratory faults reveal period-multiplying slow and fast slip events before entering into a fully dynamic regime (PhD project DeepaMeleVeedu).

5) Fault slip behaviour during fluid pressure stimulation in calcite and shales (Scuderi Marie Curie, project).

Finally, we have used BRAVA for teaching rock-physics at Master students of the Petrophysics course at La Sapienza University of Rome and for outreach with high-school students.

Analog laboratory

Rheometer

15 rheological experiments have been conducted on natural suspensions composed by different proportion of mud powder of Fermo and LUSI.

In 2017 the analog laboratory hosted a campaign of shock-tube experiments aiming at investigating the jet-particle dynamics during explosive volcanic eruptions. 94 experiments were performed using a plexiglass shock-tube apparatus.

### FAMoUS (Fast Multiparametric Setup) TOOLBOX

The fourth BAcIO (Broadband Acquisition and Imaging Operation) multidisciplinary experiment was carried out at Stromboli (September 2017), in order to study the behaviour of basaltic explosive eruptions. More than 30 researchers from 5 institutions and 4 Countries (Italy, Germany, UK, USA) participated to this edition.

Microanalytical laboratory

FE-SEM and EMP performed 149 days of analysis in the frame of the following 23 research proposals.

Proposals

1. Experimental fault rocks at the microscale
   T. Tesei I INGV Roma 1

2. The role of crystal mushes in the differentiation processes of calcalkaline magmas: field relationships, petrography, geochemistry and experimental modeling
   V. Tecchiato - P. Scarlato I Sapienza University of Rome - INGV Roma 1

3. Experimental determination of magma ascent rates at Mt. Etna volcano based on clinopyroxene growth rates, sector zoning and crystal size distribution
   M. Masotta - M. Nazzari I University of Pisa - INGV Roma 1

4. Solidification of a rhyolitic magma beneath the Krafla caldera
   M. Masotta - M. Nazzari I University of Pisa - INGV Roma 1

5. Characterisation of the mud emissions occurred after M 6.5 earthquake in Central Italy
   T. Ricci I INGV Roma 1

6. Textural and micro-chemical features of fault rocks from Central Apennines
   G. Iezzi - M. Nazzari I Chieti University - INGV Roma 1

7. Crystal-chemical variations induced by variable cooling rate in sub-alkaline silicate liquids
   G. Iezzi - V. Misiti I Chieti University - INGV Roma 1

8. Understanding clinopyroxene zoning as recorder of pre-eruptive magmatic processes
   T. Ubide - S. Mollo - P. Scarlato I The University of Queensland - INGV Roma 1
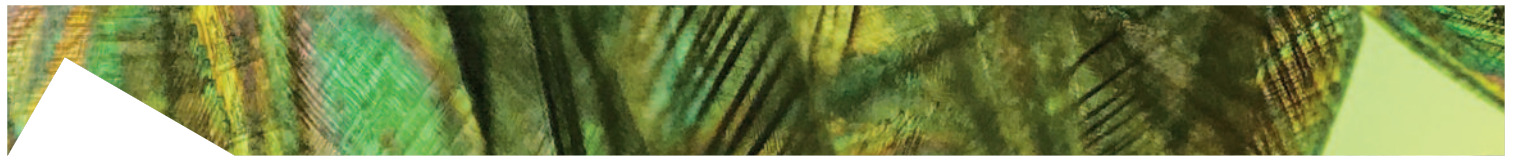
9. Study of the petro-physical characteristics of volcanic rocks through 2D and 3D textural micro-analyzes: implications on the subvulcanic processes
   L. Pappalardo I INGV-OV

10. Experimental investigation of mechanisms generating phonolites in the Dunedin Volcano, New Zealand
    A. Pontesilli - M. Nazzari I The University of Otago - INGV Roma 1

11. The Earth's deep volatile cycle over geological time as function of mantle redox state, pressure and temperature
    M. Caruso - P. Scarlato I Sapienza University of Rome - INGV Roma 1

12. Oxygen fugacity, pressure and temperature conditions at which elemental carbon turns into CO_2-bearing melts within eclogite and peridotite assemblages
    V. Stagno - M. Nazzari I Sapienza University of Rome - INGV Roma 1

13. Wall rock-magma interaction at 2kbar and 1000-1300 °C
    V. Stagno - M. Nazzari I Sapienza University of Rome - INGV Roma 1

14. Geochemical characterization of geological obsidian sources
    M. Carapezza I INGV Roma 1

15. A combined FE-SEM/EDS and -IR analysis of Carbonaceous Chondrites meteorites, analogue of the next returned asteroid samples and HED meteorites in relation to infrared spectra of Vesta-like asteroids
    E. Palomba - M. Nazzari I Institute for Space Astrophysics and Planetology (IAPS) - INAF - INGV Roma 1

16. Physical-chemical constraints of the magmatic feeding system of the 2014-2015 explosive eruptive activity at Mt. Etna
    P.P. Giacomoni - P. Scarlato I University of Ferrara - INGV Roma 1

17. Origin and dispersal of volcanic ash in the Austral Hemisphere: a database for the volcanology, chronostratigraphy and paleoclimate of the Earth system
    P. Del Carlo I INGV PI

18. Volcanic ash resuspention
    E. Del Bello I INGV Roma 1

19. Igneous rocks as source and sink of abiotic hydrocarbons and CO_2
    G. Etiope I INGV Roma 2

20. Dynamic crystallisation in magmas
    M. Nazzari I INGV Roma 1

21. Characterisation of anthropogenic pollutants in natural snow deposit, magnetic contribution and geochemical determination
    L. Alfonsi I INGV Roma 2

22. Crystal-chemistry and texture of a 2015 Mt. Etna bomb
    G. Iezzi - M. Nazzari I Chieti University - INGV Roma 1

23. Analysis of chemical and physical properties of nominally anhydrous minerals at high pressure and high temperature in order to study dynamic processes occurring within the Earth's mantle
    A. Del Vecchio - V. Misiti I INGEO Chieti University - INGV Roma 1

5I RESEARCH PROJECTS

1. **European research project I** EPOS 'European Plate Observing System' Implementation Phase, WP 16 Multi-scale Laboratories **I P.I. Cocco M.**

2. **European Research Infrastructures Transnational Access EUROPLANET 2020 I** Agreement n.654208 (15-EPN-003). Approved proposal grant n. 10341: 'High-Speed Imaging Of Gas-Particle And Particle-Particle Interactions In Lab-Sized Volcanic Jets/plumes' **I P.I. Taddeucci J., Del Bello E.**

3. **International Continental Scientific Drilling Program - ICDP I** Krafla Magma Drilling Project **I P.I. Eichelberger J.**

4. **Italian Civil Protection, INGV 2016 Agreement I** B2, Objective 4 - 'Centro di Pericolosità Vulcanica' **I P.I. Macedonio G., Calvari S.**

5. **MIUR Progetti Premiali 2015 I** Ash-RESILIENCE A research infrastructure for volcanic ash hazard assessment to aviation and communities living near Italian active volcanoes **I P.I. Costa A., Andronico D.**

6. **Sapienza Progetti di Ateneo I** Quantitative understanding of magma reservoirs feeding large-scale volcanic eruptions at Campi Flegrei. **I P.I. Mollo S.**

7. **Sapienza Progetti di Ateneo I** Kinetic controls on the partitioning of chemical species between olivine, clinopyroxene and melt during solidification of terrestrial and extraterrestrial basaltic rocks: Implications for the understanding of the crystallization conditions of magmas **I P.I. Mollo S.**

8. **Marie Curie Individual Fellow FEAT (n° 656676) I** The role of Fluid pressure in EArthquake Triggering **I P.I. Scuderi M.**

9. **Sapienza Progetti Ateneo I** The role of fluid pressure in carbonate-fault frictional stability and earthquake-triggering **I P.I. Collettini C.**

10. **École polytechnique fédérale de Lausanne I** Frictional properties of Opalinus clay **I P.I. Violay M.**

11. **Sapienza Progetti di Ateneo I** The role of fluid pressure in the mechanics of slow earthquakes: insights from rock deformation experiments **I P.I. Collettini C.**

12. **European research project I VERTIGO ITN FP7 Framework "FP7-PEOPLE-2013-ITN" I** Volcanic ash: Field, experimental and numerical investigations of processes during its lifecycle **I P.I. Kueppers U.**

13. **Sapienza Progetti di Ateneo I** From small to large, to very large: a multiscale study of the influence of fractures on physical properties of carbonate rocks **I P.I. Trippetta F.**

14. **European Research Project I ERC Consolidator Grant Project I** NOFEAR: New Outlook on seismic faults: From EARthquake nucleation to arrest **I P.I. Di Toro G.**

6I PARTNER LABORATORIES

1. **Planetary Environmental Facilities I** Aarhus University **I Denmark**

2. **Experimental & Physical Volcanology I** Ludwig Maximillians Universitat **I Germany**

3. **Institute of Geochemistry and Petrology I** ETH Zurich **I Switzerland**

4. **Università di Scienze Biologiche, Geologiche e Ambientali I** Università di Catania **I Italy**

5. **Dipartimento di Fisica e Scienze della Terra I** Università di Ferrara **I Italy**

6. **Petro- Volcanology Research Group (PVRG) Department of Physics and Geology I** University of Perugia **I Italy**

7. **School of Earth and Environmental Sciences I** University of Queensland **I Australia**

8. **Department of Geology I** University of Otago **I New Zealand**

9. **Institute of Fluid Dynamics and Technical Acoustics (ISTA) I** Technische Universität **I Berlin**

10. **Petro-Volcanology Research Group (PVRG) I** Department of Physics and Geology **I University of Perugia**

7I PARTNER INSTITUTIONS

1. Department of Geology and Geophysics **I SOEST I** USA

2. Department of Physics and Astronomy **I Aarhus University I Denmark**

3. HVO Hawaiian volcano observatory **I USGS I** USA

4. Ludwig Maximillians Universitat Munchen **I Munich I Germany**

5. School of Earth and Environmental Sciences **I University of Queensland I** Australia

6. Department of Geology **I University of Otago I New Zealand**

8.1 PETROLOGY, MINERALOGY, VOLCANOLOGY

Anthropogenic magnetic particulate in the central Apennines snow deposit and Urban area: a comparison

L. Alfonsi, P. Macrì, M. Nazzari.

We utilize rock magnetic mineralogy and FESEM and EDS analysis of Fe-particles to investigate characters of the magnetic content of the solid residual contained in snow samples collected in the central Apennines area and in Urban Rome. The snow samples are collected in the Apennines in the late spring season, this to allow the maxim deposition of the possible particulate and taken in both rural and exploited areas (Gran Sasso, Sirente and Campo Felice, and Campo Imperatore natural reserves). For what concerns the sampling in urban district we collected snow samples in Rome in February 2012; in that case the samples were taken a week after the snow storm that heavily affected the city of Rome. The whole set of analyses are devoted to discriminate the anthropogenic contribution to the soil and atmospheric pollution in different environments utilizing the snow as a neutral micro-particles collector. Magnetic particles associated to anthropogenic pollution are often related to heavy metal content and, iron oxides.

A total of 63 samples, snow and terrain samples of the sampling location (this latter aspect was necessary to discriminate between natural provenance of the Fe and Fe-oxides and hydroxides and the anthropogenic contribution on the snow residual). The snow samples were collected with a bottle (one liter volume) on selected snow patches (Fig. 1A), the snow is then melted at room temperature and filter utilizing a vacuum filtering system, specifically designed to fulfill the purposes
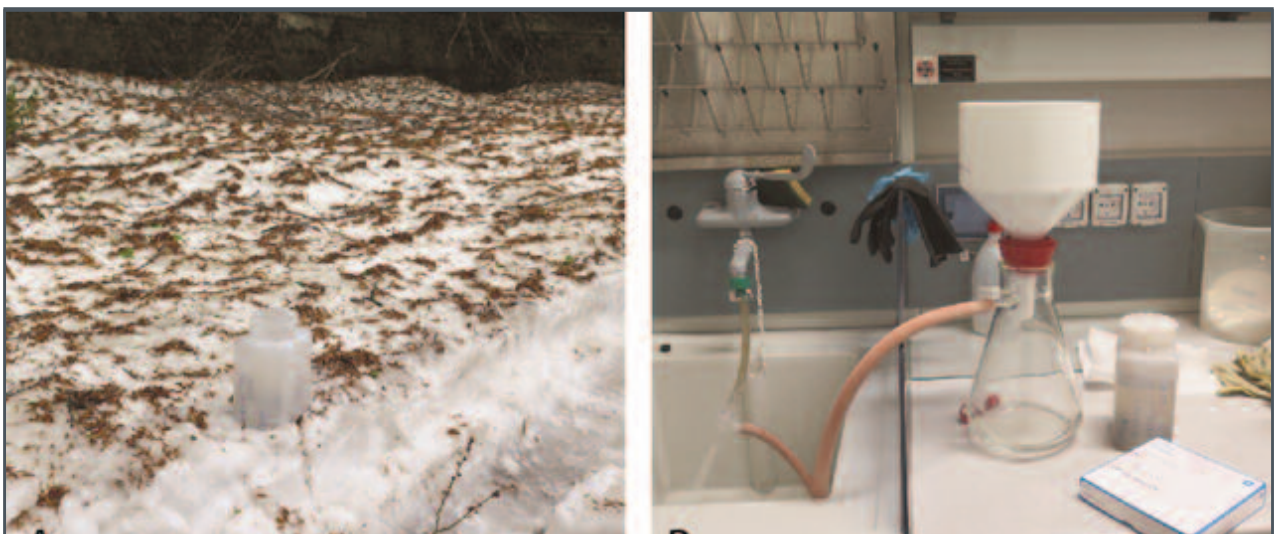

Fig. 1 I A) typical sampling locality in the Apennines; B) Vacuum filtering system employing a Whatmann filter n.42.
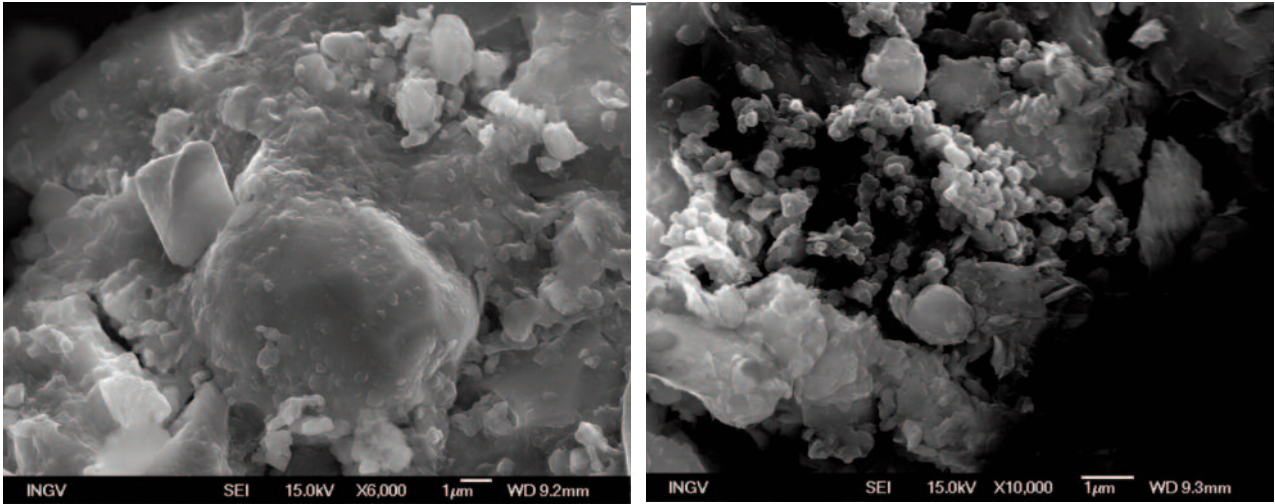
Fig. 2 I Magnetite spherules in aggregates, Ovindoli and Sirente area.

of this research topic (i.e. the need to retain particles greater or equal than 0,25 micron; Fig. 1B). The preliminary rock magnetism analysis, necessary to select the suitable samples for the subsequent FESEM and EDS analyses, have been carried out and we are on the way to perform the second step of the research. The rock magnetic analysis carried on the solid residual obtained from the snow showed, unexpectedly, quite high values of magnetic susceptibility, confirming the presence of magnetic material. Titanomagnetite, and is some cases haematite are the magnetic carriers found in the samples analysed. The microscope observations, on selected samples will help to qualitatively characterize the chemical content and identify the morphological aspects of the magnetic fraction. For this the JEOL JSM 6500F Field Emission Scanning Electron Microscope (FESEM, resolution of 1.5 nm), operating at 10/15 kV equipped with detectors for x-ray (EDS, with a resolution of 133 eV) will be used to analyze the material extracted from the snow samples. The shape of the ferromagnetic particles of anthropogenic origin is well known in the literature; the FESEM and EDS analyses of Fe-particles is a specific technique widely used as a fundamental instrument to identify magnetic particles produced by anthropogenic combustion processes. A suitable result would be to discriminate if any amo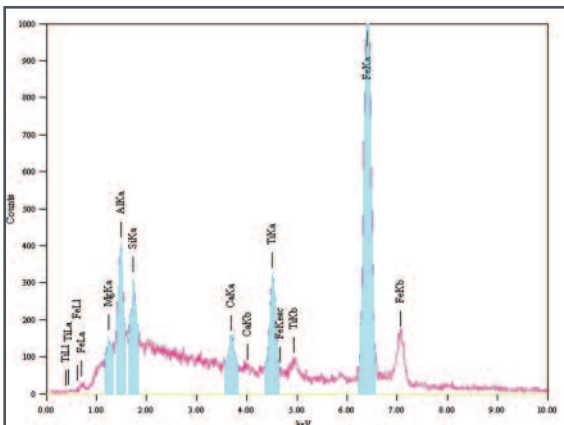ng the natural and anthropogenic content of Fe rich particles in natural environments and urban area and qualitatively characterize it. On the basis of the results of the rock magnetic analyses 7 suitable samples have been selected for FESEM and EDS analysis. The first two samples analysed enhanced the presence of anthropogenic magnetic material. We identified irregular magnetite aggregates this magnetic mineral has been identified as a combustion-derived component of vehicle exhaust materials with spherical shapes and as aggregates.

Fig. 3 I Examples of FESEM analysis on an antropogenic magnetite spherule.

The effect of decompression and water content on the degassing pattern of magmas
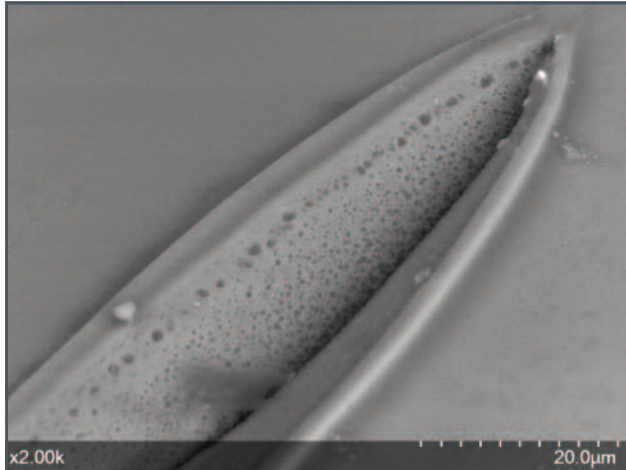
A. Kazarian, C. Romano, B. Scheu, V. Misiti

Fig. 1 I The vesicle size distribution in experimental sample.

The aim of the project is to investigate how the physical state of magma (anhydrous chemical composition, volatile content, bubble content and shape, as well as dP/dT conditions) can influence the degassing process of magma and to relate this to the intensity eruptive activity. The hydrous samples were synthesized at INGV Rome with the Piston Cylinder apparatus and with the Quick Press. The starting material is a trachytic glass from Agnano Monte Spina eruption (Phlegrean Fields Italy). Gold-Palladium and Platinum capsules of internal diameter 3 mm and 15 mm long were used. Those were filled with powder and different amount of water (between 0.5 and 2.5 wt% H_2O). We run a total of 8 synthesis experiments. The piston cylinder experiments were performed at 5 Kbar of pressure and 1200°C for 2 hours to allow dissolution and complete homogeneization of water through the samples. Some additional experiments were performed with the Quick Press apparatus at 3 Kbar of pressure and 1200°C. Hydrous glasses were then cut into pieces and prepared for the decompression experiments. The decompression experiments were conducted at the fragmentation lab at LMU (Munich University, Germany), using the following apparatus:

- Split-tube furnace, used for heating of the samples.

- Shock-tube apparatus, main experimental device used for the fragmentation experiments.

A total of 8 decompression experiments were performed. In every experiment the decompression profile was varied while the temperature was kept constant at 850°C: ie. in the first set of experiments the samples were decompressed to ambient pressure, in the second set of experiments the samples were decompressed to a P>Patm (oversaturated) and then quenched isobarically; finally in the third set of experiments the samples were decompressed to ambient pressure in a stepwise fashion. Decompression rate was around 1 MPa/s for each experiment.

Samples were recovered after the experiments and analyzed by optical microscopy. Each sample presented a different vesicle distribution (Fig. 1). The degassing pattern experienced by each samples will be investigated through SEM analyses and Raman spectroscopy at the University of Roma Tre. The vesicle size distribution will be then related to the different decompression patterns and original water contents.

New insight into the provenance of the obsidian fragments of the island of Ustica (Palermo, Sicily)

F. Foresta Martin, M.L. Carapezza, A. Di Piazza, C. D'Oriano, M. Nazzari, A. Paonita, S.G. Rotolo, L. Sagnotti

Since the mid-1990s, it had been believed that the obsidian fragments found on Ustica were all imported from the neighbouring island of Lipari, located about 160 km eastward. In 1995, Tykot studying the chemical composition of some obsidian fragments from the Faraglioni village archaeological site (Middle Bronze Age), attributed the provenance of one of them to the island of Pantelleria, situated about 230 km to the SSW. This single finding paved the way for further confirmation of the presence on Ustica of obsidians from the island of Pantelleria.

The primary goal of this multidisciplinary study (coupling physical and chemical analyses) was to perform an investigation on the provenance of a representative population of Ustica obsidians (170 flakes), collected on the volcanic island of Ustica (Sicily). On this island there are some prehistoric settlements dated from the Neolithic to the Middle Bronze Age. Despite not having geological outcrops of obsidian rocks, the countryside of Ustica is rich in fragments of this volcanic glass, imported from other sources. The study of obsidian findings was carried out first through visual observations and density measurements. At least two different obsidian families have been distinguished, probably imported from Lipari and Pantelleria islands. Then, the analysis of the magnetic properties of the samples was carried out and results confirmed these two main sources, but the possibility of other provenances, notably from Palmarola (Latium) and Monte Arci (Sardinia), was also inferred. To verify this hypothesis, we characterized the geochemical signature of the Ustica obsidians by performing microchemical analyses through electron microprobe (EMPA) and laser ablation (LA–ICP–MS). The results were compared with literature data, confirming the presence of the Lipari and Pantelleria sources (Sicily) and indicating, for the first time, in this part of Italy a third provenance from Palmarola island (Latium). At the same time, the trace element composition indicated the absence of fragments from Sardinian sources. We thus came to the conclusion that about 87.6% of the analysed Ustica obsidian fragments come from Lipari, 11.8% come from Pantelleria and only 0.6% come from Palmarola. By means of this study, through the comparison of different analytical methodologies, we can confirm that the analysis of trace elements using laser ablation ICP–MS is the most effective way to discriminate among different sources of provenance for obsidian fragments. Our study confirms the significant presence of obsidians from Pantelleria on the island of Ustica, as already inferred by Tykot. In addition, we presented the first occurrence of a Palmarola obsidian flake in Ustica samples. This result extends the known diffusion area of obsidians southward from Palmarola that until now was limited to northern and central Italy. Our results shed new light on the commercial exchanges in the peri-Tyrrhenian area during the prehistoric age.

Geological evidence for recurrent collapse-driven blast pyroclastic density currents in the Stromboli basaltic stratovolcano (southern Italy)

F. Lucchi, G. De Astis, C.A. Tranne, L. Francalanci, E. Braschi

Three different pyroclastic successions - i.e. positioned in different stratigraphic positions within the Holocene volcano-stratigraphy and known as: Semaforo Nuovo (SN), Secche di Lazzaro (SL) and Semaforo Labronzo (LB) and with distinctive lithologic and volcanological features - have been studied to understand their origin in the ordinary magmatic activity of the Stromboli volcano. They are coherent to unconsolidated, ash-rich and accretionary lapilli-bearing pyroclastic deposits that crops out in scattered sites along the lower slopes of the Stromboli volcano (southern Italy). Although they share a composition identified as the most evolved high-K shoshonites erupted in the Neo Stromboli Eruptive Epoch, their juveniles have slightly different major and trace element compositions (whole-rock and glass), isotopic ratios and mineralogical characteristics. The three successions were independently recognized in distinct sectors of the volcano, displaying an asymmetric areal distribution interpreted as the result of temporally distinct eruptive blasts from summit vents that produced laterally-directed pyroclastic density currents and minor fallout deposits. In the frame of this multidisciplinary geological study we performed a morphoscopic investigation of their glass fragments in the grain size fraction < 125μ, aimed to unravel the dilemma – also present in other strombolian volcanoes - between magmatic vs. phreatomagmatic fragmentation affecting the magma along the eruptive process. Particle morphology and features (contours, shapes, walls of ruptured bubbles and degrees of vesicularity) were investigated by using a Scanning Emission Microscope (SEM) equipped with Energy Dispersion System (EDS) microanalysis available at HPHT Lab (INGV, Rome).

We analyzed one sample from SL and LB, whereas a sequence of 3 samples from 3 different layers of SN. All the samples from these pyroclastic successions are composed of glass fragments, with minor amounts of lithic clasts and crystals (pyroxene, olivine, plagioclase, K-feldspar). Overall, glass particles show variable shapes and textures. Basically, we have observed two types (Fig. 1a) of coexisting particles: i) one represented by blocky, equant in shape, poorly vesiculated glass, with micro-crystalline groundmass (type-A); (ii) the other, by fluidal, medium to highly vesiculated fragments up to spongy forms (type-B). The latter are mostly sub-aphyric and resemble sideromelane according to the nomenclature of basaltic ash. Some transitional shapes between these two end-members have been also observed (Fig. 1a). The relative proportions between these two types change from one to another sample of the studied layers. SL is mainly composed of type A blocky particles with sharp edges (Fig. 1a, b, c) and frequent secondary features such as stepped surfaces (Fig. 1b), chemical pitting (Fig. 1c), secondary skins, V-shaped pits (Fig. 1d), and very fine adhering particles. By contrast, quenching cracks are quite rare. Type-B glass shards are subordinately present, represented either by medium to highly vesicular fragments (Fig. 1e), in places

with tube-vesicles, or by angular clasts with sub-spherical vesicles showing concave–convex contours.

Although heavily altered, ash fragments from LB display similar amounts of type-A blocky shards and type-B highly vesiculated, irregular or spiny ones, with rare spongy shards (Fig. 1f). 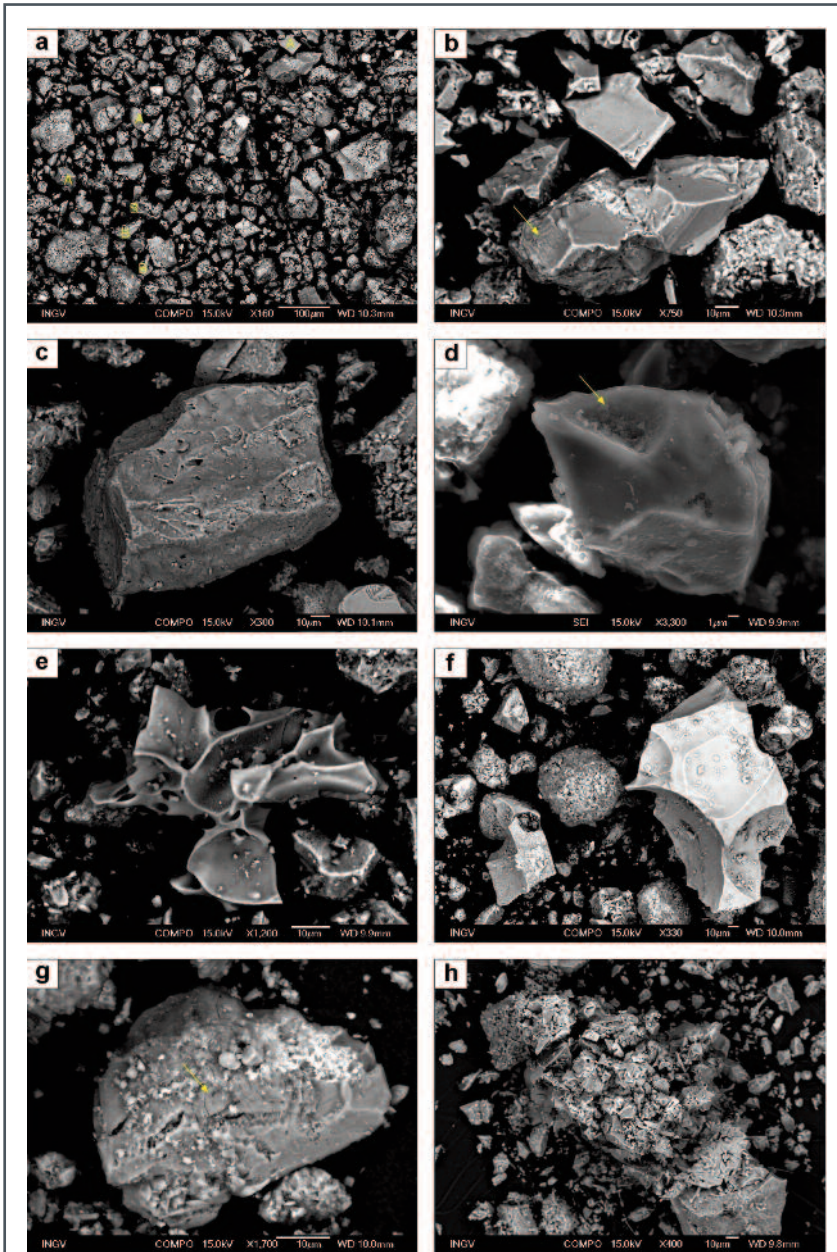Both blocky and, more variably, vesicular particles show wide and generally severe chemical pitting. In this unit, armoured lapilli and sub-spherical ash pellets are frequently formed by the aggregation of fine ash fragments. Moreover, also fragments (of any type) with adhering particles are quite abundant. Moss-like complex shapes, basically formed by fine blocky ash particles, are another common feature. SN displays variable features in the sampled layers, although the fine ash population is overall characterized by the coexistence of type-A and type-B glass fragments. The latter are particularly represented by angular and well vesiculated clasts, with vesicles ranging in shape from tubular to contorted or sub-spherical, and are composed of fresh glass with few features related to chemical alteration. The type-A blocky clasts are instead equant and subrounded, from non-vesicular to very poorly vesicular, and show a wide range of features, such as stepped surfaces, quenching cracks (Fig. 1g), hydration surfaces, chemical pit-

Fig. 1 l SEM images of glass fragments from the SN, SL and LB layers: **a)** double population of type-A blocky and type-B fluidal and vesicular fragments (layer SL-a), most of which are characterized by tiny fine adhering particles and often by chemical pitting; **b)** cuspidate fragment with stepped surface (arrow) and smaller blocky shards around (layer SL-a); **c)** evidence of chemical pitting on a blocky fragment (layer SL-a); **d)** V-shaped pit (layer SL-b); **e)** highly vesicular, type-B fragment (layer SL-b); **f)** blocky to cuspidate fragment with pitting (on the left) together with vesicular fragment (on the right) with thin vesicle walls and fine adhering particle on its surface, with ash pellets around (layer LB-c) **g)** blocky clast with quenching cracks (arrow) and adhering particles (layer SN-g); **h)** moss-like aggregate (layer SN-f).

ting, secondary skins, adhering particles and moss-like aggregates (Fig. 1h). Remarkably, the evidence for chemical pitting of the particles sharply increases moving from the lower to the upper (sampled) layers, together with a proportional increase of the relative amount of type-A blocky clasts and crystals.

Accordingly, the SEM study suggests a phreatomagmatic origin for SN, SL and LB, as indicated by the occurrence of type-A fragments and/or features such as surface hydration, moss-like aggregates and abundant tiny adhering particles on the larger fragments, as well as particles showing stepped fracture surfaces. The blocky glass fragments, indeed, suggest that limited bubble nucleation and growth had occurred before the magma-water interaction. Moreover, glass particles with chemical pitting and secondary skins result from the interaction with highly acidic (condensing) fluids within the eruptive cloud or during the transport in the pyroclastic current. At the same time, the (even abundant) presence of glasses (type-B) with features deriving from disruption of magmatic gas bubbles indicates that magmatic fragmentation mechanisms also played a significant role during the SN, SL and LB eruptions. Therefore, a pene-contemporaneous presence of magmatic and (prevalent) phreatomagmatic fragmentation processes should be taken into account, assuming that after the phreatomagmatic onset, the magmatic fragmentation driven by gas exsolution occurred as consequence of rapid magma decompression.

Dynamics of strombolian eruptions at Batu Tara volcano (Indonesia)

E. Del Bello, L. Spina, P. Scarlato, D. Gaudin, J. Taddeucci

In September 2014, high-speed imaging and acoustic data were acquired during 3 days of almost continuous recording (04-06/09/2015) aimed at investigating degassing and explosive dynamics using a high-speed visible camera (OPTRONIS, acquiring at 500 frames per second), a thermal infrared camera (FLIR, 50-200 fps), and two broadband microphones (freq. range of kHz to 0.1 Hz) sampled at 10 kHz. Thermal images characterization was performed by integrating the amplitude of the thermal images in a box above the vent, and then correcting for the background, obtaining a thermal amplitude signal variation over time. Each explosion can be either characterized by a single pulse or by a sequence of two or more pulses. From these signals, 69 thermal peak events were discriminated by using an sta/lta trigger algorithm. Thermally characterised events show a broad distribution in terms of event duration, with peaks at 12 and 20 seconds, and a uniform distribution of amplitudes. No direct correlation is observed between amplitude and duration. A proxy for the cumulative thermal energy of each event is obtained by integrating each signal in the trigger/detrigger time interval. In this case, event energy appears to correlate positively with amplitude and duration, becoming independent of duration for events >30 s. The picking of acoustic events was also obtained by an sta/lta trigger algorithm (STA window = 1 s, LTA window = 5 s, trigger thr. = 3). On the selected events, Short-Time Fourier Transform was performed on a window of 1 second with 0.5 second of overlap. Two type of events were identified: 1) low frequency events (Type 1), with a frequency content mostly below 5 Hz, often exhibiting monochromatic or harmonic spectra; 2) broadband events (Type 2), characterised by a frequency content ranging 0-50 Hz and emergent waveforms. These match with the thermally identified single-pulse events and multi-pulse events, respectively (Fig. 1). The peak frequency of the investigated acoustic events positively correlates with their duration suggesting that acoustic events characterized by higher frequency content were also related to more prolonged episodes of gas/ejecta release; hence they are likely to reflect differences in the source mechanism or in the local condition within the conduit.

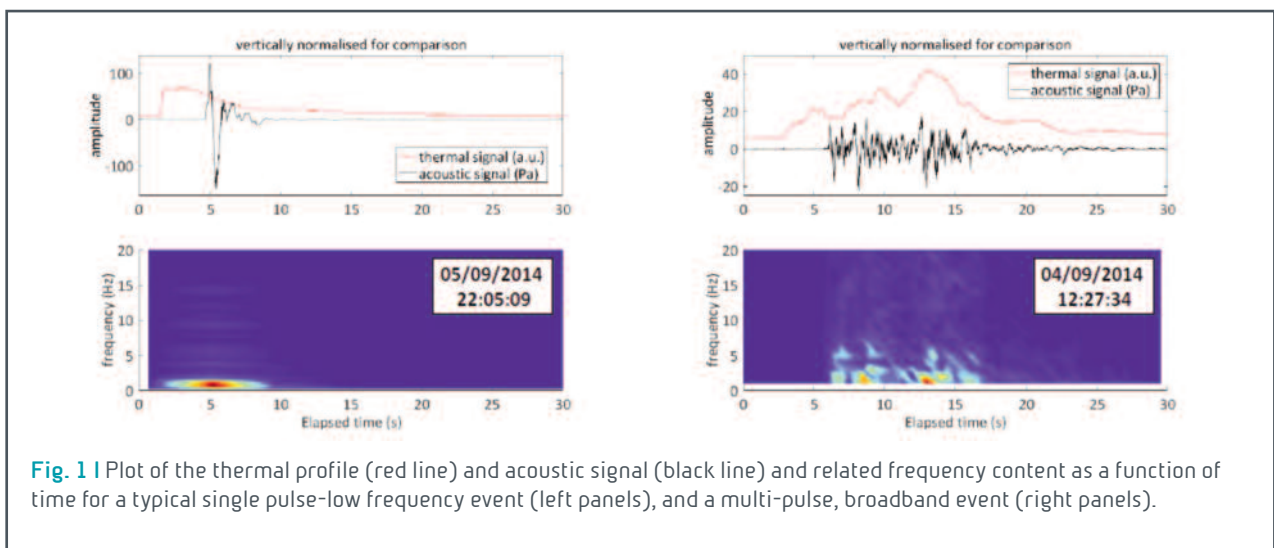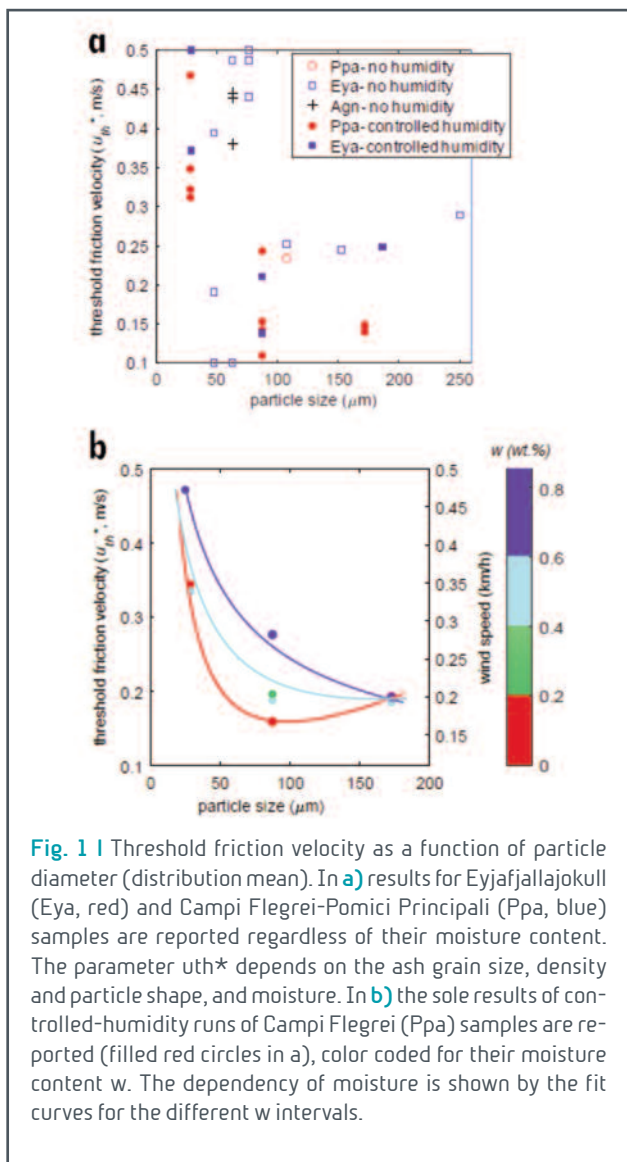**Fig. 1 I** Plot of the thermal profile (red line) and acoustic signal (black line) and related frequency content as a function of time for a typical single pulse-low frequency event (left panels), and a multi-pulse, broadband event (right panels).

Parameterization of volcanic ash remobilization by wind–tunnel erosion experiments

E. Del Bello, J. Taddeucci, J.P. Merrison, S. Alois, J.J. Iversen

In the framework of the EU-funded Europlanet project, we jointly used the environmental wind tunnel facility at Aarhus University (DK) and the state-of-the art high-speed imaging equipment of INGV experimental lab (Italy) to study the resuspension dynamics of ash-sized (half-millimetre to micron-sized) particles. In March 2017, a second campaign of experiments was conducted aiming at parameterizing the factors that influence and promote the detachment of particles from the ground and their re-entrainment into the atmosphere. Specifically, the focus of these set of experiments was to quantify the role of humidity on the threshold friction velocity, i.e. the value of friction speed beyond which particle erosion begins. To this target, the starting material (volcanic ash from Campi Flegrei- Pomici Principali deposits, and Icelandic Eyjafjallajökull May 2010 eruption) was first humidified to different degrees before each experiment by exposing plates loaded with the sample in the tunnel at controlled humidity conditions. Wind erosion experiments were then performed at the same controlled environmental conditions increasing wind tunnel velocity until detachment of the particles is seen from the plate. Detachment and resuspension processes were filmed at 2000 fps and 50-micron per pixel resolution. The plate was weighted pre and post-experiment to retrieve the eroded sample mass, and its moisture content measured by oven drying a test sample that underwent the same humidifying procedure as the sample plate. We found that increasing sample moisture dramatically increases the threshold friction velocity for particles < 125 μm. The minimum erosion threshold (uth*~ 0.16 m/s) is reached for particles with radius of about 100 μm at the lowest moisture content (w~0.15 wt.%). This parameter is roughly doubled (uth*~ 2.8 m/s) when the sample moisture is approximately 1%. Adhesive forces control the detachment behaviour of these particles, and increase by a factor of 2 in wet conditions than in dry conditions. The detachment of particles > 125 μm is largely unaffected by their moisture content, being largely dominated by torque and lift forces, inducing.

Fig. 1 | Threshold friction velocity as a function of particle diameter (distribution mean). In **a)** results for Eyjafjallajökull (Eya, red) and Campi Flegrei-Pomici Principali (Ppa, blue) samples are reported regardless of their moisture content. The parameter uth* depends on the ash grain size, density and particle shape, and moisture. In **b)** the sole results of controlled-humidity runs of Campi Flegrei (Ppa) samples are reported (filled red circles in a), color coded for their moisture content w. The dependency of moisture is shown by the fit curves for the different w intervals.

The Fourth Broadband Acquisition and Imaging Operation (BAcIO 2017) at Stromboli Volcano

P. Scarlato, J. Taddeucci, E. Del Bello, T. Ricci.

BAcIo 2017, the multi-parametric experiment at Stromboli organized by the HPHT Laboratory has reached its 4th edition. Improving the understanding of Strombolian eruptive dynamics and developing new techniques for monitoring active volcanoes is the objective of the field campaign, that, as for previous editions, involved about 30 international researchers from 5 different research institutions. Besides INGV participants (P. Scarlato, J. Taddeucci, E. Del Bello, T. Ricci, P.Y. Tournigand, D. Andronico), the experiment involved participants from LMU-Germany (U. Kueppers, V. Cigala, D. Gaudin, A. Pisello, M. Colombier, C. Cimarelli, M. Knuver), University of Bath-UK (M. Airy, K. Nicol, K. Liang Koh), University of Berlin (J. Sesterhenn), and University of Hawaii (B. Houghton, N. Turner, B. Walker, S. Müller, S. Biass). One of the novelty of this year was the presence of researchers in the meteorological field (Uni. Bath) that have carried out measurements on the electric field related to volcanic activity. For measurements in the atmosphere above the volcano, probe flasks were used, equipped with sensors for measuring atmospheric parameters in the volcanic cloud, such as temperature, humidity, ash concentration and electric field. For the imaging and sensing of the eruptive dynamics, four high-speed/high-resolution cameras and two synchronized thermal cameras were used, plus several infrasonic microphones. Four drones, equipped with high-resolution cameras to observe in real time the crater area from above. These allowed to detect the morphological changes occurred with respect to last year, and revealed the presence of magma at very shallow levels inside the active vents (Fig. 1). From the high definition images of the craters taken from the drones of BAcIO 2016, it was finally possible to create a digital model of the high-resolution Stromboli summit area. The result was published in American Geophysical Union EOS.

Fig. 1 I Picture taken from a drone of an active vent in the northeast crater at Stromboli in September 2017, showing magma residing at a shallow level. Credits: ITN VERTIGO project (@VERTIGO_ITN), Ludwig Maximilian University.

Origin and dispersal of volcanic ash in the Austral Hemisphere: a database for the volcanology, chronostratigraphy and paleoclimate of the Earth system.

P. Del Carlo

Fig. 1 I Back scattered electron (BSE) images showing some of the studied tephra sampled in Patagonia (Chile).

Explosive volcanic eruptions inject into the atmosphere solid materials (tephra) whose finest fraction (ash, <2 mm) represents a major contributor to the particle atmospheric load affecting climate parameters and nutrient availability to ecosystems as well. Furthermore, the knowledge of atmospheric particle paths is invaluable in reconstructing atmospheric currents at different layers and their temporal variabilities. In the Austral Hemisphere, the Antarctic continent has a barycentric position and an integral snow-ice cover, making it a prime sink for atmospheric particles, infact Antarctic ice contains plenty of volcanic ash layers. Their study is a fundamental tool for paleoclimatic interpretations in Antarctica and surrounding areas. Using tephra layers as chronostratigraphic markers and atmospheric path tracers is nevertheless possible only when their provenance can be tightly constrained. It is therefore mandatory to compare the volcanological, geochemical and chronological data of these materials with as many as possible potential sources (volcanoes) for which the same parameters are known. That is, this type of studies completely relies on the availability of a comprehensive database including data for all the volcanoes with activity during the Holocene. Ash layers in the Antarctic ice offer a hemispheric-scale record of the explosive volcanic activity as well as implications on atmospheric circulation and hence on paleoclimate. Such an investigation needs a comprehesive database including all the volcanoes active during the Holocene-late Pleistocene time span in the Austral Hemisphere. Such a database is not yet available, and among those set up by the research institutions no one is specifically designed for this function. This project is designed to set up a specific database integrating available data and new data on available samples as well as on ash layers (Fig. 1). To this aim, we have started to analyse several Holocene-late Pleistocene ash layers sampled in Patagonia produced by Southern America volcanoes and compared their geochemical compositions with those recovered in Antarctica in order to find correlations and the volcanic sources for the extra-Antarctic tephra. This work is still in progress and results will be available within this year.

Rheology of mixed clay-silt and silt-sand water-rich suspensions at high shear rates and implications for the flow of slurries, mudflows and sludge

P. Del Gaudio, G. Ventura

Natural and artificial water-rich clay to sand suspensions like mud-flows, slurries and sludge are characterized by a complex, share rate dependent flow behavior.

The rheology of such suspensions depends on the size and shape of the suspended particles and by the water (solid) content; small quantity of clay fraction plays an important role on the rheology of that suspensions. Comprehension of the appropriate rheological model (e.g., Netwonian, Bingham or Herschel-Bulkley), which is also a function of particle interaction and lubrication processes, is of primary importance for geological, hydraulic, mining, and civil engineering applications and studies. Here, we present the results of experimental rheological measurements of water-rich (40 to 60 wt.%) clay to silt (population A) and silt to sand (population B) suspensions mixed in different proportions. The data are consistent with the Herschel-Bulkley model. At high shear rates (>200 s^{-1}) most of the studied suspensions show a dilatant (shear thickening) behavior with values of the flow index n >1. The viscosity, consistency K and yield stress τ_0 decrease as the A+B fraction decreases and the content of B particles increases.

This behavior is due to competing effects of the lubrication and frictional processes as function of particle size and water content. Results from an application of the Herschel-Bulkley model to suspensions flowing on an inclined plane show that the flow velocity significantly changes as small variations of water or coarse (fine) fraction occur. This has relevant interest for the studies on the hazard related to floods.

Rheology of mud derived by liquefaction occurred during Amatrice 2016 earthquakes
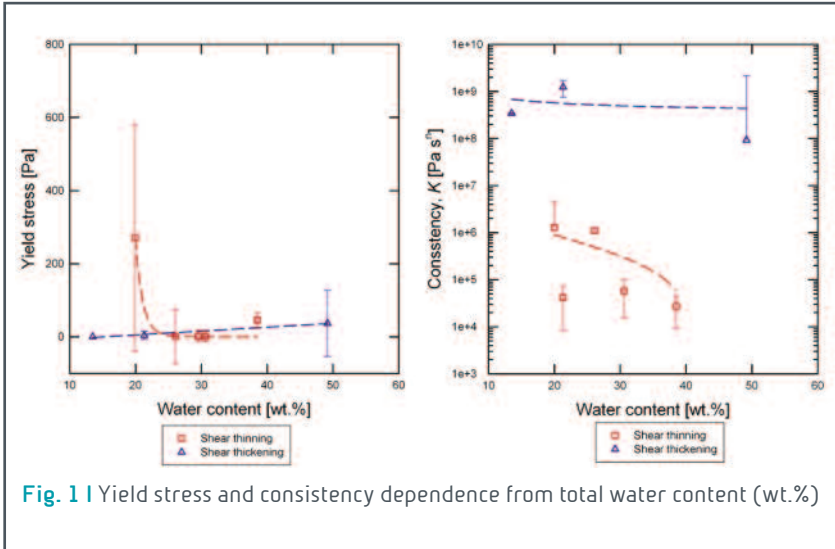
P. Del Gaudio, V. Misiti

Fig. 1 I Yield stress and consistency dependence from total water content (wt.%)

Study on liquefaction features have showed their correlation to strong earthquakes. However, other natural causes can produce or mimic liquefaction features, e.g. structures of syndepositional origin, due to artesian condition, formed by weathering or in periglacial environment. Liquefaction is the transformation of a granular deposit from a solid state to a liquefied state as a consequence of the increased pore-water-pressure determined by cyclic shaking. The most common surficial features of liquefaction are sand blows occurring in sand volcanoes or along fissures. Liquefaction features usually occurs during strong earthquakes, $M_s > 6.5$. Galli and Meloni (1993) and Galli (1999) account for a large number of moderate earthquakes, $M_s > 4.2$, producing liquefaction. We have experimentally studied the rheology of mud derived from liquefaction occurred during Amatrice 2016 earthquakes (30th October 2016, 6.5 Mw).
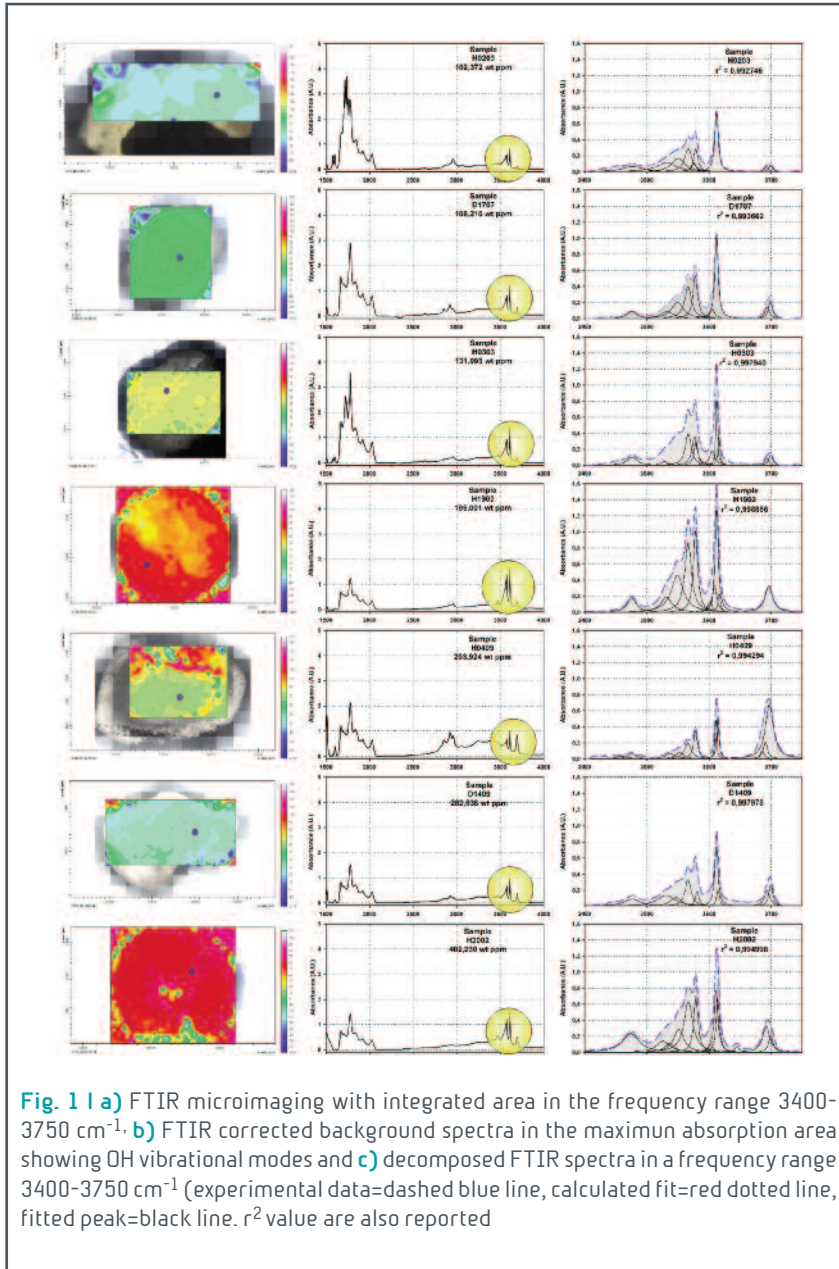
Water content of all mud suspensions (in total 8 samples) was measured by LOI and is ranging between 13 and 49 wt.%. Rheological experiment were performed in an Anton Paar MCR301 rheometer equipped with vane rotor geometry with (CSS) controlled stress at INGV. Flow curves display a shear thinning behavior (material is one in which viscosity decreases with the rate of shear strain) for 5 samples and shear thickening (material is one in which viscosity increases with the rate of shear strain) behavior for 3 samples. Such different behavior seems to be independent from the total water content of suspensions. In figure 1 we show the yield stress and consistency dependence from total water content (wt.%). Yield stress of shear thinning suspensions decreases as total water content increases while seems to have no variation for shear thickening suspensions. The consistency is decreasing by two order of magnitude since total water content increases.

These preliminary study exhibits a strong effect of total water content in liquefied mud suspensions just in shear thinning suspensions at shear rate investigated (ranging between 10^{-7} and 10^{-4} s^{-1}) while is not influencing the shear thickening suspensions.

Synthesis and characterization of hydrous and nominally anhydrous minerals at upper mantle conditions

A. Del Vecchio, B.T. Poe, V. Misiti, M. Cestelli Guidi

Fig. 1 | a) FTIR microimaging with integrated area in the frequency range 3400-3750 cm^{-1}, **b)** FTIR corrected background spectra in the maximun absorption area showing OH vibrational modes and **c)** decomposed FTIR spectra in a frequency range 3400-3750 cm^{-1} (experimental data=dashed blue line, calculated fit=red dotted line, fitted peak=black line. r^2 value are also reported

The presence of water in the crystal lattices of nominally anhydrous minerals plays a key role in the field of the dynamic processes occurring at greater depths in the Earth, mainly because it influences several chemical-physical properties such as electrical conductivity, rheology and seismic velocities.

Experimental methods in the field of experimental mineralogy and petrology allow us to synthesize samples at the Earth's mantle conditions, and then eventually be able to compare them with natural samples coming from the mantle itself. As starting materials, we used a natural San Carlos olivine and a synthetic forsterite obtained by thermo−mechanical activation with known chemical composition. In this case, we used talc $Mg_3Si_4O_{10}(OH)_2$ and hydroxyl magnesium carbonate $MgCO_3*Mg(OH)_2*H_2O$, in a stechiometric ratio Mg : Si equal to 2:1 suitable for the formation of the forsterite. Heat treatment was carried out putting starting powders in a platinum crucible and using a Nabertherm LHT 04/18 chamber furnace at National Institute of Geophysics and Volcanology in Rome. Synthesis was performed through a series of steps of heating − locking system until to reach a temperature value of 1600 °C, with a gradient of about 11-15 °C/min. X-Ray Powder Diffraction and Raman spectroscopy analyses confirmed the presence of iron-free forsterite. Synthesis runs were carried out at 1100 °C and with pressure values up to 4 GPa, con-

ditions of the upper mantle. We performed 11 runs, using multi anvil apparatus for higher pressure, ¾ inch end loaded piston cylinder apparatus and ½ inch non-end loaded quick press for lower pressure.

Polycrystalline powders of olivine and forsterite (about 1,5 g) and liquid hydrogen source (H_2O and D_2O for different isotopic content) were inserted in a platinum capsule ($Pt_{0,95} Rh_{0,05}$). Piston and assembly diameter was ¾" (1,91 cm), the cylinders were made by NaCl, Pyrex and graphite, coaxial to the capsule, which acts as the furnace. Capsules were arranged exactly into the isothermal region through a cylindrical support made by Al_2O_3 with keeps it in a vertical position. Alumina cylinders show a central hole inside which the thermocouple is passed. Temperature was monitored using a $W_{95}Re_5/W_{75}Re_{25}$ (C type) thermocouple inserted within an alumina sleeve. Using a Walker type 6/8 Multi-Anvil apparatus 2 runs at 4 GPa were annealed at 1100 °C for a duration of 300 min. The runs were performed using 25/17 assembly configuration, with a 25-mm edge length Cr_2O_3-doped MgO octahedral pressure medium and 17 mm WC anvil truncation. After syntheses, samples were recovered, sectioned and embedded in an epoxy resin for about 24 hours. Then, sections were thinned and polished to obtain a thickness ranged between 300 - 700 microns. In order to evaluate the effective presence of water in our samples after HP and HT syntheses, FTIR represents the best powerful tool to identify bands associable with vibrational modes of OH groups in the crystal lattices. Through FTIR micro imaging we mapped all the sample area and we integrated the whole area in a frequency range equal to 3400 - 3800 cm^{-1}, in order to observe a strong heterogeneity of the distribution of water throughout the sample (Fig. 1a). Then, we acquired a spectrum from the maximum absorption zone (Fig. 1b). Total water content was calculated by using the Paterson calibration for unpolarized spectra, with final concentrations ranged from 100 -450 ppm. Fitting process of FTIR spectra was performed using Peakfit 4.2 software, and peaks were best approximated by Lorentzian function with three parameters (intensity/absorbance, frequency and FWHM), in order to identify the main incorporation mechanisms of hydrogen in the crystal lattice. We succeed to identify main vibrational modes in a frequency range of 3550 – 3650 cm^{-1}, and between the main models of incorporation mechanisms known by literature data (Hydro garnet defect, Magnesiac vacancies defect, Titanoclinohumite defect, Trivalent Cations defect and Interstitial defect), all fitting process indicated Si vacancy as the main incorporation mechanism, and more specifically, the Si^{2-} and Si^{3-} configurations. Furthermore, we identified two bands at 3566 and 3610 cm^{-1} that can be also related to interstitial OH position (Fig. 1c). No vibrational modes were observed below 3500 cm^{-1}, frequency range of magnesium vacancy. This behavior may be explained 1) by an absence of any material buffering the silica activity in the HP and HT assemblies and 2) by the presence of MgO traces in XRPD spectra that probably played a key role in the buffering of Mg-vacancy. Now, we are trying to apply the same experimental design using D_2O as hydrogen source. Being able to obtain FTIR spectra would allow us to study the hydrogen self-diffusion processes in these types of minerals, in order to be improve our knowledge regarding the processes and the physical, chemical and mineralogical properties of minerals representing the Earth's mantle.

Carbonaceous Chondrites and HED meteorites characterized combining SEM/EDS, FT-IR and IRµ-spectroscopy

F. Dirri, M. Ferrari, M. Nazzari

This work reports the results of the µ-IR, FT-IR and SEM/EDS characterization of three Carbonaceous Chondrites (CC) and three HED meteorites. The FT-IR analysis performed on meteorite powders provided bulk information on the mineralogy of the samples. To corroborate the FT-IR results and to obtain textural and chemical information, several SEM/EDS and µ-IR analytical spots have been performed on the samples.

The analysed CC meteorites belong to CV, CI and CM classes. The combined analysis of the most interesting regions of CCs indicate that: the NWA2086 (CV3 group, with considerable amount of large mm-size chondrules and inclusions surrounded by igneous rims) chondrules are essentially enriched in Mg-pyroxene while the matrix is mainly composed by olivine; the NWA8267 (CM2 group, characterized by small chondrules and refractory inclusions) chondrules (Fig. 1a) and their rim are enriched in low-Ca pyroxene with small inclusions of sulphides in the inner rim; the Murchison meteorite (CM2 group) shows two types of inclusions: the "white" ones that can be ascribed to Mg-olivine with minor serpentine and the "yellow" inclusions formed by olivine with minor sulphides and hydrates silicates.

The results of the Fourier Transform Infrared Spectroscopy and SEM/EDS combined study of three HED meteorite samples indicates that: the NWA 7159 is a monomictic brecciated eucrite consisting of exsolved orthopyroxene and anorthite with accessory silica polymorph and ilmenite; the NWA 7490 is a diogenite with a cumulate texture dominated by orthopyroxene, with Ca-plagioclase, minor olivine and chromite and troilite as accessory
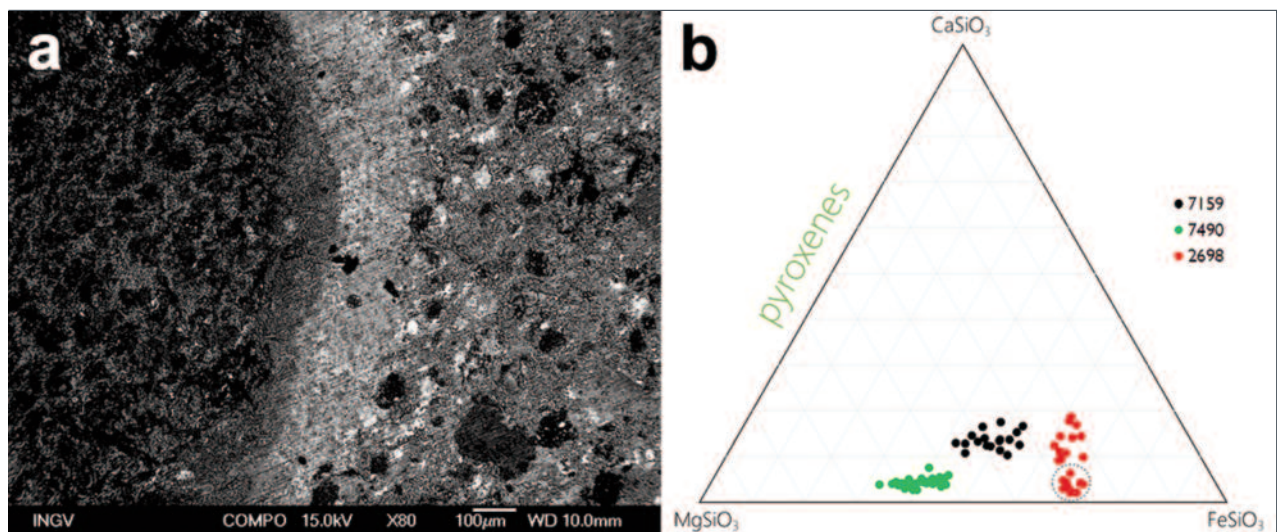

Fig. 1 I **a)** SEM/BSE detail of NWA8267 meteorite. The chondrula (dark region) with its rim (bright region) were studied and the main mineral composition was inferred; **b)** Pyroxene compositions in the three HED meteorites plotted on a standard $MgSiO_3$–$CaSiO_3$–$FeSiO_3$–ternary diagram (wt%).

minerals; the NWA 2698 is an howardite with eucritic pyroxene. The SEM/EDS wt% data related to pyroxenes in the HEDs are potted in the ternary diagram in figure 1b. The composition of the pyroxene of NWA 7159 fall in the pigeonite area with a spread in the Fe/Mg ratio. The NWA 7490 pyroxene showing a low-Ca composition with a slightly variable Mg/Fe ratio. The average composition can be ascribed to a hypersthene. The NWA 2698 meteorite shows two different domains: the low-Ca (dotted circle in Fig. 1b) and the higher one that can be ascribed at two different pyroxene, the diogenitic pyroxene and the eucritic one respectively.

Igneous rocks as source and sink of abiotic hydrocarbons and CO_2

G. Etiope, M. Nazzari, G. Ventura

This research is aimed at evaluating, through laboratory experiments and field surveys, the process of hydrocarbon generation and CO_2 removal during serpentinization in geologic environments, with particular emphasis on the abiotic methanation in ultramafic rocks. Rock milling and gas analyses performed in previous experiments revealed the presence of considerable amounts of hydrocarbons in some ultramafic rocks collected from ophiolites in Greece. It is not clear, however, how and where this gas is stored within the rock, whether dispersed in the voids and microfractures or in fluid inclusions. Classic literature on gas in igneous rocks generally considers the presence of methane only as trace amounts in fluid inclusions of minerals. The amount of gas detected by us would suggest, however, that it is dispersed in the rock voids, similar to the gas in shales or reservoir rocks. Accordingly, we performed accurate analyses in order to know the geometry and distribution of voids and microfractures that can host hydrocarbons within the ultramafic rocks. This has been done using optical microscopy and a Field Emission Scanning Electron Microscope (FESEM, JEOL JSM 6500F).

The first analyses performed in 2017 allowed to identify a series of microfractures and porous structures in the methane-bearing rocks. Chromitites, in particular, which host considerable amounts of methane, are characterized by high porosity and fracturing. Successive Raman analyses have confirmed that methane is stored in these microfractures and serpentine-filled veins, and not in fluid inclusions. These igneous rocks seem to have fluid-bearing properties similar to some sedimentary rocks. This finding opens a new research prospective in the framework of the origin and occurrence of abiotic methane and related implications for the environment, resource exploration and microbiology.
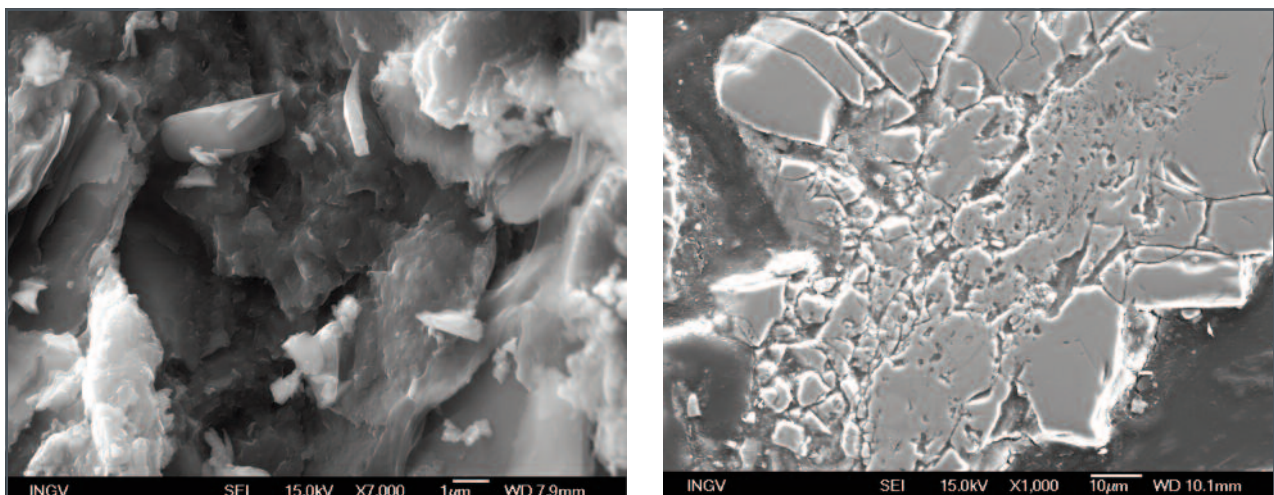

Fig. 1 l Left) fractures and pores in a crystal of Cr-spinel, and voids among crystals in a chromitite **(right)**.

The role of undercooling during crystallization of Etnean magmas

M. Masotta, A. Pontesilli, S. Mollo, P. Armienti, M. Nazzari, V. Tecchiato, P. Scarlato

Both the textural evolution and compositional changes of pyroxene are not univocally related to crystallization processes in magma chambers, but rather can be the effect of reaction kinetics along most of the crystallization path of magma controlling the final growth of minerals. In fact, with respect to the superliquidus state of magma, a certain amount of undercooling (ΔT) is always necessary for the onset of crystal nucleation and growth. Once crystal nucleation occurs, crystal growth may proceed with variable rates as a function of the magnitude of undercooling. Under such circumstances, crystals from Mt. Etna volcano exhibit significant compositional variations and, importantly, their sector zoning reflect different crystal growth velocities. The interface kinetics play the essential role in the formation of sector zoning, when the layer growth mechanism takes place during the shift from interface-controlled to diffusion-controlled crystal growth regimes. In this latter case, the crystal growth rate is limited by the ability of melt components to diffuse towards or away from the crystallizing front. Phase equilibria experiments at different undercooling (ΔT) were performed using one of the most primitive basalt erupted at Mt. Etna (M.te Maletto) at pressure of 400 MPa, in the temperature range 1050-1200 °C, and at H_2O contents of 0, 2, and 4 wt.%. All the experiments were superheated above the liquidus at 1400 °C for 30 minutes and then cooled to the experimental temperature at a rate of 80 °C/minute. Mineral assemblage is always constituted by clinopyroxene ± titanomagnetite± plagioclase. Clinopyroxene growth rates are higher at low to moderate degrees of undercooling ($\Delta T < 100$ °C) and large (>500 µm) skeletal crystals are formed at 0 wt.% H_2O (Fig. 1a). At increasing degrees of undercooling, skeletal clinopyroxene crystals that are generally smaller (<200 µm) at 2 wt.% H_2O (Fig. 1b).The diffusion of chemical elements in the melt, leads to different evolutions of the liquid line of descent, characterized by variable slopes in the SiO_2 vs. Na_2O+K_2O diagram.
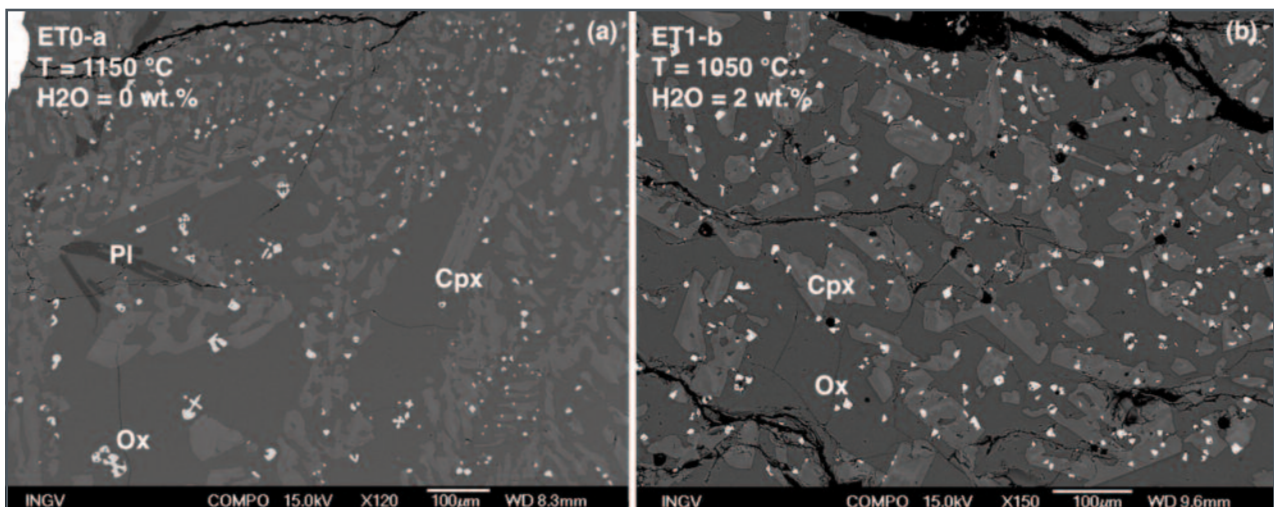

Fig. 1 I Backscattered electron (BSE) images of experimental products showing skeletal clinopyroxene crystals formed at moderate degree of undercooling, and 0 **(a)** and 2 wt.% **(b)** H_2O contents.

The imprint of thermally-induced devolatilization phenomena on radon signal: Implications for the geochemical survey in volcanic areas

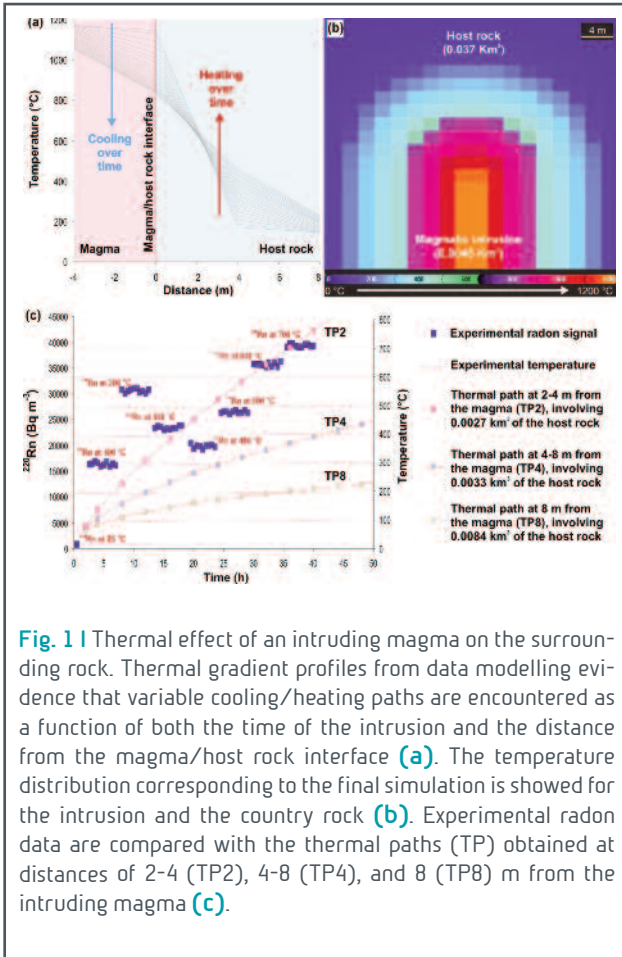*S. Mollo, P. Tuccimei, G. Galli, G. Iezzi, P. Scarlato*

Fig. 1 I Thermal effect of an intruding magma on the surrounding rock. Thermal gradient profiles from data modelling evidence that variable cooling/heating paths are encountered as a function of both the time of the intrusion and the distance from the magma/host rock interface **(a)**. The temperature distribution corresponding to the final simulation is showed for the intrusion and the country rock **(b)**. Experimental radon data are compared with the thermal paths (TP) obtained at distances of 2-4 (TP2), 4-8 (TP4), and 8 (TP8) m from the intruding magma **(c)**.
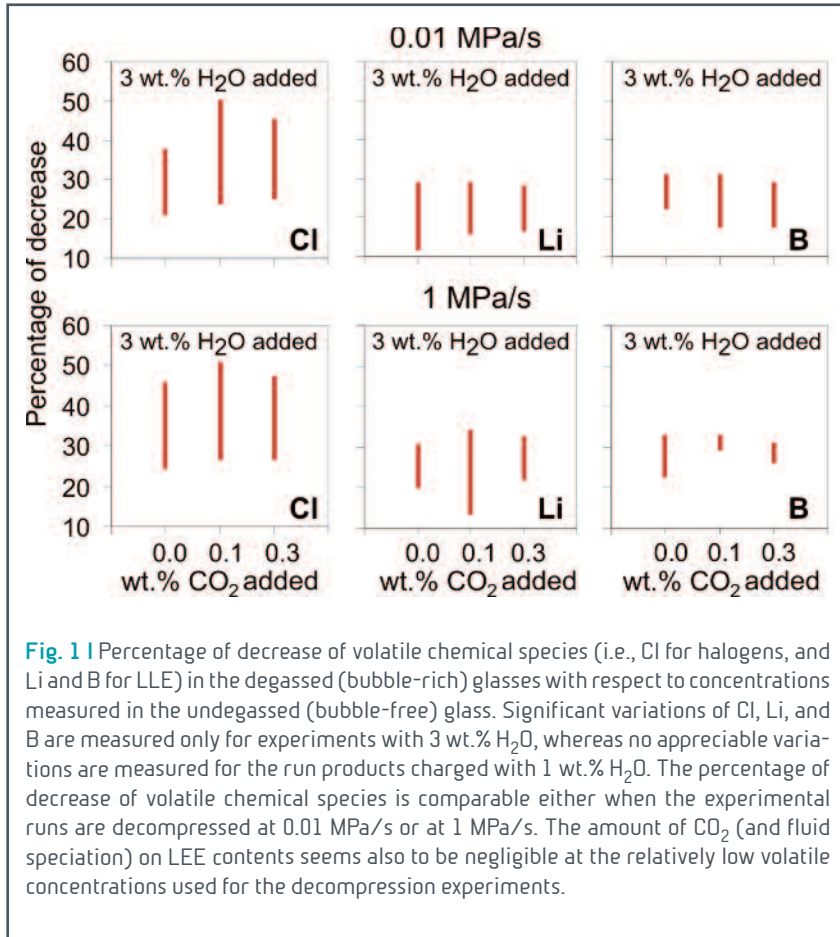
Thermal gradients due to magma dynamics in active volcanic areas may affect the emanating power of the substrate and the background level of radon signal. This is particularly effective in subvolcanic substrates where intense hydrothermal alteration and/or weathering processes generally form hydrous minerals, such as zeolites able to store and release great amounts of H_2O (up to ~25 wt.%) at relative low temperatures. To better understand the role played by thermally-induced devolatilization reactions on the radon signal, a new experimental setup has been developed for measuring in real-time the radon emission from a zeolitized volcanic tuff. Progressive dehydration phenomena with increasing temperature produce radon emissions two orders of magnitude higher than those measured during rock deformation, microfracturing, and failure. In this framework, mineral devolatilization reactions can contribute significantly to produce radon emissions spatially heterogeneous and non-stationary in time, resulting in a transient state dictated by temperature gradients and the carrier effects of subsurface gases. Results from these experiments can be extrapolated to the temporal and spatial scales of magmatic processes, where the ascent of small magma batches from depth causes volatile release due to dehydration phenomena that increase the radon signal from the degassing host rock material (Fig. 1).

The effect of degassing and volatile exsolution on the composition of a trachybasaltic melt decompressed at slow and fast rates

S. Mollo, F. Vetere, H. Beherens, V. Tecchiato, A. Langone, P. Scarlato, D. Perugini

Fig. 1 I Percentage of decrease of volatile chemical species (i.e., Cl for halogens, and Li and B for LLE) in the degassed (bubble-rich) glasses with respect to concentrations measured in the undegassed (bubble-free) glass. Significant variations of Cl, Li, and B are measured only for experiments with 3 wt.% H_2O, whereas no appreciable variations are measured for the run products charged with 1 wt.% H_2O. The percentage of decrease of volatile chemical species is comparable either when the experimental runs are decompressed at 0.01 MPa/s or at 1 MPa/s. The amount of CO_2 (and fluid speciation) on LEE contents seems also to be negligible at the relatively low volatile concentrations used for the decompression experiments.

It is widely accepted that, for the correct interpretation of bulk rock compositions, degassing process controlling both loss of magmatic volatiles and significant changes in the contents of volatile chemical species must be considered. The continuous degassing experiments presented in this study attempt to determine the absolute and relative change in abundances of volatile components in the melt at shallow levels, simulating what might occur during slow and fast ascent of magma from depth without crystallization. We performed disequilibrium decompression experiments using as starting melt a bubble-free but volatile-bearing trachybasalt.

The charges were isothermally decompressed at 1,150 °C from 400 MPa down to 50 MPa at rates of 0.01 MPa/s and 1 MPa/s. Results demonstrate that degassing of 1 wt.% H_2O of initial volatile content in the melt is not enough to induce melt compositional changes as well as H_2O supersaturation in the trachybasaltic melt. In contrast, the minimum H_2O threshold to observe Cl, B, and Li devolatilization corresponds to 3 wt.% H_2O and volatile supersaturation is attained at the fast decompression rate of 1 MPa/s. An increase of CO_2 up to 0.3 wt.% do not change the partitioning behaviour of these chemical species between vapor and trachybasaltic melt. Moreover, CO_2 degassing is less efficient with respect to H_2O transfer from the melt into the vapor phase. As a consequence, the trachybasaltic melt is preferentially supersaturated in CO_2 with decreasing pressure. Disequilibrium degassing does not change the bulk oxidation state of the melt (Fig. 1).

Clinopyroxene-melt element partitioning during interaction between trachybasaltic magma and siliceous crust: Clues from quartzite enclaves at Mt. Etna volcano

S. Mollo, J. Blundy, P.P. Giacomoni, M. Nazzari, P. Scarlato, M. Coltorti, A. Langone, D. Andronico

A peculiar characteristic of the paroxysmal sequence that occurred on March 16, 2013 at the New South East Crater of Mt. Etna volcano (eastern Sicily, Italy) was the eruption of siliceous crustal xenoliths representative of the sedimentary basement beneath the volcanic edifice. These xenoliths are quartzites that occur as sub-spherical bombs enclosed in a thin trachybasaltic lava envelope. At the quartzite-magma interface a reaction corona develops due to the interaction between the Etnean trachybasaltic magma and the partially melted quartzite. Three distinct domains are observed: (i) the trachybasaltic lava itself (Zone 1), including Al-rich clinopyroxene phenocrysts dispersed in a matrix glass, (ii) the hybrid melt (Zone 2), developing at the quartzite-magma interface and feeding the growth of newly-formed Al-poor clinopyroxenes, and (iii) the partially melted quartzite (Zone 3), producing abundant siliceous melt.

These features makes it possible to quantify the effect of magma contamination by siliceous crust in terms of clinopyroxene-melt element partitioning. Major and trace elemen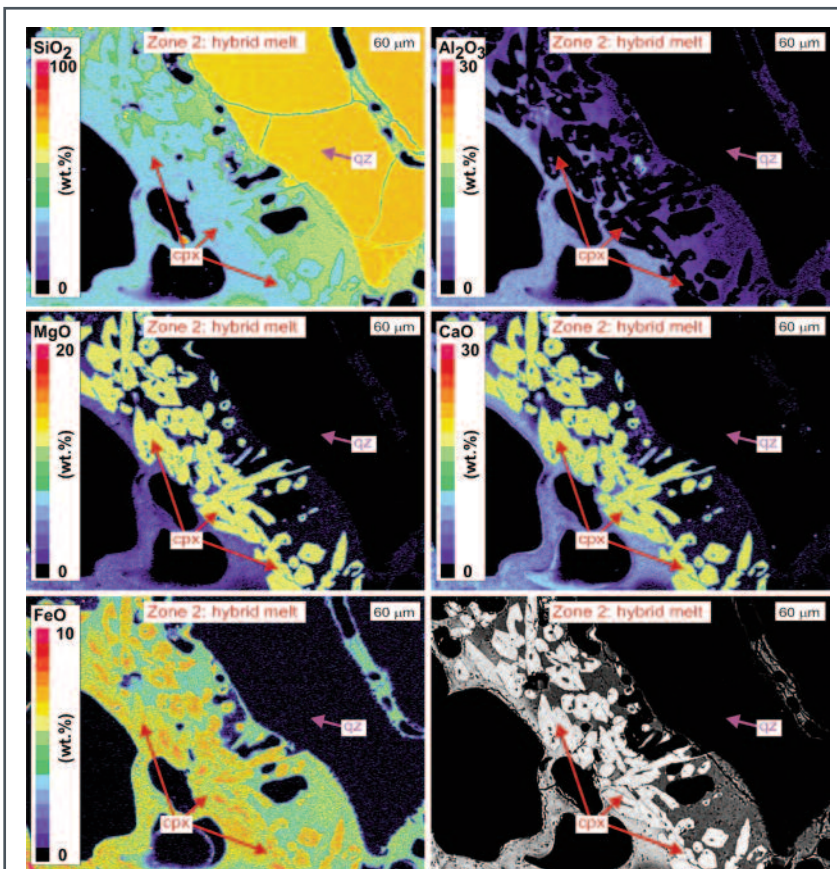t partition coefficients have been calculated using the compositions of clinopyroxene rims and glasses next to the crystal surface. Zone 1 and Zone 2 partition coefficients correspond to, respectively, the chemical analyses of Al-rich phenocrysts and matrix glasses, and the chemical analyses of newly-formed Al-poor crystals and hybrid glasses. For clinopyroxenes from both the hybrid layer and the lava flow expected relationships are observed between the partition coefficient, the valence of the element, and the ionic radius. However, with respect to Zone 1 partition coefficients, values of Zone 2 partition coeffi-

Fig. 1 | Backscattered electron (BSE) images of experimental products showing skeletal clinopyroxene crystals formed at moderate degree of undercooling, and 0 **(a)** and 2 wt.% **(b)** H_2O contents.

cients show a net decrease for transition metals (TE), high-field strength elements (HFSE) and rare earth elements including yttrium (REE+Y), and an increase for large ion lithophile elements (LILE). This variation is associated with coupled substitutions on the M1, M2 and T sites of the type $^{M1}(Al, Fe^{3+}) + TAl = {}^{M2}(Mg, Fe^{2+}) + {}^{T}Si$. The different incorporation of trace elements into clinopyroxenes of hybrid origin is controlled by cation substitution reactions reflecting local charge-balance requirements. According to the lattice strain theory, simultaneous cation exchanges across the M1, M2, and T sites have profound effects on REE+Y and HFSE partitioning. Conversely, both temperature and melt composition have only a minor effect when the thermal path of magma is restricted to ~70 °C and the value of non-bridging oxygens per tetrahedral cations (NBO/T) shifts moderately from 0.31 to 0.43. As a consequence, Zone 2 partition coefficients for REE+Y and HFSE diverge significantly from those derived for Zone 1, accounting for limited cation incorporation into the newly-formed clinopyroxenes at the quartzite-magma interface (Fig. 1).

Olivine compositional changes in primitive skarn environments: A reassessment of divalent cation partitioning models to quantify the effect of carbonate assimilation

S.F. Di Stefano, S. Mollo, K. Putirka, P. Scarlato, M. Nazzari, O. Bachmann, M. Caruso

The geochemical evolution of olivine from primitive skarn environments has been studied by atmospheric pressure experiments carried out at 1,250, 1,200, and 1,150 °C under QFM oxygen buffering conditions. The starting materials were three synthetic basalts (i.e., $^{melt}Mg\#_{78}$, $^{melt}Mg\#_{75}$, and $^{melt}Mg\#_{72}$) doped with variable amounts of $CaCO_3$, in order to reproduce the natural concentration levels of CaO-rich magmas interacting with the skarn rock shells. Results from decarbonation experiments evidence that the crystallization of Fo-CaO-rich, Ni-poor olivines is more favored at higher temperatures when primitive basaltic magmas assimilate increasing amounts of carbonate materials. The number of large size Ca cations entering olivine crystal lattice is proportional to the amount of Ca-O-Si bonds available in the melt. Due to differences between Fe^{2+} and Mg cation radii, the Ca-Fe^{2+} substitutions into M2 crystallographic site are more facilitated than Ca-Mg ones, thus enhancing the forsterite component in olivine. The partitioning behavior of Ni, Mg, Fe^{2+}, Mn and Ca between olivine and melt has been also investigated to better understand cation redistribution mechanisms at the magma-carbonate reaction zone. In this context, some partitioning models from literature have been refined to more accurately quantify the geochemical evolution of primitive skarn systems. Under the effect of $CaCO_3$ assimilation, the partitioning of divalent cations, can be parameterized as a function of temperature, bulk composition (mostly, CaO and MgO contents in both olivine and melt) and melt structure (expressed as the number of non-bridging oxygens per tetrahedrally coordinated cations). Conversely, the exchange partition coefficients between Fe^{2+}/Ca/Mn/Ni and Mg do not vary significantly as a function of temperature and $^{melt}Mg\#$, due to the limited influence of these parameters on the melt structure. In turn, cation exchange reactions are primarily controlled by the strong depolymerizing effect of $CaCO_3$ assimilation that increases the number of structural sites critically important to accommodating network-modifying cations in the melt phase (Fig. 1).
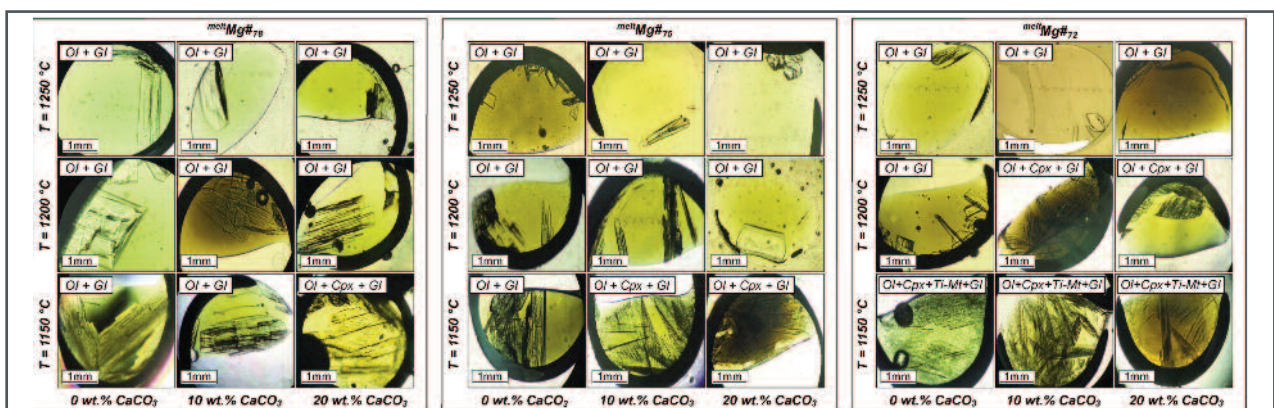

Fig. 1 I Photomicrographs showing the textural evolution of minerals from the experimental charges obtained at 1150, 1200, 1250 °C, using three different basalts (i.e., $^{melt}Mg\#_{78}$, $^{melt}Mg\#_{75}$, and $^{melt}Mg\#_{72}$) doped with 0, 10, and 20 wt.% $CaCO_3$. Ol, olivine. Cpx, clinopyroxene. Ti-Mt, titanomagnetite. Gl, glass.

Crystallization kinetics of clinopyroxene and titanomagnetite growing from a trachybasaltic melt: New insights from isothermal time-series experiments

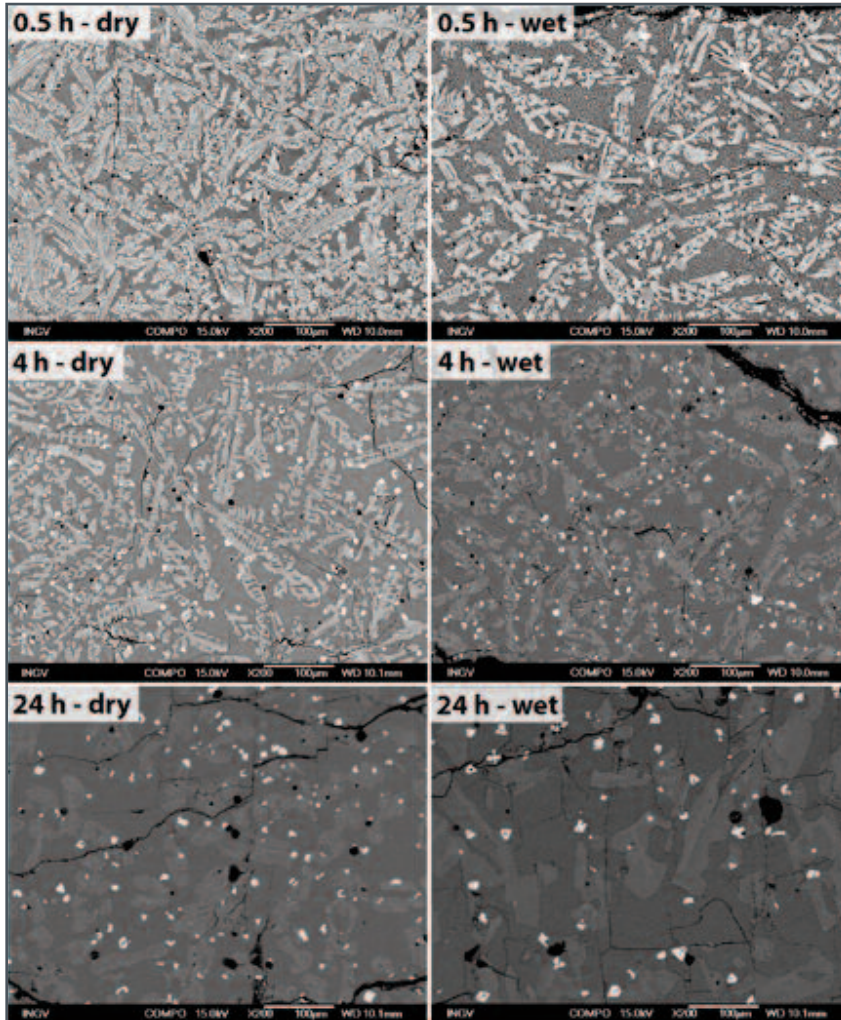*A. Pontesilli, M. Masotta, M. Nazzari, S. Mollo, P. Scarlato, M. Brenna*

Fig. 1 | Backscatter Electron images of experimental products from both anhydrous and hydrous (2wt.% H_2O) time series. Brighter crystals are titanomagnetites, while clinopyroxene is grey to whitish, always brighter than the glass in the background. The panel shows the evolution of crystal textures with experimental time, as evidenced by an increase in euhedrality of clinopyroxene crystals and crystal sizes.

The final textures of igneous rocks, being fundamentally determined by crystallization kinetics, have the potential of giving insights into both physicochemical conditions of former magma bodies and on the dynamics of magmatic processes. Indeed, the experimental study of crystal growth and nucleation represents the most reliable approach to the estimation of the rates characterizing these processes, thus providing a tool for the evaluation of timescales in both volcanic and intrusive systems.

In order to investigate crystal growth kinetics in a synthetic trachybasaltic liquid reproducing one of the most primitive alkaline magma compositions (SiO_2 = 47.6 wt.%, MgO = 6.5 wt.%, Na_2O+K_2O = 5.1 wt.%) ever erupted at Mt.Etna Volcano (belonging to Mt.Maletto formation), we performed isothermal/ isobaric piston cylinder experiments under both hydrous (2 wt.% H_2O) and anhydrous conditions. Reversal experiments has been performed through superheating the sample material from room T to 1300°C at a heating rate of 80°C/min and maintaining the superliquidus temperature for 30 min, then attaining run temperature with a cooling rate of 80°C/min and keeping the sample material at constant experimental conditions of P = 400 MPa, T = 1100°C, f_{O2} = NNO+2 buffer for variable dwell times (0.5, 1, 2, 4, 8, and 24 h). Isobaric quench of 100°C/s have been applied in order to preserve experimental textures.

Electron Microprobe Analyses revealed a mineral assemblage always consisting of clinopyroxene (titanaugite) and titanomagnetite. Scanning Electron Microscope observations enabled to study the evolution of crystalline textures with experimental time, revealing a progressive increase of crystal size with experimental time and a maturation of clinopyroxene textures, whose crystals show a transition from dendritic to close-to-euhedral habits with increasing experimental time (Fig.1). Being also this phenomenon associated with a limited change in crystal area fraction with time (with clinopyroxene always representing by far the more abundant crystalline phase), it points to an important role for crystal aggregation in determining coarsening of crystal populations. Estimated growth kinetics for both phases decline at a steady pace, ranging from 4.98×10^{-8} to 1.84×10^{-6} cm/s (anhydrous conditions) and from 9.87×10^{-8} to 1.80×10^{-6} cm/s (hydrous conditions) for clinopyroxene, and from 1.48×10^{-7} to 6.62×10^{-9} cm/s (anhydrous conditions) and from 2.51×10^{-7} to 1.70×10^{-8} cm/s (hydrous conditions) for titanomagnetite, witnessing approach to near-equilibrium crystallization after the early "burst" of crystal nucleation and growth driven by the large degrees of initial undercooling (around 100°C). Results from this study give insights into the fast crystallization kinetics of primitive alkaline magmas experiencing large degrees of undercooling, and add new experimental data of interest with respect to the evolution of crystallization processes during solidification of magmas (Fig. 1).

Crystallization and partial melting of rhyolite and felsite rocks at Krafla volcano: A comparative approach based on mineral and glass chemistry of natural and experimental products
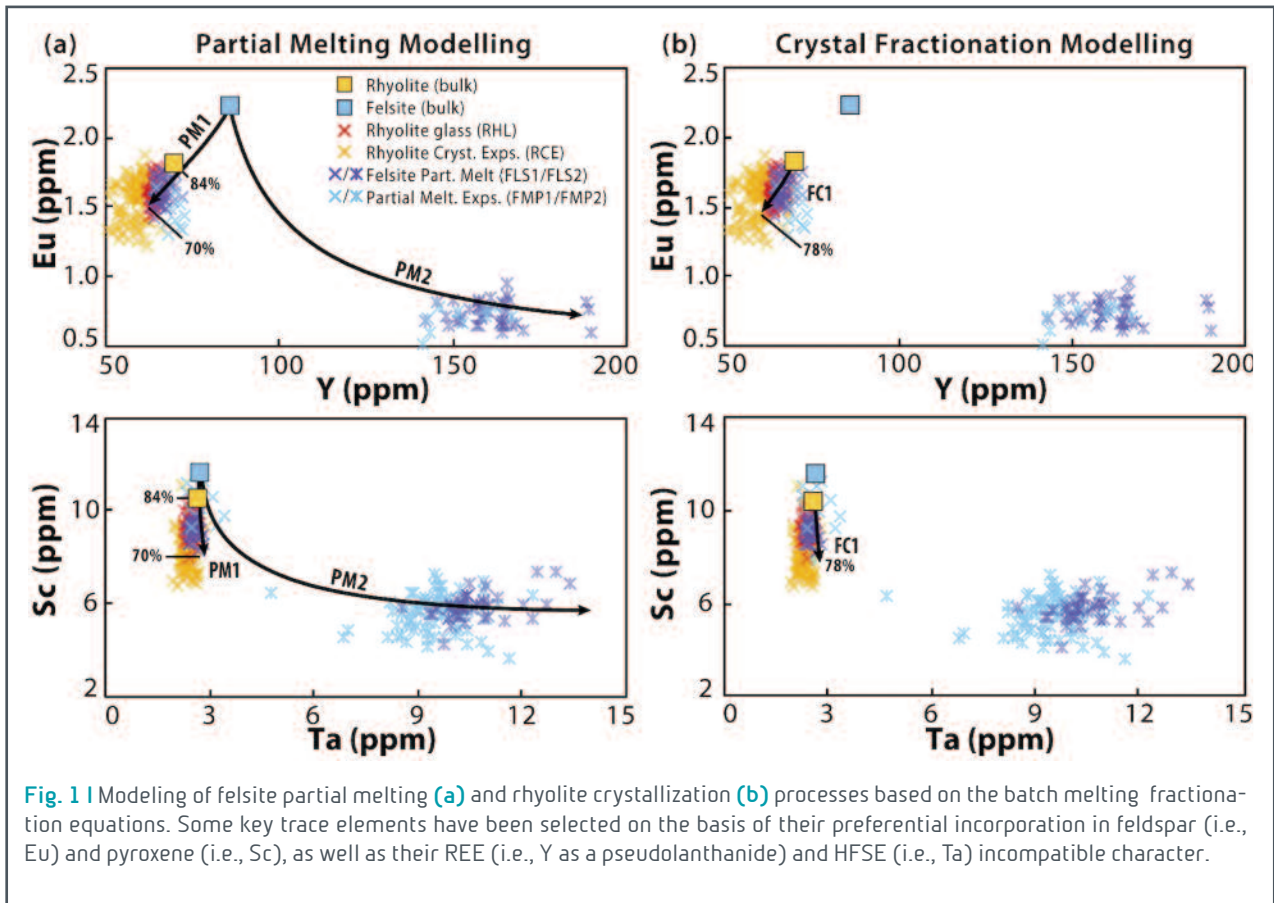
M. Masotta, S. Mollo, M. Nazzari, V. Tecchiato, P. Scarlato, P. Papale, O. Bachmann

Rhyolite and felsite cuttings were collected at Krafla volcano during the perforation of the Iceland Deep Drilling Project Well 1 (IDDP-1). The perforation was stopped at a depth of 2,100 m due to intersection with a rhyolite magma that intruded the felsite host rock.

Rhyolite cuttings are vitrophiric (glass ~95%, RHL) and exhibit a mineral assemblage made of plagioclase + augite + pigeonite + titanomagnetite. Felsite cuttings display evidences of partial melting, responding to variable degrees of quartz + plagioclase + alkali feldspar + augite + titanomagnetite dissolution. The interstitial glass analyzed close to (i.e., FLS1) and far from (i.e., FLS2) the reaction surface of pyroxene from felsite cuttings shows continuous changes between the two end-members. FLS1 is compositionally similar to RHL, showing Na_2O + K_2O + REE depletions, counterbalanced by MgO + CaO enrichments. Conversely, FLS2 exhibits opposite chemical features. REE-exchange thermobarometric calculations reveal that plagioclase and augite cores from rhyolite and felsite formed under identical conditions, along a thermal path of 940-960 °C. However, in terms of major and trace element concentrations, plagioclase and augite crystal cores are not in equilibrium with the rhyolite magma, suggesting the incorporation of these minerals directly from the host felsite. To better understand the petrogenetic relationship between rhyolite and felsite, two sets of crystallization and partial melting experiments have been carried out at P = 150 MPa and T = 700-950 °C. Rhyolite crystallization experiments (RCE) reproduce the two-pyroxene assemblage of IDDP-1 rhyolite cuttings only at T <800 °C, when the crystal content (>19%) is higher than that observed in the natural rhyolite (~5%). Under such conditions, the RCE glass is much more differentiated (i.e., marked CaO depletion and Eu anomaly) than RHL. On the other hand, felsite partial melting (FPM) experiments show interstitial glass with a bimodal composition (i.e., FPM1 and FPM2) comparable to FLS1 (=RHL) and to FLS2, only at T = 950 °C. This effect has been quantified by fractional crystallization and batch melting modeling, denoting that FLS1 (=RHL) and FLS2 reflect high (>70%) and low (<8%) degrees of felsite partial melting, respectively. In contrast, modeling RHL by crystal fractionation requires the removal of an amount (~22%) of solid material that is inconsistent with the low crystal content of the natural IDDP-1 rhyolite. It is therefore concluded that natural rhyolite and felsite represent, respectively, the near-liquidus and sub-solidus states of a virtually identical silicic magma, either feeding aphyric to subaphiric rhyolitic eruptions, or solidifying at depth as phaneritic quartzofeldspathic rocks. Felsite lenses from the Krafla substrate may explore variable degrees of remelting and remobilization processes. The intrusion into fel-

site of a fresh silicic magma from depth may lead to low degrees of partial melting, whereas the persistent heat release from intense basaltic intrusive events at Krafla may be the source of high degrees of felsite partial melting and consequent rejuvenation of the previously solidified silicic magma.

Fig. 1 I Modeling of felsite partial melting (a) and rhyolite crystallization (b) processes based on the batch melting fractionation equations. Some key trace elements have been selected on the basis of their preferential incorporation in feldspar (i.e., Eu) and pyroxene (i.e., Sc), as well as their REE (i.e., Y as a pseudolanthanide) and HFSE (i.e., Ta) incompatible character.

Trace element decoupling in clinopyroxene reflects magma recharge and kinetic effects

T. Ubide, S. Mollo, J. Blundy, J.X. Zhao, M. Nazzari, P. Scarlato

Early mineral phases hold key information on the architecture of magma plumbing systems. Clinopyroxene can provide information on the mechanisms, depths and timescales of magmatic processes, including mafic recharge events which are considered efficient triggers of volcanic eruptions. However, volcanic clinopyroxene commonly shows sector zoning, which complicates the study and interpretation of compositional records and thermobarometric estimates. Here we tackle fundamental understanding of sector zoning by investigating clinopyroxene crystals in basaltic products of recent eruptions at Mt. Etna volcano (Sicily, Italy). We investigate titanoaugite crystals from primitive, undegassed, so-called 'eccentric' or 'deep-dyke-fed' eruptions in 1974 (southwest flank eruption) and 2002-03 (south flank eruption). We apply a combination of in-situ quantitative methods for the visualisation and modelling of major and trace element zoning at the m-scale, including spot analyses and mapping by electron microprobe and laser ablation mass spectrometry (LA-ICP-MS). Major element maps illustrate sharp sector zoning in titanoaugite crystallising along or perpendicular to the c crystallographic axis (Fig. 1). Sector {-111} is systematically enriched in Si and Mg and depleted in Al, Ti and to a lesser extent Fe, relative to sectors {100}, {110} and {010} growing perpendicular to the c axis and similar in composition. This behaviour is explained by substitution of Si^{4+} for Al^{3+} in the tetrahedral site, which requires the incorporation of Ti^{4+} and Fe^{3+} in the M1 octahedral site for charge balance. Ca and Na do not show compositional variations with sector zoning. At the trace element level, there is a sharp decoupling between sector zoned and oscillatory zoned elements in single crystals (Fig. 1). Trivalent cations of Rare Earth Elements (REE) and tetravalent and pentavalent cations of High field strength elements (HFSE) show sector zoning that correlates with aluminium. Si^{4+}-Al^{3+} substitution promotes preferential incorporation of REE+Y^{3+} in the M2 site, and incorporation of $HFSE^{4+}$ and $HFSE^{5+}$ in the M1 site. This translates into enrichments in REE and HFSE in Al-rich sectors (perpendicular to the c axis). Strikingly, however, we find that incorporation of divalent and trivalent cations into M1 is independent of Al. Rather than reflecting sector zoning, the distribution of Cr^{3+}, Sc^{3+} and Ni^{2+} defines oscillatory zoning, where zones of enrichment correlate with slight increases in Mg and show textural signs of resorption, suggesting the arrival of a hotter, more primitive magma into the crystallising clinopyroxene mush.

Importantly, it follows that cation incorporation into the M1 site is a function of cation charge: low charge, compatible transition metals reflect fractional crystallisation and recharge whereas high charge, incompatible HFSE (as well as M2 REE-Y^{3+} cations) are strictly controlled by tetrahedral Al, responding to kinetic effects such as the development of sector zoning under conditions of relatively high undercooling. To our knowledge, this is the first report of cation decoupling in sector zoned crystals and provides new insights into trace element incorporation
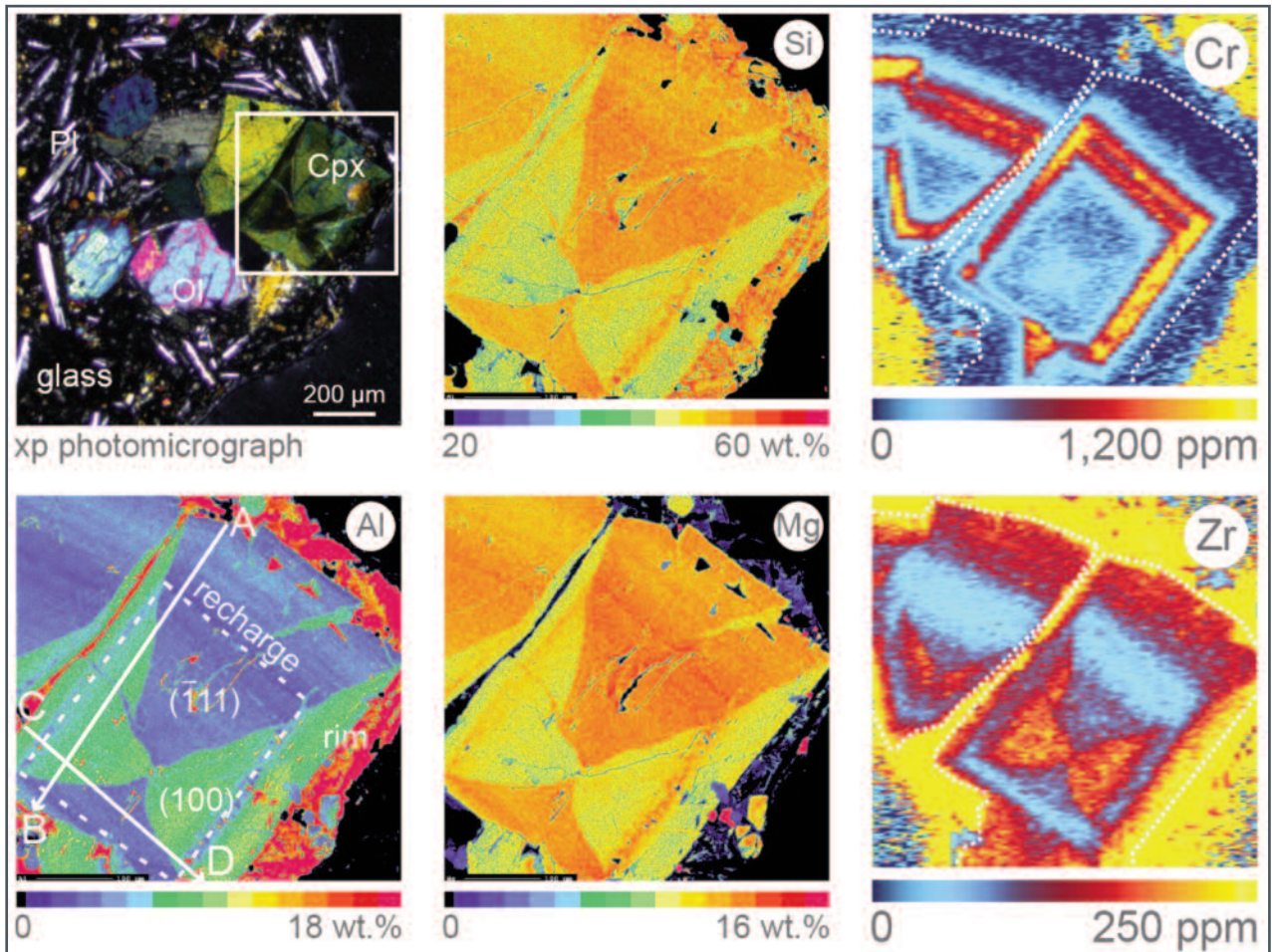
Fig. 1 | Major and trace element maps of titanoaugite microphenocrysts from Mt Etna volcano, obtained by electron microprobe and LA-ICPMS, show elemental decoupling as a function of cation site and charge. The hourglass form {-111}, growing along the c crystallographic axis, is enriched in Si-Mg and depleted in Al, high charge M1 cations (e.g., Zr) and M2 cations relative to form {100}, growing perpendicular to the c axis. The dashed white line marks a mafic recharge zone, relatively enriched in Mg and transition metals (low charge M1 cations, which do not show sector zoning; e.g., Cr; the dotted line represents the outline of the crystal). The photomicrograph (transmitted light, crossed polars) provides context: the crystals belong to a glomerocryst composed of titanoaugite and olivine, embedded in a hypocrystalline groundmass with microlites of plagioclase, microcrysts of clinopyroxene, olivine and titanomagnetite, and glass.

mechanisms and their response to kinetic effects vs. open system processes such as magma recharge and mixing.

Our study shows that while the incorporation of major and many trace cations into the clinopyroxene structure are controlled by Si-Al substitution and strongly skewed in cases of sector zoning, transition metals and particularly Cr are faithful recorders of mafic replenishment and magma mixing at depth (Fig. 1).

2D and 3D textural and geochemical investigation to explore the trigger mechanisms of Plinian eruptions: a Somma-Vesuvius volcano case study

L. Pappalardo, G. Buono, P. Petrosino

In this case study we explored the internal microstructure of pyroclasts erupted during the first and most intense Plinian eruption of Somma-Vesuvius (Pomici di Base eruption, 22 ka) by generating high-resolution three-dimensional digital maps via X-ray microtomography. A peculiar aspect of this eruption, that marks the passage to the explosive character of the volcano as well as the beginning of the caldera collapse, is its high intensity that remained stable during all the course of the Plinian fallout phase despite the strong magma compositional variation towards mafic terms; thus requiring that complex mechanisms may have acted at sub-volcanic level and magnified the eruption intensity.

Our 2D and 3D quantitative textural data combined with Sr and Nd isotopic investigations, demonstrated that during the eruption the transfer of magma towards the surface was related to the occurrence of rapid vesiculation pulses driven by limestone assimilation (skarn recycling) during magma ascent through the carbonatic bedrock. Limestone assimilation can hence be a syn-eruptive process, able to trigger further gas nucleation with deep impact on the eruption intensity, particularly crucial in the case of mafic-intermediate magma compositions (Fig. 1).
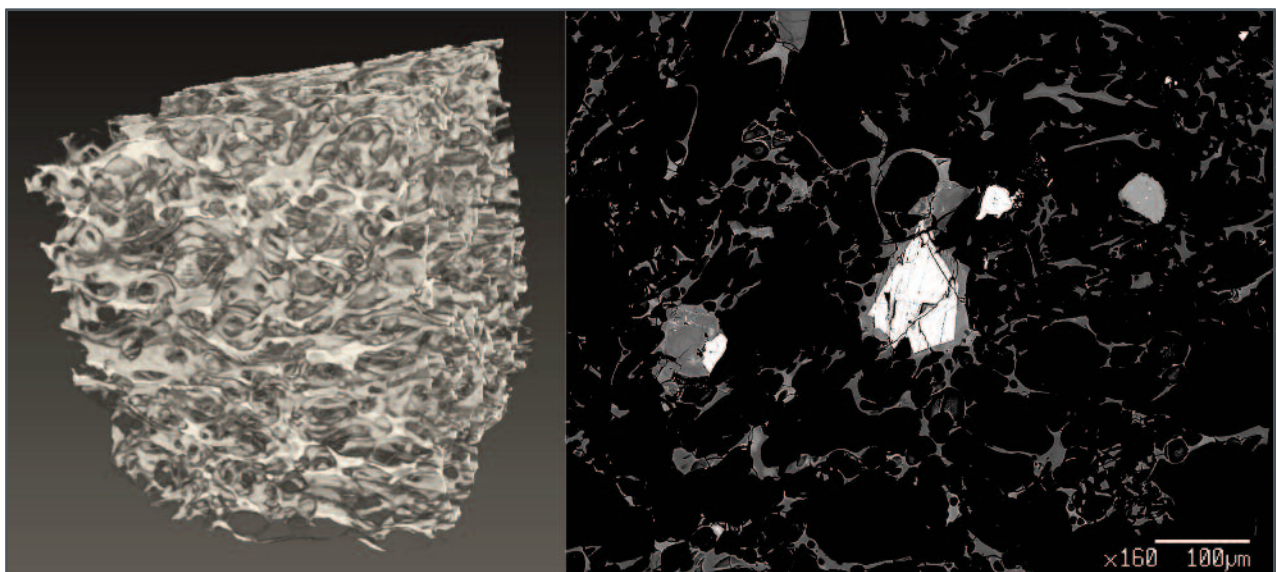

Fig. 1 | Example of volume rendering and SEM image showing 3D and 2D microstructure of Pomici di Base trachytic rocks. Cube side: 500 pixels (pixel size=1 micron).

Experimental constraints on limestone-ultrabasic/basic melt interaction at 2 kbar: implications for the origin of the pseudo-carbonatites

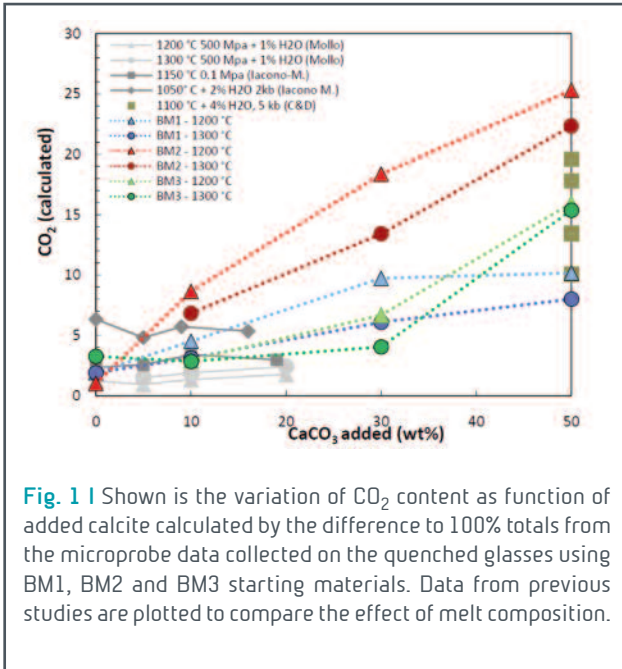*S. Narzisi, V. Stagno, N. Luciani, M. Lustrino, M. Nazzari, P. Scarlato*

Fig. 1 | Shown is the variation of CO_2 content as function of added calcite calculated by the difference to 100% totals from the microprobe data collected on the quenched glasses using BM1, BM2 and BM3 starting materials. Data from previous studies are plotted to compare the effect of melt composition.

Carbonatites are very rare igneous rocks generated by low-degree of partial melting of carbonated mantle rocks or by immiscibility processes of a CO_2-bearing silicatic magma after prolonged fractional crystallization processes. The worldwide distribution of carbonatites is generally associated with that of Archean cratons, but rare lithologies of this type have found in several Cenozoic volcanic districts around the Mediterranean area in central-southern Italy, Central Spain, Morocco, France and Germany.

An alternative hypothesis considers that at least some of the rocks classified in literature as carbonatites could be the result of a shallow depth process, involving digestion of sedimentary carbonates (limestones and dolostones) by silicatic magma. Several experimental studies focused on basaltic compositions (i.e., plagioclase-bearing melts) to reproduce assimilation paths as function of pressure, temperature and fractional crystallization steps. To date no experiments have been performed to investigate the products of limestone assimilation by strongly SiO_2-undersaturated melts. On this ground we performed experiments at 2 kbar and 1100, 1200 and 1300 °C using the Quickpress apparatus available at the HPHT lab of the INGV (Rome). The starting materials employed in this study were three glasses obtained by melting at 1450 °C three natural samples with increasing SiO_2 content such as vesecite (~30.3 wt% SiO_2; BM2), melilite-olivine-nephelinite (~38.5 wt% SiO_2; BM1), and basanite (~43 wt% SiO_2; BM3). Each starting glass was then mixed with 10, 30 and 50 wt% synthetic pure calcite ($CaCO_3$).

The recovered run products showed vesicles that testify CO_2 saturation during the experiments. The results from runs at 1300 °C surprisingly show the complete dissolution of the added calcite with consequent formation of a Ca-rich/Si-poor melt coexisting with high-forsterite Ca-rich olivine (up to Fo_{97}). The CO_2 content of these melts (calculated by difference to 100% totals) is observed to increase with the amount of added calcite, and ranges from ~3 wt% (10 wt% calcite added) to ~25 wt% (50 wt% calcite added) in case of BM2 composition (Fig. 1). Interestingly, these experimentsalso show the presence of monticellite formed as rim around olivine crystals
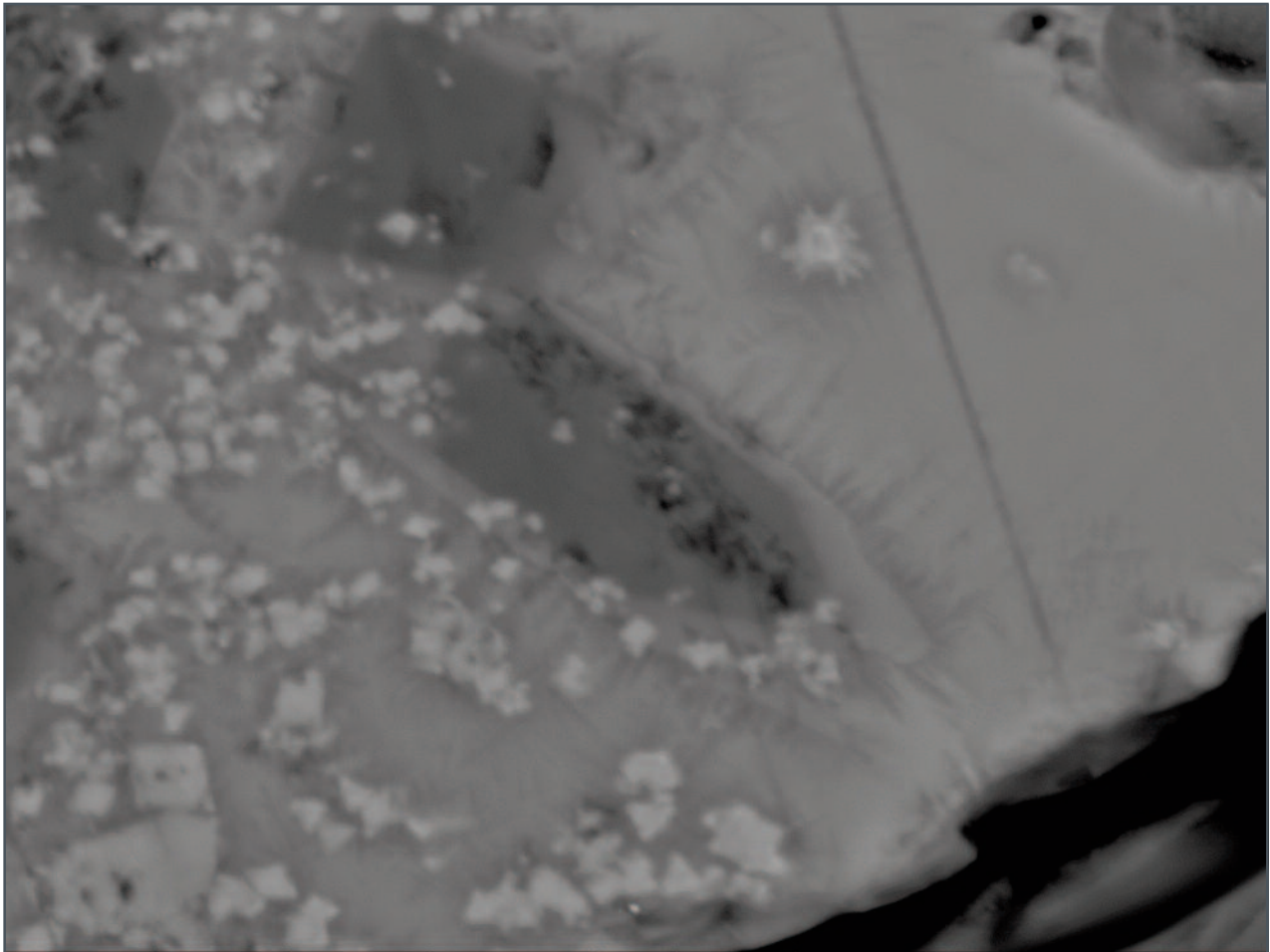
Fig. 2 | BSE images relative to a run at 2 kbar and 1300 °C with 30% of $CaCO_3$ mixed with the starting glass (BM2) where it is possible to distinguish the glass (grey) coexisting olivine crystal (dark) rimmed by monticellite (light grey).
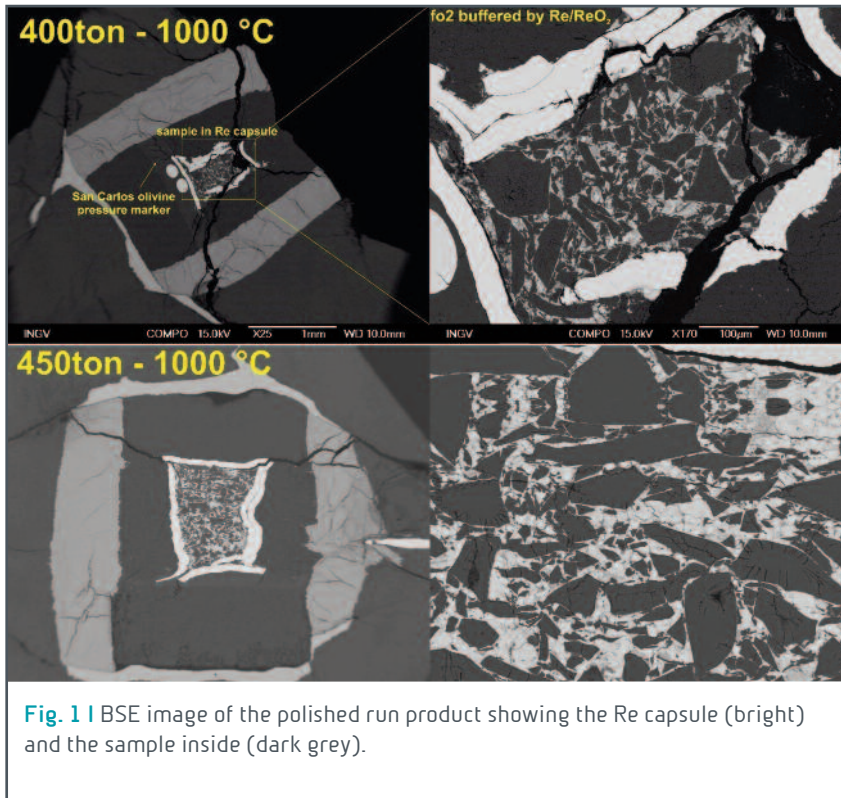
(Fig. 2) similarly to what reported in natural cases (e.g., Polino, central Italy).

Our experimental results extend the knowledge on the effect of magma composition on limestone assimilation in case of strongly silica-undersaturated melt compositions, and provide an alternative explanation to the origin of CO_2-rich magmas at shallow depths, known as pseudo-carbonatites.
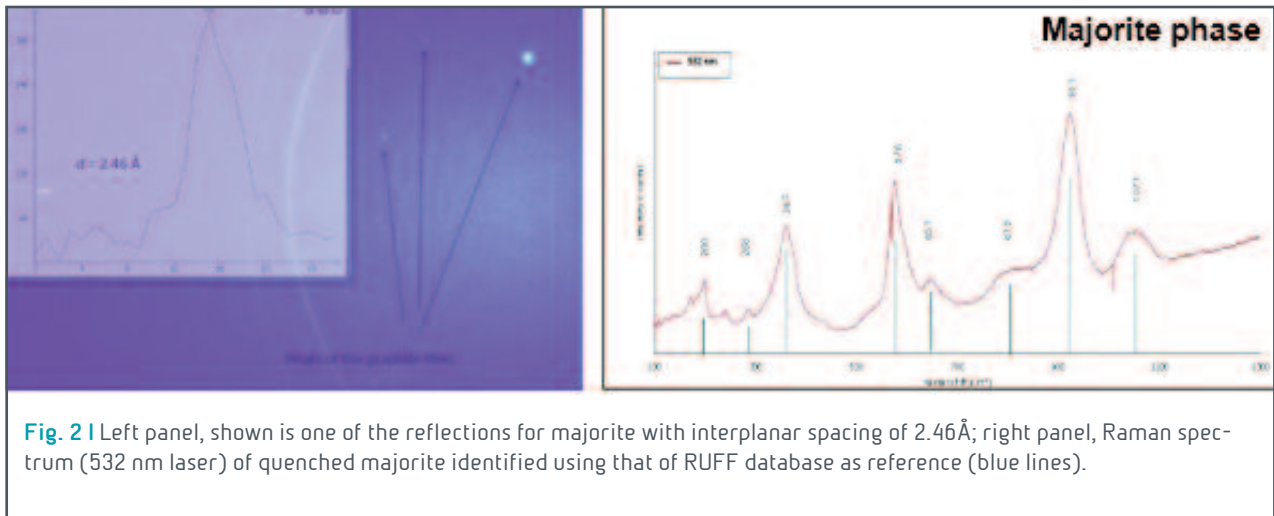
Synthesis of Na-, Si-rich majorite from omphacitic glass at conditions of the deep Earth's mantle

V. Stagno, B. Bonechi, L. Bindi, S. Greaux, B.T. Poe, C. Romano, M. Nazzari, P. Scarlato

Fig. 1 I BSE image of the polished run product showing the Re capsule (bright) and the sample inside (dark grey).

The transport of chemical elements down to the Earth's interior links to the stability of minerals during subduction that, in turn, can affect the rheology of the slab (i.e. stagnation vs. sinking). Among the several mineral phase transformations occurring during subduction, the breakdown of eclogitic clinopyroxene (i.e. omphacite) to majoritic garnet is of particular interest because of its use as geobarometer of sublithospheric diamonds, and the associated increase in the slab density at about 200-450 km depth. At cold slab temperatures, the cpx-majorite transformation is kinetically inhibited, and hence, cpx can occur as a metastable phase, thus contributing to the deceleration and potential stagnation of the slab in the transition zone. Experimental studies on the stability of omphacitic cpx as function of pressure are few in literature and show contrasting results as either decomposition to an assemblage of majorite + Ca-perovskite + stishovite, or formation of an unknown post-clinopyroxene phase. To address the stability of omphacitic cpx during subduction of the oceanic crust, we performed high pressure and temperature experiments using the multi anvil press technique.

The starting material used in this study is a synthetic omphacitic glass with composition as reported for natural Bavarian (Weissenstein) eclogite mixed with 25% Re and ReO_2 to act as redox buffer. Two experiments were performed at pressures of~18, and~25 GPa at 1000 °C using the 840-ton Walker-type press available at the High Pressure High Temperature laboratory of the National Institute of Geophysics and Volcanology (INGV, Italy). Textural observations and chemical compositions of the run products were performed using a Jeol JSM-6500F scanning electron microscope at the Microanalysis Lab of National Institute of Geophysics and Volcanology (INGV, Rome). The crystallinity of the recovered products was first checked by Raman spectroscopy using the Spectrometer Horiba Jobin Yvon LABRAM HR800 at Experimental Volcanology and Petrology Laboratory (EVP Lab) at University of Roma Tre.

Fig. 2 | Left panel, shown is one of the reflections for majorite with interplanar spacing of 2.46Å; right panel, Raman spectrum (532 nm laser) of quenched majorite identified using that of RUFF database as reference (blue lines).

Successive X-ray diffraction(XRD) investigations were performed with an Oxford Diffraction Xcalibur3 CCD single-crystal diffractometer available at the CRIST (Centro di Studi per la Cristallografia Strutturale, Università of Florence)using a small fragment (size about $17 \times 22 \times 34\ \mu m^3$) extracted from the polished samples.

The recovered products were found to retain the same chemical composition of the initial cpx glass with ~5.8 wt% Na_2O content and 55 wt% SiO_2 corresponding to ~20% Na-majorite ($Na_2MgSi_5O_{12}$) and ~58% majorite ($Mg_4Si_4O_{12}$) end-members. The results from single-crystal and powder XRD revealed reflections belonging to the cubic garnet structure only with cell parameter a ~10.5 Å.

According to the pyrolite model, the portion of garnet within the depth range from 410 to 660 km may exceed 50 vol %. Calculations show that at a bulk concentration of ~0.4 wt% Na_2O, Na content in garnet resulting from incorporation of the $Na_2MgSi_5O_{12}$ end-member would not exceed 0.8-0.9 wt % Na_2O. If we accept the heterogeneous or layered structure of the mantle, according to which eclogite transforms to garnetite at pressures above 15-18 GPa and predominates in the transition zone, garnet of these rocks would contain from ~1 to ~5 wt % Na_2O depending on the bulk eclogite (garnetite) composition. As it is evident from previous experiments on the diopside-hedenbergite-jadeite join at 12-24 GPa and studies of MORB-eclogite, $Na_2MgSi_5O_{12}$ solubility is quite significant and exceeds 30 mol % in pyrope-grossular garnet with increasing pressure. Although the limits of Na solubility in garnets and the character of solid solutions in the pyrope-$Na_2MgSi_5O_{12}$ join require additional study, the ability of the garnet phase to accumulate significant concentrations of Na under the conditions of the lower parts of the upper mantle and transition zone has been confirmed by the present study. Furthermore, our results show the formation of a Na, Si-rich majorite phase crystallized directly from an omphacitic glass at conditions of the Earth's lower mantle thus extending the pressure-dependent exchange reaction $Na^X + Si^Y = Mg^X + Al^Y$. The produced Na,Si-rich phase may represent the product of the isochemical phase transformation of clinopyroxenites during subduction of cold slabs down to Earth's lower mantle causing, therefore, the sinking of the slab itself.

Development of the Voggenreiter 840t multi anvil press to generate pressures and temperatures of the Earth's transition zone and lower mantle

V. Stagno, B. Bonechi, S. Greaux, M. Caruso, B.T. Poe, C. Romano, M. Nazzari, P. Scarlato
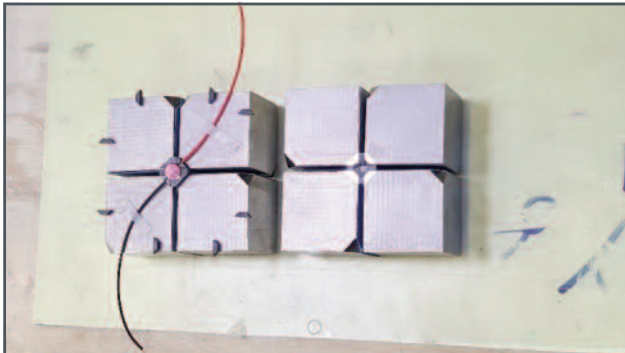
Fig. 1 I Shown is the set of WC anvils with a Co-doped octahedron used for synthesis of ringwoodite. The thermocouple wires (C-type) are used to monitor the temperature during the experiments.

Our knowledge of the mineralogy and chemical composition of the interior of Earth relies on the analyses of mantle rocks (i.e. xenoliths) or inclusions in deep diamonds, other than interpretative models of seismic wave propagation through the solid Earth. The use of high pressure facilities such as the multianvil press has been widely used over the last decades in the field of experimental petrology and mineral physics to investigate the behavior of Earth materials in the lower crust, throughout the upper mantle and in the shallower parts of the lower mantle, including the rheology of mantle phases, transformation mechanisms, reaction kinetics, diffusion, electrical conductivity, and sound velocity at high pressure. The HP-HT Lab at National Institute of Geophysics and Volcanology (INGV, Rome) is equipped with the Voggenreiter 840t multi anvil press that employs a Walker-type module. This press was installed in 2004, and it can operate in both multi anvil and piston cylinder mode simply by switching a valve controlling the circulation of oil in the hydraulic system.

We performed several experiments at the aim to test new cell assemblies that allow to extend the range of pressures and temperatures from the upper mantle (3-11 GPa) to the shallower part of the lower mantle (22-26 GPa). A range of pressures between 3 and 25 GPa was reached using different Cr(or Co)-doped MgO octahedra with edge length (OEL) of 25, 18, 14 and 7 mm, in combination with eight second-stage tungsten carbide anvils (F grade) cut with truncation of 17, 11, 8 and 3mm in length (TEL). A technique was developed to prepare home-made pyrophyllite gaskets acting as pressure media (Figure 1). Cylindrical $LaCrO_3$ and graphite tubes
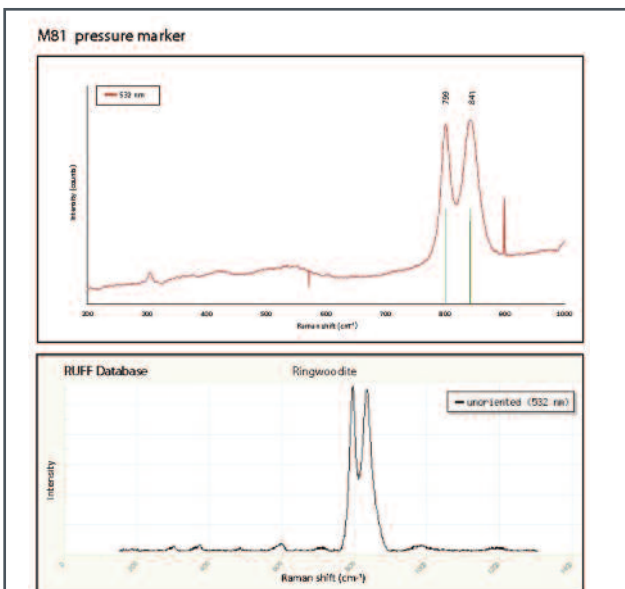
Fig. 2 I Raman spectrum collected from the recovered run product quenched at about 8 GPa and 1000 °C. The sample was identified to be ringwoodite after a comparison with a typical spectrum taken from RUFF database.

were used as heaters, while the powdered sample (either natural rocks or oxide mixture) was loaded in capsules of different materials such as Re, Mo and graphite.

As example, figure 2 shows the Raman spectrum of a ringwoodite synthesized from natural olivine (San Carlos - Arizona, USA) used as a starting material and pressurized applying a ram load of 450 ton, then heated and kept at a constant temperature of 1000 °C for ~30 minutes.

To date, preliminary tests have showed 1) the synthesis of ringwoodite at a pressure of 18 GPa; 2) the observation of the decomposition of ringwoodite to bridgmanite + periclase at a pressure of about 21 GPa.

An important aspect of this implementation is the possibility to investigate polymorphic transformations and mineral decomposition as origin of deep earthquakes.

Snapshots of primitive arc magma evolution recorded by clinopyroxene textural and compositional variations: The case of hybrid crystal-rich enclaves from Capo Marargiu Volcanic District (Sardinia, Italy)

V. Tecchiato, M. Gaeta, S. Mollo, O. Bachmann, A. von Quadt, P. Scarlato

Fig. 1 | Clinopyroxene major element compositions. The Al_{tot} vs. Mg-number and Ti diagrams show that Type 1 and Type 2 evolve along the same path controlled by olivine + clinopyroxene + amphibole fractionation, whereas Type 3 appears as an isolated group of data recording the effect of plagioclase fractionation.

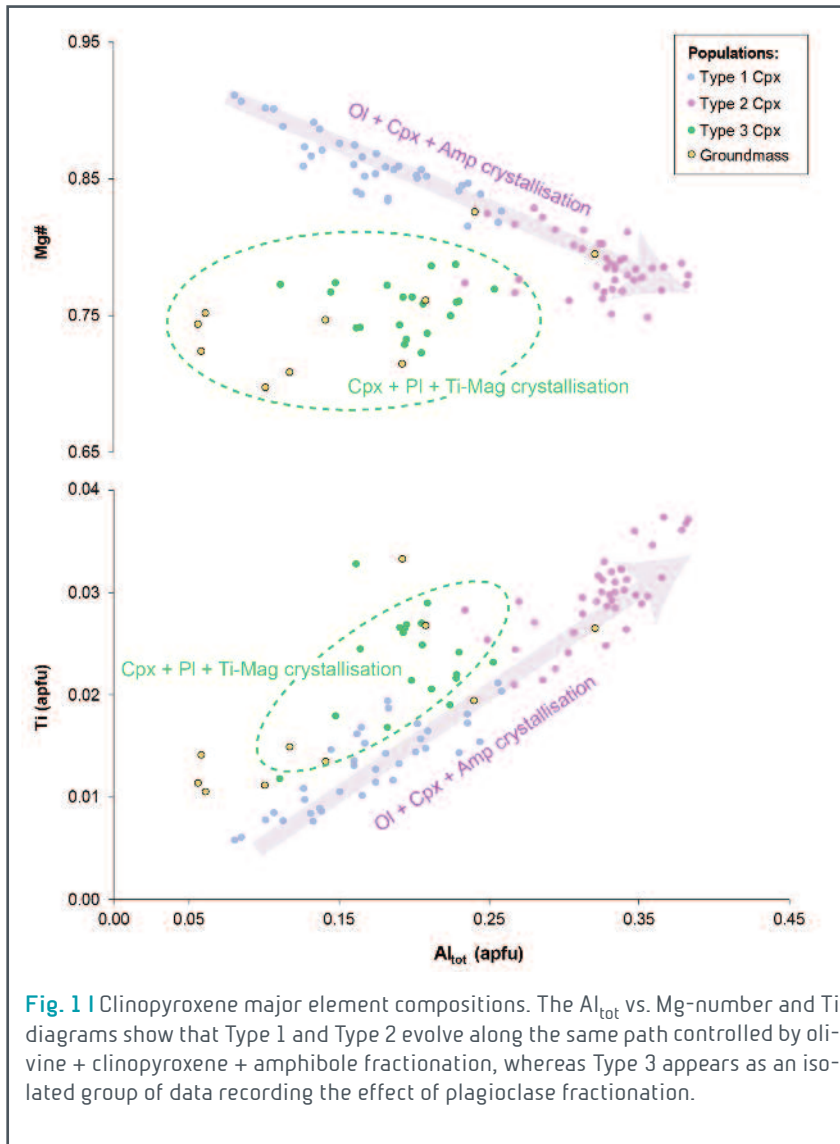Capo Marargiu Volcanic District (CMVD) is an Oligo-Miocene calc-alkaline complex located in north-western Sardinia (Italy) and characterized by the widespread occurrence of basaltic to andesitic domes. One of these domes hosts abundant crystal-rich enclaves with millimeter-to-centimeter-sized clinopyroxenes showing intriguing textural features due to complex magma dynamics. With the aim to better understand the mechanisms governing the early evolution of the CMVD magmatic system, such clinopyroxene phenocrysts have been investigated in terms of their major, trace element and isotopic compositions. Three distinct clinopyroxene populations have been identified, i.e.,

Type 1, Type 2, and Type 3. Type 1 appears as the sub-rounded cores of clinopyroxenes with overgrowth textures corresponding to Type 2 and Type 3. These latter populations may also occur as single isolated crystals. Type 2 exhibits oscillatory zoning and spongy cellular textures with Type 3 overgrowths, whereas Type 3 are polycrystalline glomerocrysts with occasional Type 2 overgrowths. The crystal overgrowths are striking evidence of magma recharge dynamics. Type 1 (cpxMg#83-92), Type 2 (cpxMg#75-82) and Type 3 (cpxMg#72-79) are, respectively, in equilibrium with Sardinian mantle-derived high-Mg basalts (HMB with meltMg#56-73), primitive basaltic andesites (PBA with mmeltMg#45-56) and evolved basaltic andesites (EBA with meltMg#41-50). Type 1 and Type 2 are diop-

sidic phenocrysts evolving along a similar geochemical path (i.e., linear increase of Al, Ti, La, and Hf contents, as well as negligible Eu-anomaly) controlled by olivine + clinopyroxene + amphibole fractionation (Fig. 1). This differentiation path is addressed to phenocryst crystallization from hydrous HMB and PBA magmas stalling at moderate crustal pressures. The occurrence of globular sulfides within Type 1 suggests saturation of the HMB magma with a sulfide liquid under relatively low redox conditions. Moreover, Type 1 isotopic systematics denote variable $^{87}Sr/^{86}Sr$ ratios ascribable either to assimilation of crustal material by HMB magma or a mantle source variably contaminated by crustal components. In contrast, Type 3 are augitic phenocrysts recording the effect of plagioclase and titanomagnetite fractionation (i.e., low Al and Ti contents associated with high La and Hf concentrations, as well as important Eu-anomaly; Fig. 1) from more degassed EBA magmas ponding at shallow depths. Rare titanite associated to Type 3 and titanomagnetite crystals point to high oxidizing conditions for EBA magmas. The $^{87}Sr/^{86}Sr$ ratios of both Type 2 and Type 3 are almost constant, accounting for a limited interaction of PBA and EBA magmas with the country rock. The overall textural and compositional features of Type 1, Type 2 and Type 3 clinopyroxene phenocrysts lead to the conclusion that CMVD is characterized by a polybaric plumbing system where geochemically distinct magmas crystallize and mix under variable environmental conditions (Fig. 1).

Initial development of transient volcanic plume as a function of source conditions

P.Y. Tournigand

Transient volcanic plumes, having similar eruption duration and rise timescales, characterize many unsteady Strombolian to Vulcanian eruptions. Despite being more common, such plumes are less studied than their steady state counterpart from stronger eruptions. Here we investigate the initial dynamics of transient volcanic plumes using high-speed (visible light and thermal) and high-resolution (visible light) videos from Strombolian to Vulcanian eruptions of Stromboli (Italy), Fuego (Guatemala), and Sakurajima (Japan) volcanoes. Physical parameterization of the plumes has been performed by defining their front velocity, velocity field, volume, and apparent surface temperature. We also characterized the ejection of the gas-pyroclast mixture at the vent, in terms of number, location, duration, and frequency of individual ejection pulses and of time-resolved mass eruption rate of the ejecta's ash fraction. Front velocity evolves along two distinct trends related to the initial gas-thrust phase and later buoyant phase. Plumes' velocity field, obtained via optical flow analysis, highlights different features, including initial jets and the formation and/or merging of ring vortexes at different scales. Plume volume increases over time following a power law trend common to all volcanoes and affected by discharge history at the vent. Time-resolved ash eruption rates range between 102 and 107 kg/s and may vary up to 2 orders of magnitude within the first seconds of eruption. Our results help detailing how the number, location, angle, duration, velocity, and time interval between ejection pulses at the vents crucially control the initial (first tens of second), and possibly later, evolution of transient volcanic plumes (Fig. 1).
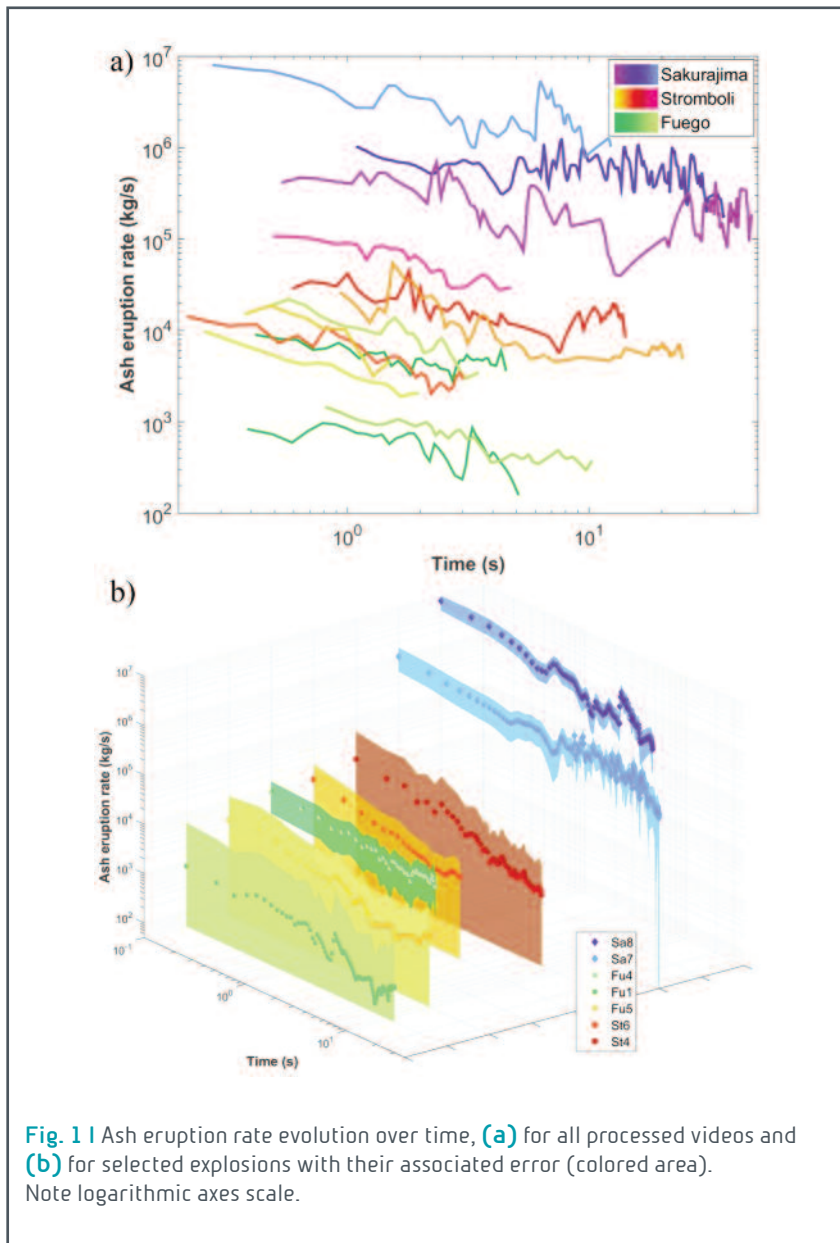
Fig. 1 I Ash eruption rate evolution over time, **(a)** for all processed videos and **(b)** for selected explosions with their associated error (colored area). Note logarithmic axes scale.

Fractal analysis: A new tool in transient volcanic ash plume characterization

P.Y. Tournigand

Fig. 1 I Average Ash Eruption Rate (AER) in function of the fractal increase rate power law coefficient (α_D). Color groups are referring to the source instability factor (β). Dashed line correspond to the power-law fit of the data (AER=0.009$\alpha_D^{-6.602}$, R^2 = 0.48).
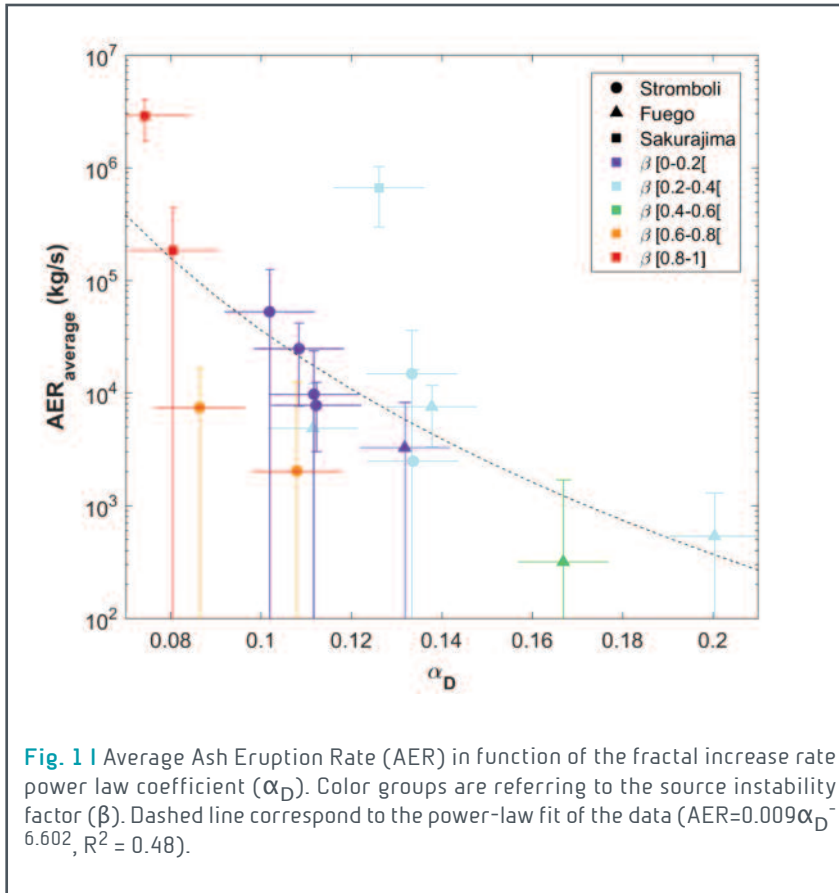
Transient volcanic plumes are time-dependent features generated by unsteady eruptive sources. Their morphological evolution reflects both the discharge history at the vent and air entrainment, crucial parameters controlling volcanic ash dispersal and impact on the environment and human activities. However, transient plume morphology has been so far scarcely quantified, due to both observational and analytical hindrances. In this study, we quantify the initial morphological evolution of transient volcanic plumes by applying fractal analysis to thermal high-speed and visible-light high-resolution videos of eruptions. Eruptive plumes from Sakurajima (Japan), Stromboli (Italy), and Fuego (Guatemala) volcanoes were recorded during several field campaigns in 2012 - 2016. The eruption dataset has been complemented by the fractal analysis of three numerical gas-jet simulations at different Reynolds number (2×10^3, 5×10^3 and 10×10^3) in order to provide reference cases to compare with the natural ones. The two shape analysis methods used show different sensitivities. The perimeter ratio method appears to be more perceptive of punctual dynamical variations, while fractal analysis reflects the overall plume evolution. Both methods highlight the plume shape complexity increase over time related to the formation and development of smaller scale vortexes. Fractal increase rates (α_D) variability can thus be used to reveal different plume's air entrainment abilities. It also appears that the plume fractal evolution over time (α_D) correlates with the ash eruption rate (AER) and source instability factor (β) (see Figure 1). This study shows that discharge history and intensity at the vent are the first order control on plume's shape evolution and air entrainment ability.
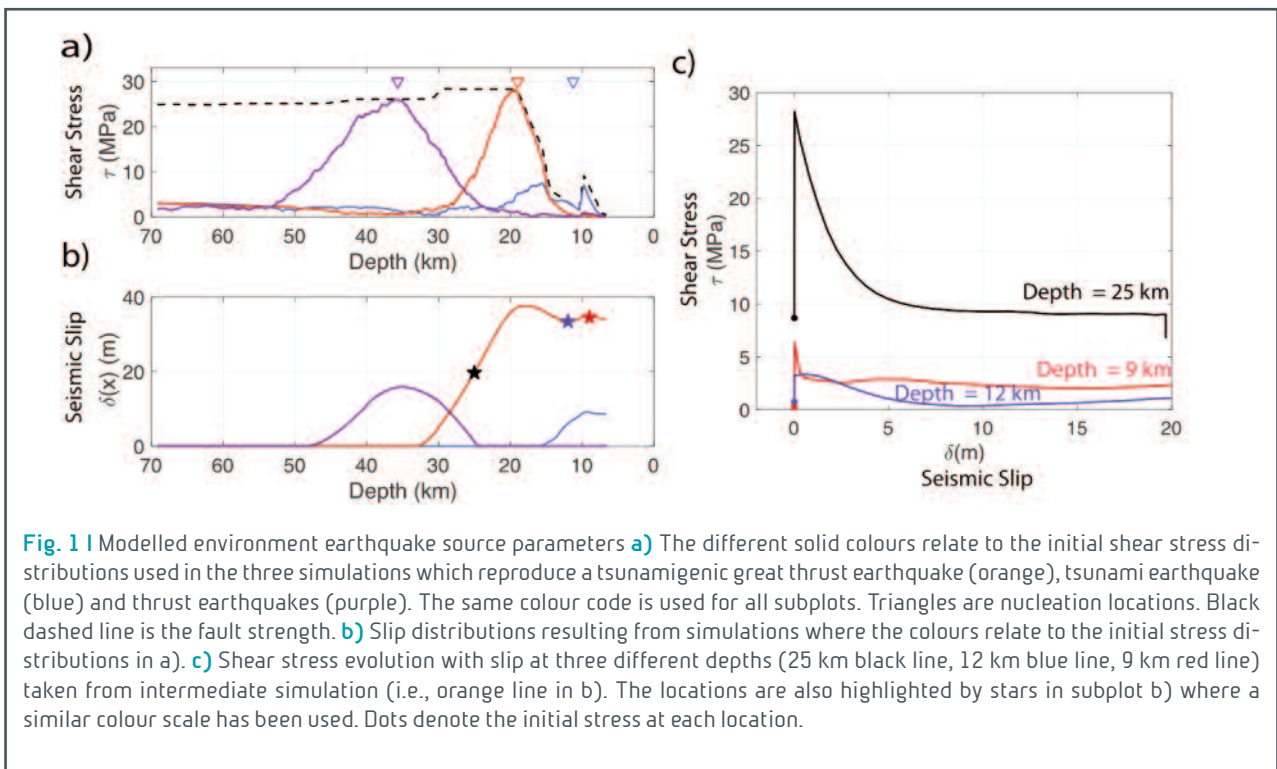
8.2 I ROCK PHYSICS

Tsunamigenic earthquake simulations using experimentally derived friction laws

S. Murphy, G. Di Toro, F. Romano, A. Scala, S. Lorito, E. Spagnuolo, S. Aretusini, G. Festa, A. Piatanesi, S. Nielsen

Seismological, tsunami and geodetic observations have shown that subduction zones are complex systems where the properties of earthquake rupture vary with depth as a result of different pre-stress and frictional conditions. A wealth of earthquakes of different sizes and different source features (e.g. rupture duration) can be generated in subduction zones, including tsunami earthquakes, some of which can produce extreme tsunamigenic events. Here we offer a geological perspective on these depth-dependent features. Subduction zone fault rocks are dominantly incohesive and clay-rich near the surface, transitioning to cohesive and more crystalline at depth.
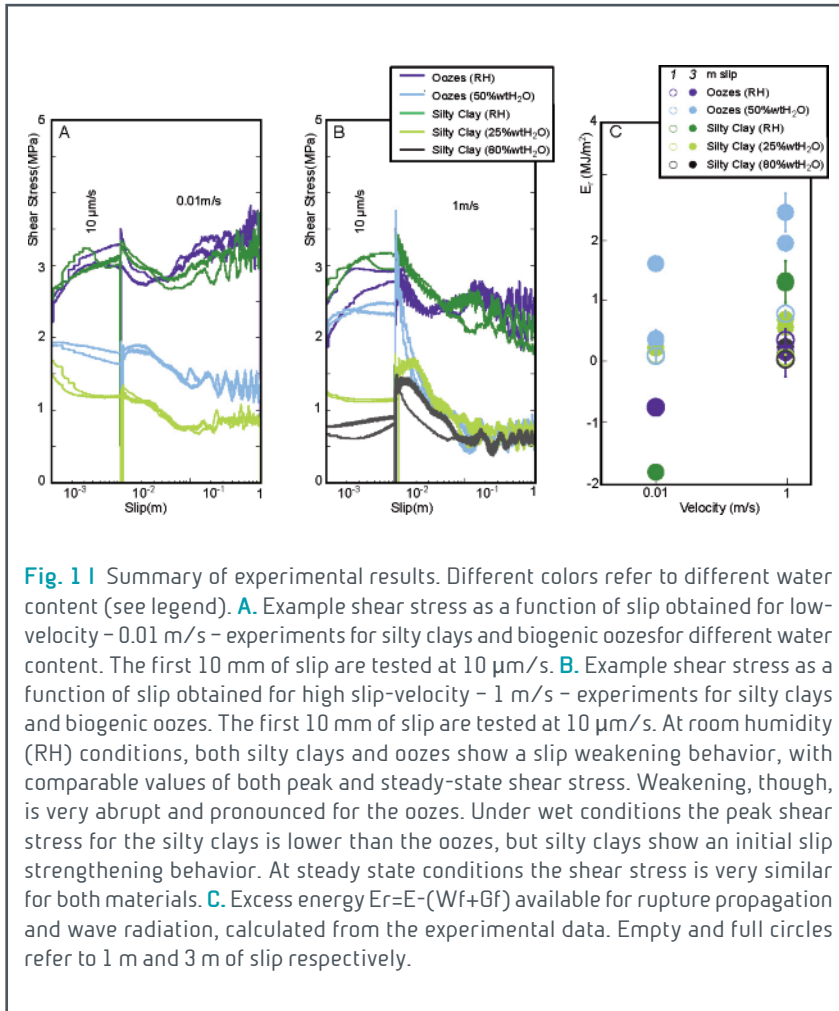
We combine a lithology-controlled, depth-dependent experimental friction law with elastodynamic rupture simulations for a Tohoku-like subduction zone. By using simplified pre-stress distributions, we show that by shifting along fault dip the location of the high shear stress regions ("asperities"), moderate to great thrust earthquakes and tsunami earthquakes are produced, consistent with seismological, geodetic, and tsunami observations. Central to this depth dependence is that slip is confined to the high stress asperity at depth; near the surface rupture is impeded by the rock-clay transition constraining slip to the clay-rich layer. However, when the high stress asperity is located in the clay-to-crystalline rock transition, great thrust earthquakes can be generated similar to the Mw 9 Tohoku (2011) earthquake (Fig. 1).

Fig. 1 I Modelled environment earthquake source parameters a) The different solid colours relate to the initial shear stress distributions used in the three simulations which reproduce a tsunamigenic great thrust earthquake (orange), tsunami earthquake (blue) and thrust earthquakes (purple). The same colour code is used for all subplots. Triangles are nucleation locations. Black dashed line is the fault strength. b) Slip distributions resulting from simulations where the colours relate to the initial stress distributions in a). c) Shear stress evolution with slip at three different depths (25 km black line, 12 km blue line, 9 km red line) taken from intermediate simulation (i.e., orange line in b). The locations are also highlighted by stars in subplot b) where a similar colour scale has been used. Dots denote the initial stress at each location.

Past seismic slip-to-the-trench recorded in Central America megathrust

P. Vannucchi, E. Spagnuolo, S. Aretusini, G. Di Toro, K. Ujiie, A. Tsutsumi, S. Nielsen

Fig. 1 I Summary of experimental results. Different colors refer to different water content (see legend). **A.** Example shear stress as a function of slip obtained for low-velocity – 0.01 m/s – experiments for silty clays and biogenic oozesfor different water content. The first 10 mm of slip are tested at 10 µm/s. **B.** Example shear stress as a function of slip obtained for high slip-velocity – 1 m/s – experiments for silty clays and biogenic oozes. The first 10 mm of slip are tested at 10 µm/s. At room humidity (RH) conditions, both silty clays and oozes show a slip weakening behavior, with comparable values of both peak and steady-state shear stress. Weakening, though, is very abrupt and pronounced for the oozes. Under wet conditions the peak shear stress for the silty clays is lower than the oozes, but silty clays show an initial slip strengthening behavior. At steady state conditions the shear stress is very similar for both materials. **C.** Excess energy Er=E-(Wf+Gf) available for rupture propagation and wave radiation, calculated from the experimental data. Empty and full circles refer to 1 m and 3 m of slip respectively.

The 2011 Tohoku-Oki earthquake revealed that co-seismic displacement along the plate boundary megathrust can propagate to the trench. Co-seismic slip to the trench amplifies hazards at subduction zones, so its historical occurrence should also be investigated globally. Here we combine results from IODP Exp. 344 offshore SE Costa Rica with 3D reflection seismic interpretation and experimental data to identify and document a geologic record of past co-seismic slip-to-the-trench. IODP Exp. 344 drilled an old, < 1.9 Ma, megathrust frontal ramp – at ca. 325 mbsf – that superimposes older Miocene biogenic oozes onto late Miocene-Pleistocene silty clays. Stratigraphy and geophysical imaging constrain the position of the basal decollement to lie within the biogenic oozes.

Friction experiments show that when wet, silty clays and biogenic oozes are both slip-weakening at subseismic and seismic slip velocities. Oozes are stronger than silty clays at slip velocity 0.01 m/s, and wet oozes only become as weak as silty clays at slip velocity of 1 m/s. The implication is that the geological structures found in the forearc offshore SE Costa Rica were deformed during seismic slip-to-the-trench events. During slower aseismic creep, deformation would have preferentially localized within the silty-clays.

Mechanical behavior of fluid lubricated faults.

C. Cornelio, E. Spagnuolo, G. Di Toro, S. Nielsen, M. Violay

Fluids are pervasive in fault zones cutting the Earth's crust, however the effect of their viscosity on fault mechanics is mainly conjectured by theoretical models. Here, we present the results of 30 friction experiments performed at normal effective stress up to10 MPa (drained conditions), sliding velocity ranging between 10 ms^{-1} and 10 ms^{-1} and under both dry and fluid-present conditions. Four different fluid viscosities were tested: distilled water (ŋ~1mPas) and three mixtures of water and glycerol with concentrations of 40/60 wt%, 15/85 wt% and 1/99 wt% (i.e. n=10.9,108.0 and 1226.6 mPas respectively).

Highly viscous fluids strongly decreases the static and the dynamic friction coefficients, in agreement with the elasto-hydrodynamic lubrication theory. However, for small slip events, the high viscosity of the fluid increases the frictional weakening distance D_c, thus decreasing the available energy for rupture propagation and potentially inhibiting earthquake propagation. Extrapolation of experimental results to seismogenic conditions suggests that elasto-hydrodynamic lubrication may be an efficient mechanism for dynamic fault weakening at mid-crustal conditions for moderate to large in magnitude earthquakes (Fig. 1).
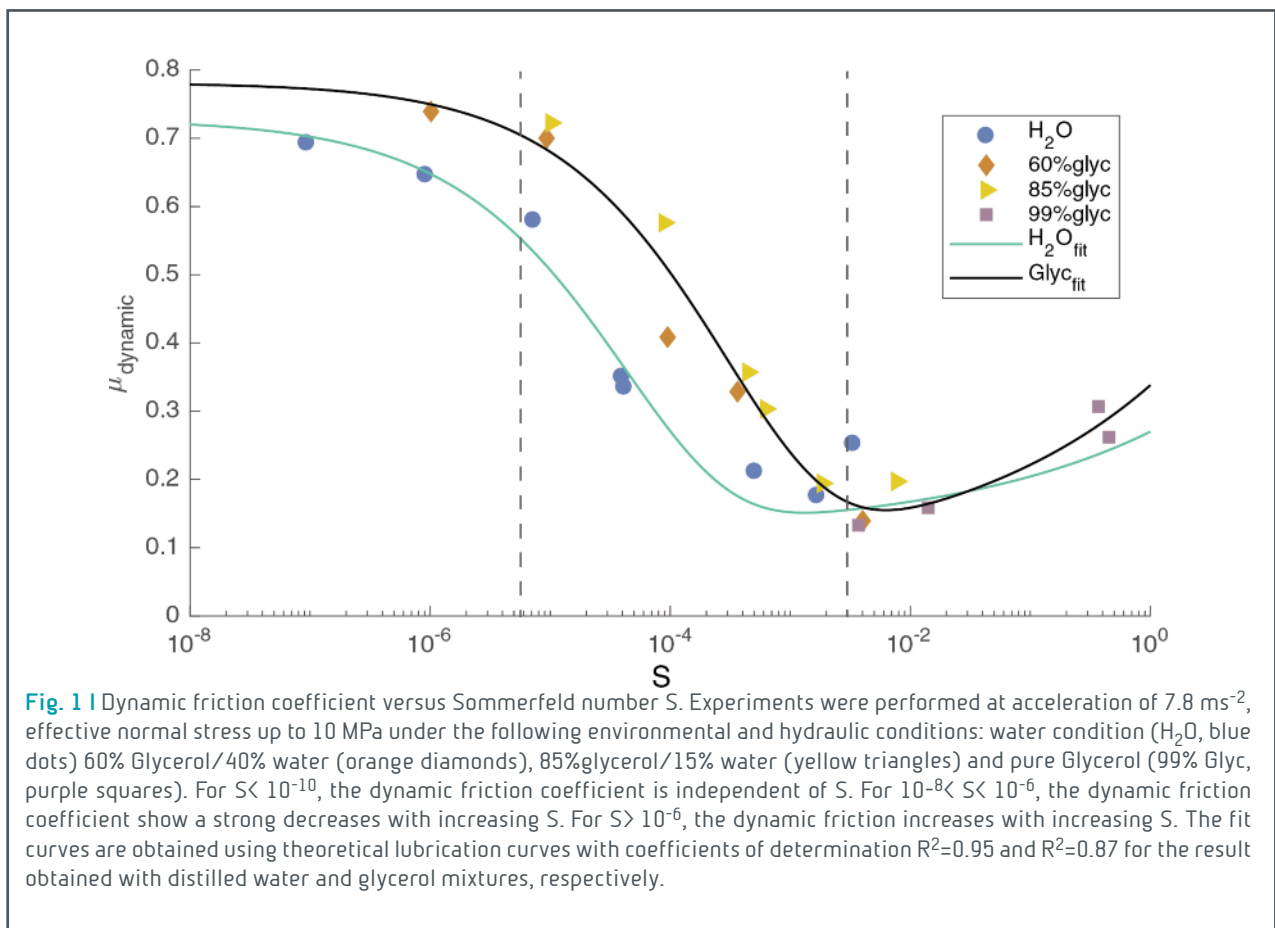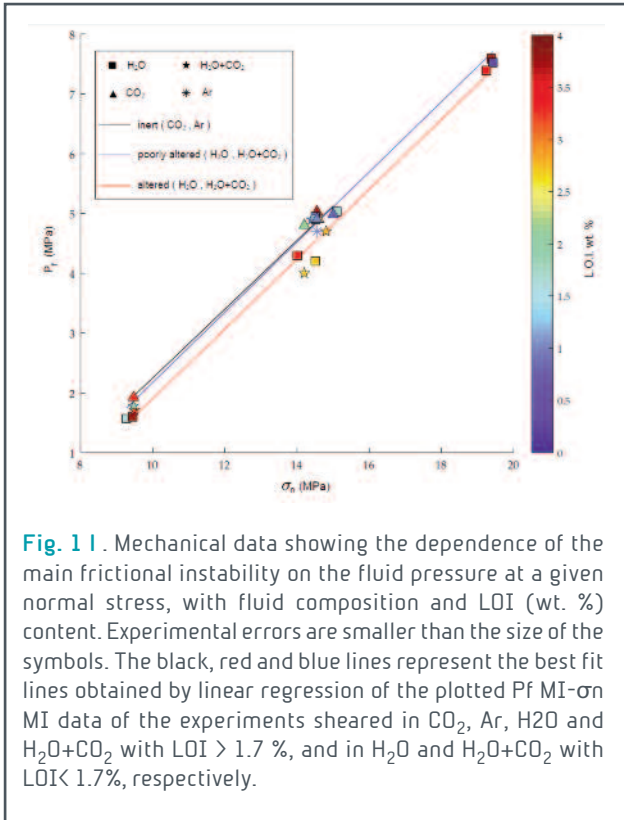

Fig. 1 I Dynamic friction coefficient versus Sommerfeld number S. Experiments were performed at acceleration of 7.8 ms^{-2}, effective normal stress up to 10 MPa under the following environmental and hydraulic conditions: water condition (H$_2$O, blue dots) 60% Glycerol/40% water (orange diamonds), 85%glycerol/15% water (yellow triangles) and pure Glycerol (99% Glyc, purple squares). For S< 10^{-10}, the dynamic friction coefficient is independent of S. For 10^{-8}< S< 10^{-6}, the dynamic friction coefficient show a strong decreases with increasing S. For S> 10^{-6}, the dynamic friction increases with increasing S. The fit curves are obtained using theoretical lubrication curves with coefficients of determination R^2=0.95 and R^2=0.87 for the result obtained with distilled water and glycerol mixtures, respectively.

Frictional instabilities and carbonation of basalts triggered by injection of pressurized H$_2$O- and CO$_2$- rich fluids

P. Giacomel, E. Spagnuolo, M. Nazzari, A. Marzoli, F. Passelegue, N. Youbi, G. Di Toro

Fig. 1 | . Mechanical data showing the dependence of the main frictional instability on the fluid pressure at a given normal stress, with fluid composition and LOI (wt. %) content. Experimental errors are smaller than the size of the symbols. The black, red and blue lines represent the best fit lines obtained by linear regression of the plotted Pf MI-σn MI data of the experiments sheared in CO$_2$, Ar, H2O and H$_2$O+CO$_2$ with LOI > 1.7 %, and in H$_2$O and H$_2$O+CO$_2$ with LOI< 1.7%, respectively.

The assessment of the hazards and risks of seismicity is crucial to the success of geological carbon storage and must be based on the understanding of how earthquakes can be induced by fluid injection.

In this regard, we performed friction experiments using a rotary shear apparatus on pre-cut basalts with variable degree of alteration by injecting distilled H$_2$O, pure CO$_2$ and H$_2$O+CO$_2$ fluid mixtures under temperature, fluid pressure and stress conditions relevant for large scale CO$_2$ storage reservoirs.

The main frictional instabilities were preceded by short-lived slip bursts and occurred at comparable fluid pressures (Fig. 1) and normal stresses regardless of the fluid injected and degree of alteration of basalts, suggesting a secondary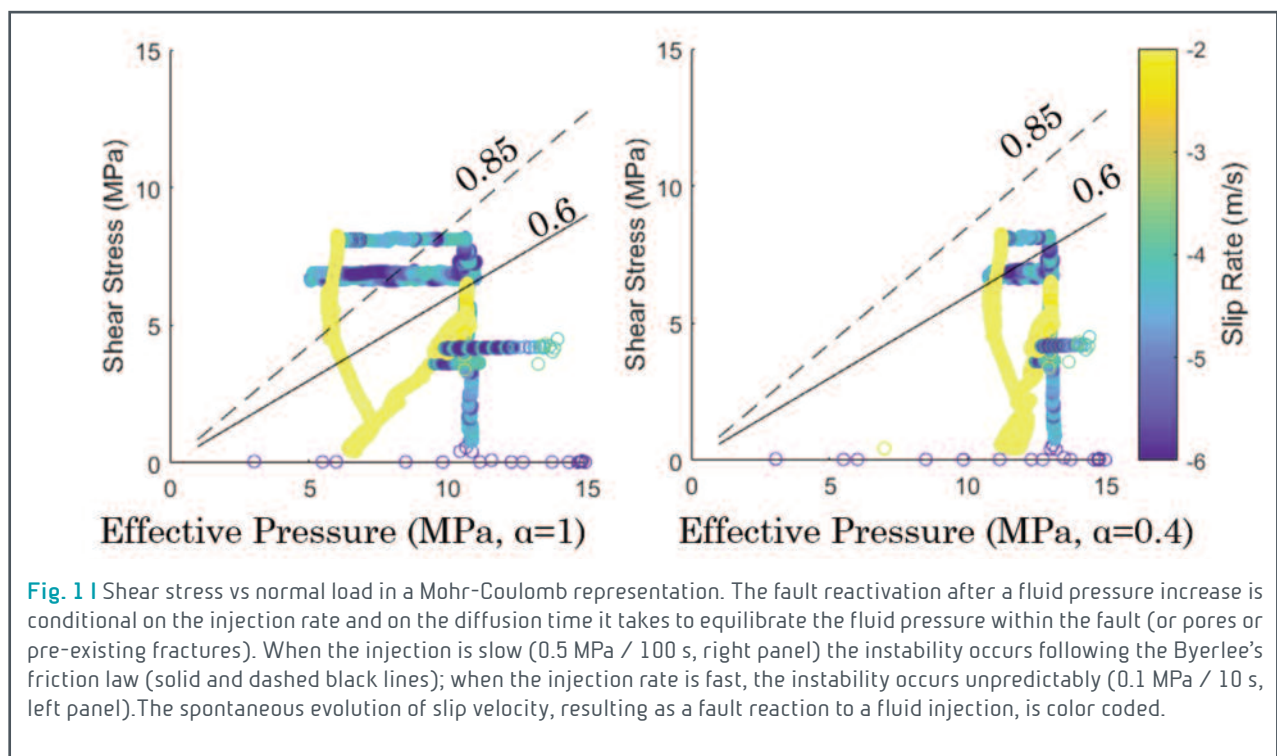 effect of H$_2$O-rich fluids – clay minerals interaction on fault weakening. Dolomite grains due to mineral carbonation of basalts were found only in experiments performed with H$_2$O+CO$_2$ mixtures, providing evidence for the effectiveness of this technique for CO$_2$ storage.

Susceptibility of experimental faults to pore pressure increase: insights from load-controlled experiments on calcite-bearing rocks

E. Spagnuolo, M. Violay, S. Nielsen, C. Cornelio, G. Di Toro

Fluid pressure has been indicated as a major factor controlling natural (e.g., L'Aquila, Italy, 2009 Mw 6.3) and induced seismicity (e.g., Wilzetta, Oklahoma, 2011 Mw 5.7). Terzaghi's principle states that the effective normal stress is linearly reduced by a fluid pressure (Pf) increase $\sigma_{eff}=\sigma_n(1-\alpha Pf)$, where the effective stress parameter (the coupling parameter) α, may be related to the fraction of the fault area that is flooded. A value of $\alpha =1$ is often used by default, with P_f shifting the Mohr circle towards lower normal effective stresses and anticipating failure on pre-existing faults. However, within a complex fault core of inhomogeneous permeability, α may vary in a yet poorly understood way. To shed light on this problem, we conducted experiments on calcite-bearing rock samples (Carrara marble) at room humidity conditions and in the presence of pore fluids (drained conditions) using a rotary apparatus (SHIVA). A pre-cut fault is loaded by constant shear stress τ under constant normal stress $\sigma_n=15$ MPa until a target value corresponding roughly to the 80 % of the frictional fault strength. The fluid pressure P_f is then raised with regular pressure and time steps to induce fault instability. Assuming $\alpha=1$ and a threshold for instability $\tau_{p\_eff}=\mu_p\sigma_{eff}$, the experiments reveal that an increase of P_f does not necessarily induce an instability even when the effective strength threshold is largely surpassed (e.g., $\tau_{p\_eff}=1.3\,\mu_p\sigma_{eff}$). This result may indicate that the P_f increase did not instantly diffuse throughout the slip zone, but took a finite time to equilibrate with the external imposed fluid pressure increase due to finite permeability. Under our experimental conditions, $\alpha=1$ and fault reactivation

Fig. 1 | Shear stress vs normal load in a Mohr-Coulomb representation. The fault reactivation after a fluid pressure increase is conditional on the injection rate and on the diffusion time it takes to equilibrate the fluid pressure within the fault (or pores or pre-existing fractures). When the injection is slow (0.5 MPa / 100 s, right panel) the instability occurs following the Byerlee's friction law (solid and dashed black lines); when the injection rate is fast, the instability occurs unpredictably (0.1 MPa / 10 s, left panel). The spontaneous evolution of slip velocity, resulting as a fault reaction to a fluid injection, is color coded.

satisfies the Byerlee's friction law when the P_f step is larger than 40 sec (right panel Fig. 1) whereas a significant departure from $\alpha=1$ is observed when the Pf step is shorter than about < 20s (left panel, Fig. 1). We interpret this behavior in relation to the diffusion time (t_d), which affects the fluid penetration length L by $L = \sqrt{\kappa t_d}$, where κ is the hydraulic diffusivity on the fault plane, and determines the distance of which the imposed fluid pressure equilibrate within the fault plane. We redefine α as the ratio between the fluid penetration length and sample dimension L resulting in $\alpha = \min(\sqrt{\kappa t_d}, L) / L$. Under several pore pressure loading rates this relation yields an approximate hydraulic diffusivity $\kappa \sim 10^{-8} m^2 s^{-1}$ which is compatible, for example, with a low porosity shale. Our results highlight that a high injection flow rate in fault plane does not necessarily induce a seismogenic fault slip (slip velocities larger than 1 cm/s): a critical fluid penetration length is necessary to trigger fault instability.

Deformation processes at seismic slip rates in water-depleted and water-rich smectite-bearing gouges

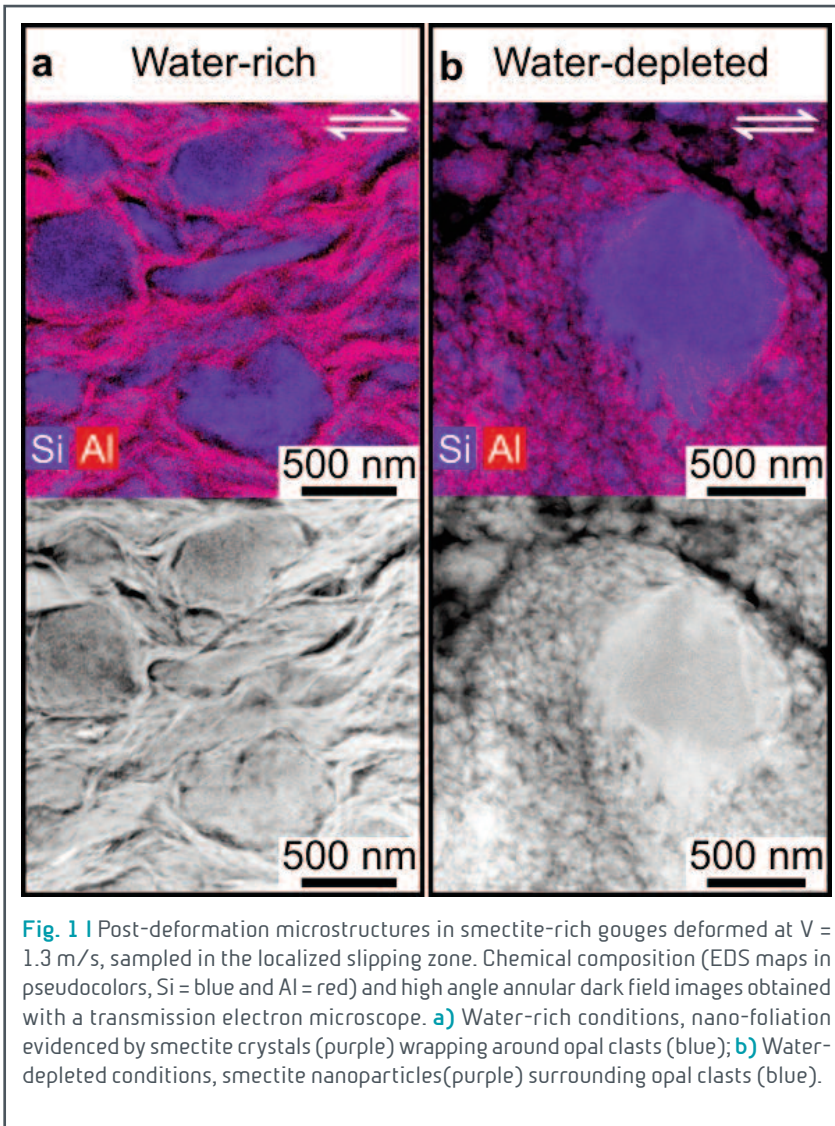*S. Aretusini, E. Spagnuolo, O. Plümper, M.C. Dalconi, G. Di Toro*

Fig. 1 I Post-deformation microstructures in smectite-rich gouges deformed at V = 1.3 m/s, sampled in the localized slipping zone. Chemical composition (EDS maps in pseudocolors, Si = blue and Al = red) and high angle annular dark field images obtained with a transmission electron microscope. **a)** Water-rich conditions, nano-foliation evidenced by smectite crystals (purple) wrapping around opal clasts (blue); **b)** Water-depleted conditions, smectite nanoparticles(purple) surrounding opal clasts (blue).

Rock Physics and geomechanical characterisation of rocks from the micro to macroscale: fabric, fractures and fluids (co-organized) Smectite clay minerals are among the most common components of fault cores in shallow sections of subduction zone megathrusts and landslide decollements.

Consequently, deformation processes at seismic slip rates (1 m/s) in smectites control the mechanics of megathrust earthquakes and landslide collapse.

To investigate the deformation processes, rotary shear experiments on smectite-rich gouge layers (70/30 wt.% Ca-montmorillonite/opal) were performed. The experiments were conducted at ambient temperature and at 5 MPa normal stress. The gouges were sheared under vacuum (10^{-3} mbar), room humidity (i.e., water-depleted) and liquid water (i.e., water-rich) conditions, at slip rates of 0.0003 V ≤ 1.5 m/s and displacements of 0.1 ≤ d ≤ 30 m. The temperature evolution with slip was determined using thermocouples and subsequently compared to numerical results obtained through a finite element model. The permeability of the gouge layer was measured using the pore pressure oscillation method prior to the rotary experiments. Before and after the experiments, mineralogic composition and amorphous material content were investigated via quantitative X-ray powder diffraction and microstructural analyses were performed using advanced electron microscopy.

The deformation processes were strongly controlled by the water content of the gouge layers. Under water-deple-

ted conditions, grain size reduction producing nanoparticles controlled the evolution of friction coefficient at all slip rates (Fig. 1a). Coseismic dynamic weakening (μca. 0.2 - 0.3) occurred by combined thermal decomposition or melting (with decreasing water content) and pressurization of water released by dehydration of smectite interlayers. Under water-rich conditions, grain size reduction was minor and development of nano-foliations occurred (Fig. 1b). Within the nano-foliations, the observed dynamic weakening ($\mu \leq 0.15$), which occurred at all slip rates and for short displacements (d < 0.1 m), was due to water lubrication resulting in combination with pore fluid pressurization by shear-enhanced compaction. The subsequent friction coefficient evolution depended on the balance between, (1) the dissipation of pore pressures, (2) the dehydration of interlayer water and (3) the thickening of the nano-foliation layers. At higher displacement and slip rates, sustained dynamic weakening was aided by vaporization of the pore water and resulted in a switch to deformation processes typical of water-depleted conditions.

These observations scaled to natural conditions would imply that the presence of liquid water in smectites has a lubricating effect, pressurizes the slipping zone and renders the smectite-rich gouges prone to accommodate large seismic slips. In megathrust environments, such lubricating effect may result in the preferential propagation of seismic ruptures during megathrust earthquakes in smectite- and water-rich sediments at shallow depths. Similarly, the presence of water can promote large displacements during landslide collapse.

Frictional stability and earthquake triggering during fluid pressure stimulation of an experimental fault

M.M. Scuderi, C. Collettini, C. Marone

Models of earthquake nucleation based on rate- and state-friction predict that fluid overpressure should stabilize fault slip rather than trigger earthquakes. To address this controversy, we conducted laboratory creep experiments to monitor fault slip evolution at constant shear stress while the effective normal stress was systematically reduced via increasing fluid pressure. We sheared layers of carbonate-bearing fault gouge in a double direct shear configuration within a true-triaxial pressure vessel. We show that fault slip evolution is controlled by the stress state acting on the fault and that fluid pressurization can trigger dynamic instability even in cases of rate strengthening friction, which should favor aseismic creep. During fluid pressurization, when shear and effective normal stresses reach the failure condition, accelerated creep occurs in association with fault dilation; further pressurization leads to an exponential acceleration with fault compaction and slip localization.

Our work indicates that fault weakening induced by fluid pressurization can overcome rate strengthening friction resulting in fast acceleration and earthquake slip. Our work points to modifications of the standard model for earthquake nucleation to account for the effect of fluid overpressure and to accurately predict the seismic risk associated with fluid injection (Fig. 1).
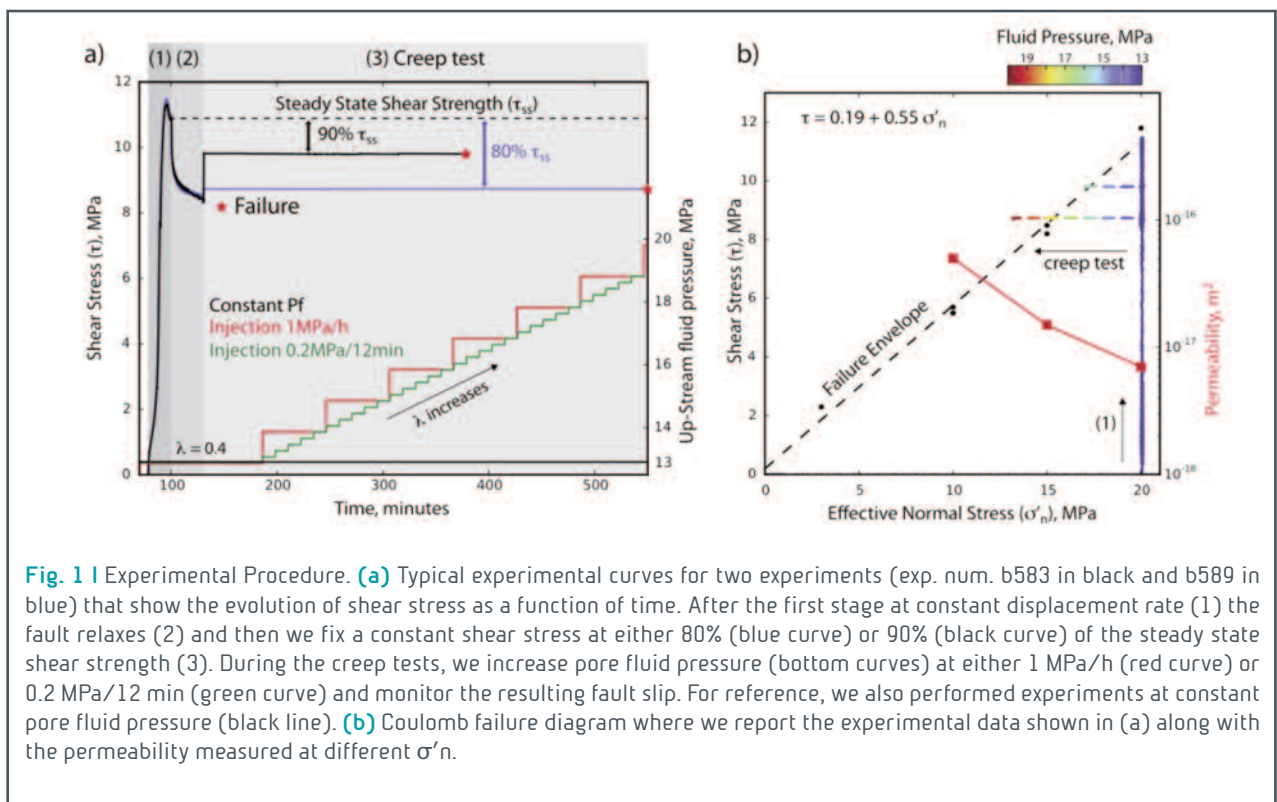

Fig. 1 I Experimental Procedure. **(a)** Typical experimental curves for two experiments (exp. num. b583 in black and b589 in blue) that show the evolution of shear stress as a function of time. After the first stage at constant displacement rate (1) the fault relaxes (2) and then we fix a constant shear stress at either 80% (blue curve) or 90% (black curve) of the steady state shear strength (3). During the creep tests, we increase pore fluid pressure (bottom curves) at either 1 MPa/h (red curve) or 0.2 MPa/12 min (green curve) and monitor the resulting fault slip. For reference, we also performed experiments at constant pore fluid pressure (black line). **(b)** Coulomb failure diagram where we report the experimental data shown in (a) along with the permeability measured at different σ'n.
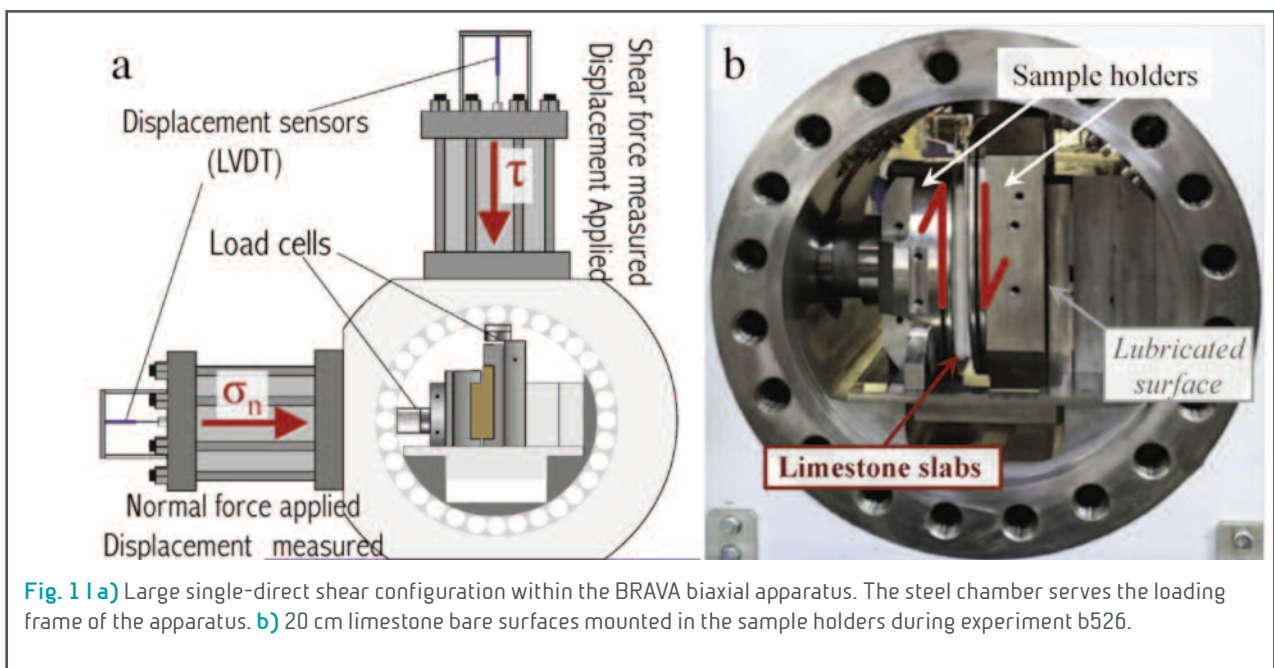
Friction and scale-dependent deformation processes of large experimental carbonate faults

T. Tesei, B.M. Carpenter, G. Giorgetti, M.M. Scuderi, A. Sagy, C. Collettini

We studied the frictional behaviour and deformation products of large (20 cm x 20 cm bare surfaces) experimental limestone faults. We sheared samples in a direct shear configuration, with an imposed normal force of 40e200 kN and shear velocity of 10 mm/s. The steady-state shearing of these surfaces yielded a coefficient of friction 0.7<m<1 (average m~0.9), significantly higher than gouge friction of the same material, m~0.6. Frictional healing, studied via slide-hold-slide tests, is null (Dm 0 upon re-shear). Moreover, sliding of these surfaces is accompanied by dilatation and production of grooves, gouge striations and fault mirrors.

These products are entirely analogous to slip surface phenomena found on natural limestone-bearing faults at both the macroscale and at the microscale. We infer that high friction, accompanied by dilatant deformation, and null frictional healing are the macroscopic effect of brittle damage on the sliding surface, constrained by the strength of the rock and by fast healing processes in the gouge. Simultaneously to brittle failure, plastic deformation occurs on the sliding surface and inside the intact rock via nanoparticle formation (mirrors) and twinning at the micron scale. Because of the similarity between experimental and natural structures, we suggest that sliding of carbonate-bearing faults in the uppermost crust could be characterized by high friction, fast healing and strongly dilatant deformation, which would help to explain shallow seismicity frequently documented in car- bonatic terrains such as the Northern Apennines of Italy (Fig. 1).

Fig. 1 l a) Large single-direct shear configuration within the BRAVA biaxial apparatus. The steel chamber serves the loading frame of the apparatus. b) 20 cm limestone bare surfaces mounted in the sample holders during experiment b526.
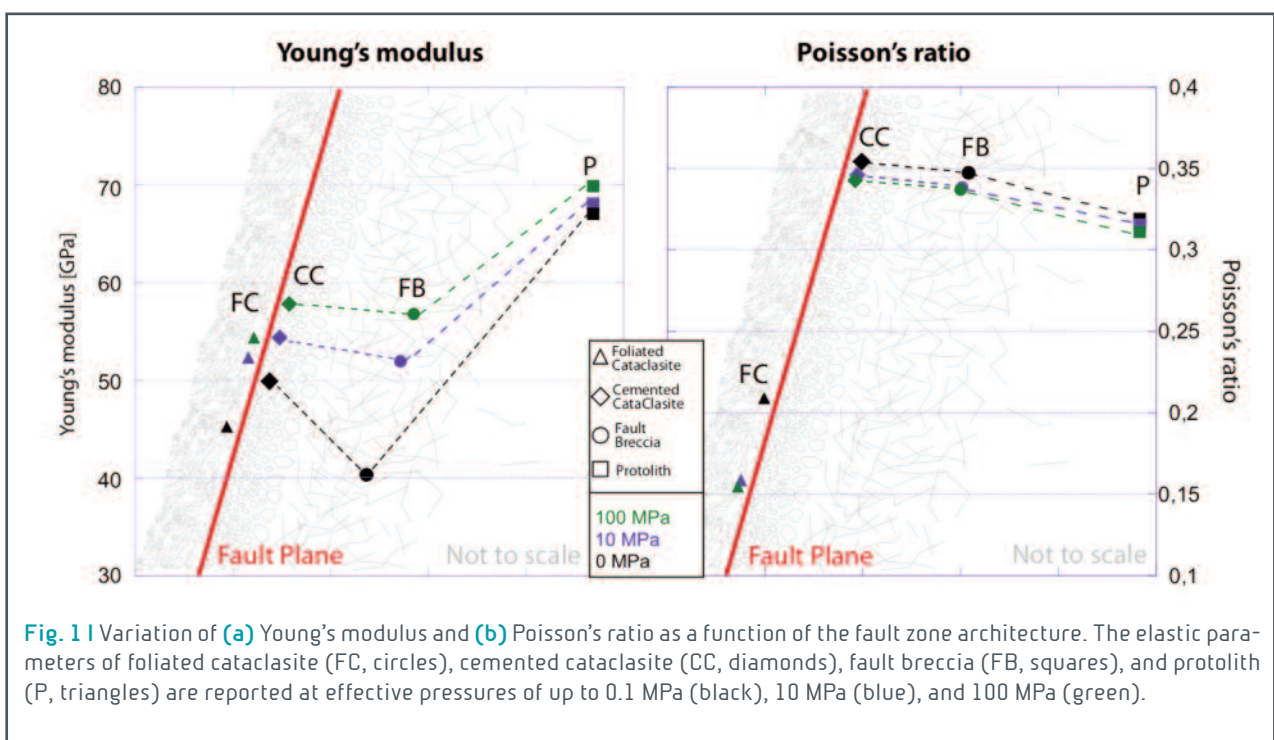
On the evolution of elastic properties during laboratory stick-slip experiments spanning the transition from slow slip to dynamic rupture

F. Trippetta, B.M. Carpenter, S. Mollo, M.M. Scuderi, C. Collettini

The physical characterization of carbonate-bearing normal faults is fundamental for resource development and seismic hazard. Here we report laboratory measurements of density, porosity, Vp, Vs, elastic moduli, and permeability for a range of effective confining pressures (0.1–100 MPa), conducted on samples representing different structural domains of a carbonate-bearing fault. We find a reduction in porosity from the fault breccia (11.7% total and 6.2% connected) to the main fault plane (9% total and 3.5% connected), with both domains showing higher porosity compared to the protolith (6.8% total and 1.1% connected). With increasing confining pressure, P wave velocity evolves from 4.5 to 5.9 km/s in the fault breccia, is constant at 5.9 km/s approaching the fault plane and is low (4.9 km/s) in clay-rich fault domains. We find that while the fault breccia shows pressure sensitive behavior, the cemented cataclasite close to the fault plane is characterized by pressure- independent behavior. Our results indicate that the deformation processes occurring within the different fault structural domains influence the physical and transport properties of the fault zone. In situ Vp profiles match well the laboratory measurements demonstrating that laboratory data are valuable for implications at larger scale. Combining the experimental values of elastic moduli and frictional properties it results that at shallow crustal levels, M 1 earthquakes are less favored, in agreement with earthquake-depth distribution during the L'Aquila 2009 seismic sequence that occurred on carbonates (Fig. 1).

Fig. 1 I Variation of (a) Young's modulus and (b) Poisson's ratio as a function of the fault zone architecture. The elastic parameters of foliated cataclasite (FC, circles), cemented cataclasite (CC, diamonds), fault breccia (FB, squares), and protolith (P, triangles) are reported at effective pressures of up to 0.1 MPa (black), 10 MPa (blue), and 100 MPa (green).

How set new functions, velocity, load and pore fluid pressure, for rocks mechanics experiments with BRAVA

G. Di Stefano, M.M. Scuderi, C. Giorgetti, C. Collettini

In some rocks mechanic experiments, performed in the laboratory, it is necessary to simulate a normal stress on the rock sample with a variable course. For example, we want to apply a normal stress with a sinusoidal pattern or to create a stress that follows a general predefined time function on a fault 50x50mm simulated fault gauge subjected to a sliding process with controlled speed.

At the same time, the pressure of the fluid inside the pores of a porous rock, subjected to stress, represents an important parameter for the process of deformation and breaking of an experimental fault rock. A particular changing in pore pressure could change the friction state inside a fault, triggering a slip of the fault rock sample.

To perform a laboratory experiment with BRAVA on rock samples, normal stress, shear stress confining pressure, pore fluid pressure and linear velocity profiles are inputs parameters generally established before or during the test. These parameters (called set-points) characterize the experiment trajectory. They are used to control the movement of the hydraulic actuators (horizontal, vertical and intensifiers pistons) of the apparatus and are pre-defined

Fig. 1 I TOF-SIMS images of the studied beryl sample after the experimental run. The color scale is proportional to the element contents from red (high) to blue (low).

in order to obtain a desiderate field stress on the rock sample and a controlled sliding between the layers of a simulated fault gauge.

The BRAVA "MAIN" program represents the first management level of the apparatus. Through a virtual interface control panel, the user can perform many operations: plan an experiment setting some parameters, have a complete view of the test, record the measured data and perform some control functions.

Using this program, the user can plan an experiment, inserting or changing the normal stress(load of the horizontal piston) and the same time the shear stress (load of the vertical piston), confining pressure and pore fluid pressure in tri-axial configuration. On a specific virtual panel "Vertical Piston Velocity steps", showed in the figure 1, it is possible also to generate a piece-wise linear profile of sliding velocity in order to realize automatic advancement of the vertical column at controlled velocity. To do this, a sequence of the velocity values are insert into a data entry records, where each one(step) contains step number, velocity, step time and data acquisition rate.

To implement set-points with variable profiles, characterized by simple or complex mathematical functions, a new program blocks (VI files in the LabVIEW environment) are been developed and linked with the MAIN program.

As showed in the figure 1, virtual buttons on the "Automatic Control" panel of the MAIN program are available to open sub-panels and in which we can build mathematical functions. For example, pushing the button in the "PPA intensifier" column a sub-panel opens where it is possible to configure a sinusoidal pore pressure profile, using an offset level Ppa_{off}(i.e. 3MPa as showed in figure1) corresponding to the real value established inside the sample rock under test(initial condition).On the panel the user can set the frequency, in the range 10mHz (or less) to 20Hz, the amplitude Ppa_{amp} of the pore fluid pressure, with ($Ppa_{off} \leq Ppa_{off}$) so that $Ppa \leq 0$, and the number of cycle of the function.

The sub-program generates a sequence of pressure values (array), which is transfer to a second level real-time computer (on board the machine) pushing the start bottom. This new set-points will be processed by a closed loop control algorithm, with a refreshing frequency fixed to 10ms up to 1ms.

Fault reactivation: insights from triaxial saw-cut experiments

C. Giorgetti, T. Tesei, M.M. Scuderi, C. Collettini

Fault zones in the brittle crust constitute planes of weakness that can be reactivated depending on their frictional properties, their orientation with respect to the stress field and the stress field magnitude. Analytical approach to evaluate the occurrence of fault reactivation is generally based on the assumption that faults are ideal planar features characterized by a constant friction. However, natural faults are complex structures characterized by the presence of fault rock. Here we aim to experimentally investigate the criterion of frictional reactivation for gouge-bearing experimental faults.

We simulated pre-existing faults by conducting triaxial experiments on sandstone cylinders containing a saw-cut, filled with clay-rich gouge, at various orientations to the maximum principal stress $\sigma 1$. Firstly, we have characterized the frictional strength of the sandstone and the frictional properties of the clay-rich gouge via triaxial and biaxial experiments, respectively. Then, triaxial saw-cut experiments on faults of variable thickness, oriented from 30° to 80° with respect to the maximum compressive stress, were performed at a constant confining
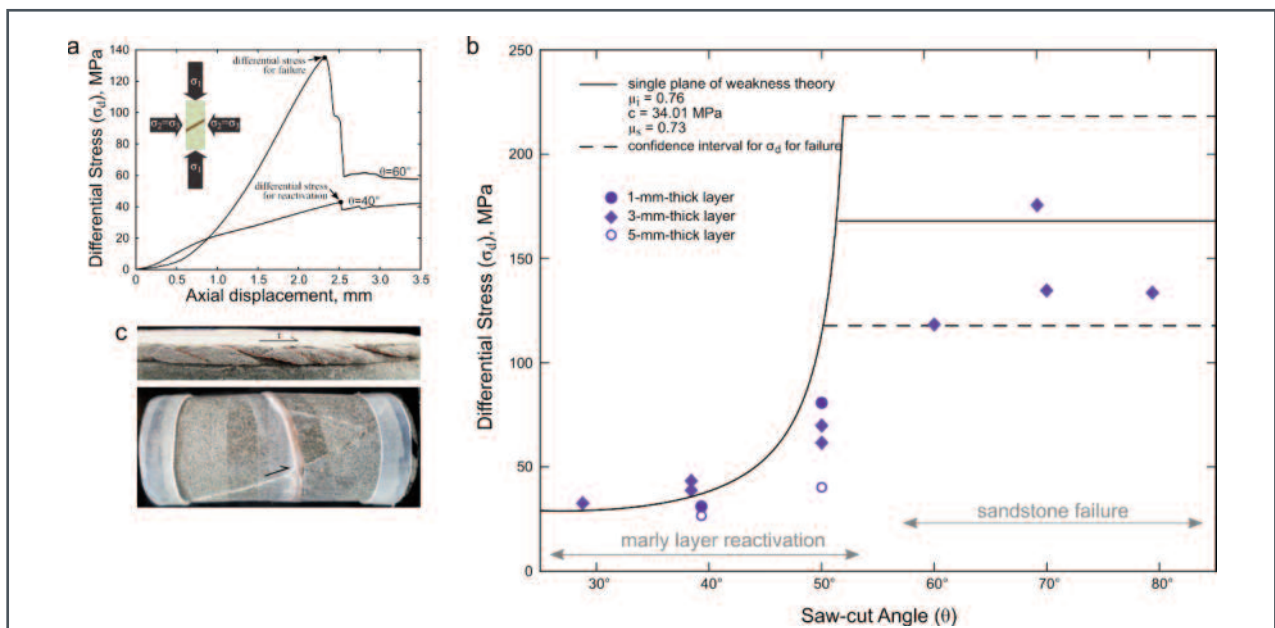
Fig. 1 I a) Evolution of differential stress plotted versus axial displacement during triaxial saw-cut experiments. The uppermost curve shows the evolution of differential stress during an experiment in which the sample deformed through the development a new fracture, whereas the lowermost curve shows the evolution of differential stress during an experiment in which the sample deformed through the reactivation of the saw-cut. Inset shows the triaxial saw-cut configuration in which confining oil is used to apply an isotropic pressure ($\sigma 3 = \sigma 2$) and the vertical loading frame applies a vertical force generating a differential stress. **b)** Results from triaxial saw-cut experiments compared to the single plane of weakness theory (black line) reconstructed on the grounds of the sandstone strength and the clay-rich gouge friction. The maximum σd supported by triaxial saw-cut samples before fault reactivation or new fracture development is plotted against the saw-cut angle. Slip within the fault occurs for $\theta = 30°-40°-50°$, whereas the development of a new fracture occurs for $\theta = 60°-70°-80°$, in agreement with theoretical predictions.c) The uppermost picture shows a sheared gouge layer at the end of a triaxial saw-cut experiment ($\theta = 30°$) showing Riedel shear planes (red dashed lines). The lowermost picture shows a new optimally-oriented fault that cuts the pre-existing gouge layer ($\theta = 70°$).

pressure of 10 MPa and at a constant axial loading rate of 0.3 μm/s.

Our results show that the reactivation of the experimental fault occurs only at 30°, 40° and 50° to σ1 and that new fractures develop in samples with experimental faults oriented at 60°, 70° and 80° to σ1, as predicted by the theory of frictional fault reactivation (Fig. 1). However, the differential stress for the reactivation differs from theoretical predictions. In particular, non-optimally oriented gouge-bearing faults appear weaker than theoretically predicted and the thickness of the fault tends to inversely relate with the apparent friction required for reactivation (Fig. 1). Our findings suggest that theoretical predictions based on the assumption of zero-thickness constitute an upper bound on fault strength and that misoriented faults can be weaker than predicted.

Strength evolution of simulated carbonate-bearing faults: the role of normal stress and slip velocity

M. Mercuri, M.M. Scuderi, T. Tesei, E. Carminati, C. Collettini

A great number of earthquakes occur within thick carbonate sequences in the shallow crust. At the same time, carbonate fault rocks exhumed from a depth < 6 km (i.e., from seismogenic depths) exhibit the coexistence of structures related to brittle (i.e., cataclasis) and ductile deformation processes (i.e., pressure-solution and granular plasticity). We performed friction experiments on water-saturated simulated carbonate-bearing faults for a wide range of normal stresses (from 5 to 120 MPa) and slip velocities (from 0.3 to 100 μm/s). At high normal stresses (n> 20 MPa) fault gouges undergo strain-weakening, that is more pronounced at slow slip velocities, and causes a significant reduction of frictional strength, from μ = 0.7 to μ = 0.47 (Fig. 1). Microstructural analysis show that fault gouge weakening is driven by deformation accommodated by cataclasis and pressure-insensitive deformation processes (pressure solution and granular plasticity) that become more efficient at slow slip velocity. The reduction in frictional strength caused by strain weakening behaviour promoted by the activation of pressure-insensitive deformation might play a significant role in carbonate-bearing faults mechanics.
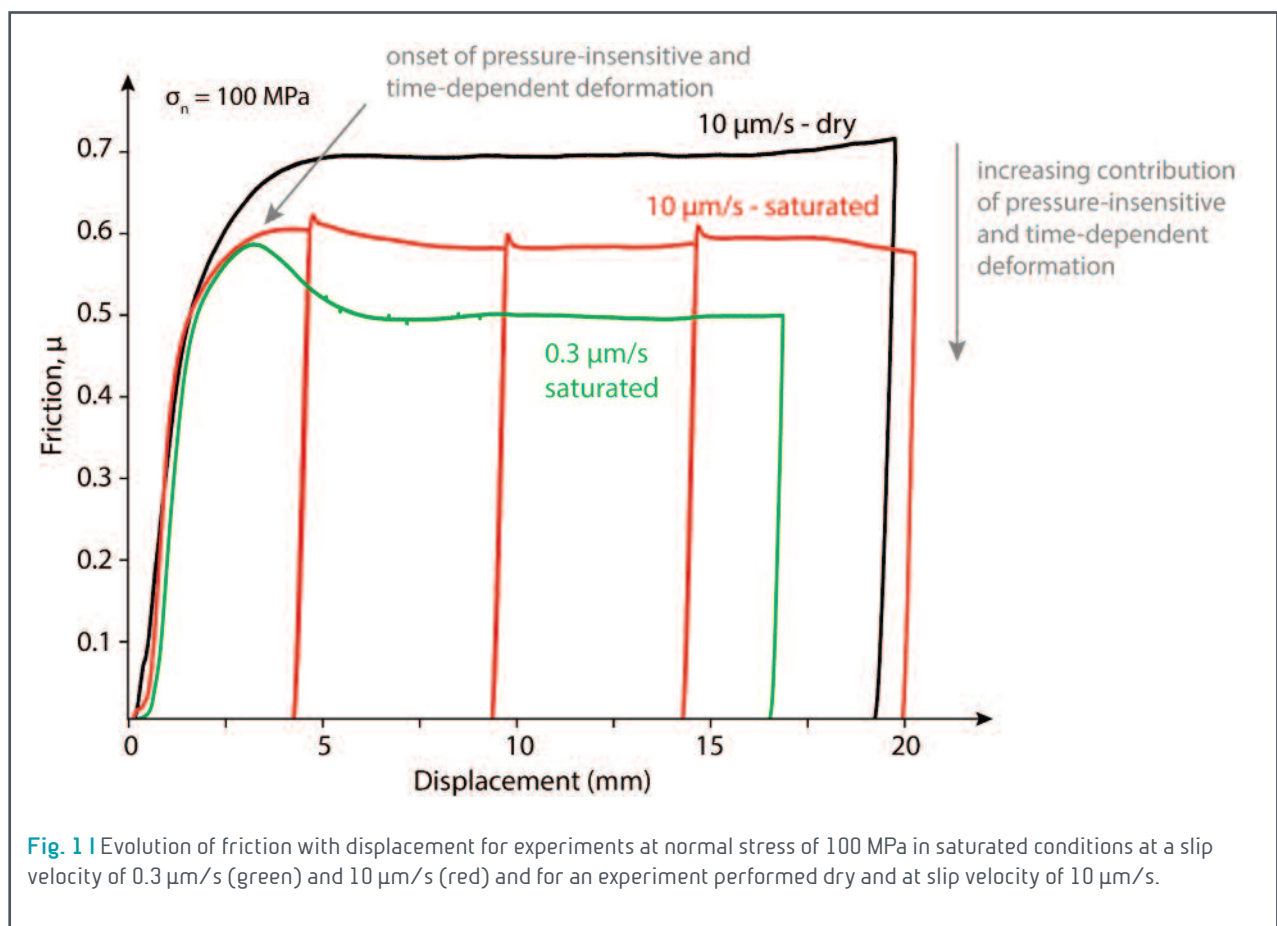
Fig. 1 I Evolution of friction with displacement for experiments at normal stress of 100 MPa in saturated conditions at a slip velocity of 0.3 μm/s (green) and 10 μm/s (red) and for an experiment performed dry and at slip velocity of 10 μm/s.

Mohr-Coulomb envelopes of fault strength under creep conditions: insights from relaxation experiments on many rock types

T. Tesei

The empirical Mohr-Coulomb criterion is the simplest description of fault strength under brittle conditions. The criterion has been developed to describe the strength of intact rocks and tectonites using classical experiments with imposed strain rates. The strength of a fault rock under imposed strain rate conditions is a good proxy of the faults resistance during accelerated motion (e.g. earthquake nucleation, slow slip, after slip) and it is strongly dependent from the internal fabric, mineral composition and the presence of interstitial fluids. However, fault strength during long geological times is poorly constrained by laboratory experiments because deformation is controlled by slow processes such as pressure-solution and subcritical crack growth. Here I present friction experiments, carried out in a biaxial apparatus, in which experimental fault gouges are allowed to relax the stress after an initial phase of externally imposed slip (slide-hold tests). When imposed slip is halted, the experimental faults creep and relax part of the stress in the loading frame. Shear stress measured during relaxation, is interpreted to indicate the maximum strength of the experimental fault (and of the given microstructure) under imposed stress conditions.

Shear stress after relaxation is linearly proportional with imposed normal stress, defining a Mohr-Coulomb envelope for the creep strength of the experimental faults. Creep fault strength is systematically 6-10% lower than strength under imposed strain rate, for a wide variety of materials, from granite, to calcite to phyllosilicate-rich natural fault gouges. The creep strength could represent the threshold between faulting by slow, long term processes and the onset of dynamic instability.

The XML Metadata Editor of GFZ Data Services

D. Ulbricht, K. Elger, T. Tesei, D. Trippanera

Following the FAIR data principles, research data should be Findable, Accessible, Interoperable and Reusable. Publishing data under these principles requires to assign persistent identifiers to the data and to generate rich machine-actionable metadata. To increase the interoperability, metadata should include shared vocabularies and crosslink the newly published (meta)data and related material. However, structured metadata formats tend to be complex and are not intended to be generated by individual scientists. Software solutions are needed that support scientists in providing metadata describing their data.

To facilitate data publication activities of 'GFZ Data Services', we programmed an XML metadata editor that assists scientists to create metadata in different schemata popular in the earth sciences (ISO19115, DIF, DataCite), while being at the same time usable by and understandable for scientists. Emphasis is placed on removing barriers, in particular the editor is publicly available on the internet without registration [1] and the scientists are not reque-sted to provide information that may be generated automatically (e.g. the URL of a specific licence or the contact information of the metadata distributor). Metadata are stored in browser cookies and a copy can be saved to the local hard disk. To improve usability, form fields are translated into the scientific language, e.g. 'creators' of the DataCite schema are called 'authors'. To assist filling in the form, we make use of drop down menus for small voca-bulary lists and offer a search facility for large thesauri. Explanations to form fields and definitions of vocabulary terms are provided in pop-up windows and a full documentation is available for download via the help menu. In addition, multiple geospatial references can be entered via an interactive mapping tool, which helps to minimize problems with different conventions to provide latitudes and longitudes.

Currently, we are extending the metadata editor to be reused to generate metadata for data discovery and contex-tual metadata developed by the 'Multi-scale Laboratories' Thematic Core Service of the European Plate Observing System (EPOS-IP). The Editor will be used to build a common repository of a large variety of geological and geo-physical dataset produced by multidisciplinary laboratories throughout Europe, thus contributing to a significant step toward the integration and accessibility of geosciences.

This presentation will introduce the metadata editor and show the adjustments made for EPOS-IP.

[1] http://dataservices.gfz-potsdam.de/panmetaworks/metaedit

Physical and Transport Property Variations Within Carbonate- Bearing Fault Zones: Insights From the Monte Maggio Fault (Central Italy)

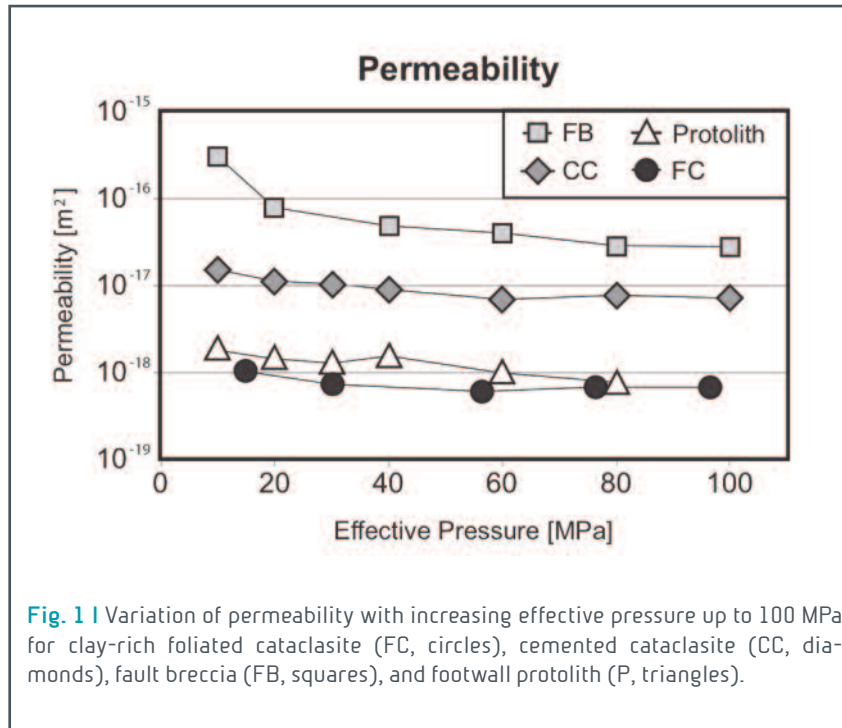*F. Trippetta, B.M. Carpenter, S. Mollo, M. M. Scuderi, P. Scarlato, C. Collettini*

Fig. 1 I Variation of permeability with increasing effective pressure up to 100 MPa for clay-rich foliated cataclasite (FC, circles), cemented cataclasite (CC, diamonds), fault breccia (FB, squares), and footwall protolith (P, triangles).

Physical properties of fault zones vary with time and space and in particular, fluid flow and permeability variations are strictly related to fault zone processes being fundamental for resource development and seismic hazard.

Here we report laboratory measurements of density, porosity, Vp, Vs, elastic moduli, and permeability for a range of effective confining pressures (0.1–100 MPa), performed at High Pressure High Temperature (HPHT) Laboratory, Istituto Nazionale di Geofisica e Vulcanologia (INGV), Rome. Collected samples represent the different structural domains of a carbonate-bearing fault (Monte Maggio normal Fault), a regional structure (length ~10 km and displacement ~500 m) located within the active system of the Apennines. In particular, we have studied an exceptionally exposed outcrop of the fault within the Calcare Massiccio formation (massive limestone) that has been recently exposed by new roadworks. Large cores (100 mm in diameter and up to 20 cm long) drilled perpendicular to the fault plane have been used to: 1) characterize the damage zone adjacent to the fault plane and 2) to obtain smaller cores, 38 mm in diameter both parallel and perpendicular to the fault plane, for rock deformation experiments.

At the mesoscale two types of cataclastic damage zones can be identified in the footwall block (i) a Cemented Cataclasite (CC) and (ii), a Fault Breccia (FB). Since in some portions of the fault the hangingwall (HW) is still preserved we also collected HW samples. After preliminary porosity measurements at ambient pressure, we performed laboratory measurements of Vp, Vs, and permeability at effective confining pressures up to 100 MPa in order to simulate crustal conditions.

We find a reduction in porosity from the fault breccia (11.7% total and 6.2% connected) to the main fault plane (9% total and 3.5% connected), with both domains showing higher porosity compared to the protolith (6.8%

total and 1.1% connected). With increasing confining pressure, P wave velocity evolves from 4.5 to 5.9 km/s in the fault breccia, is constant at 5.9 km/s approaching the fault plane and is low (4.9 km/s) in clay-rich fault domains. We find that while the fault breccia shows pressure sensitive behavior (a reduction in permeability (from 2 x 10^{-16} to 2 x 10^{-17} m^2 Fig. 1), the cemented cataclasite close to the fault plane is characterized by pressure- independent behavior (permeability 4 x 10^{-17} m).

Our dataset depicts a fault zone structure with heterogeneous static physical and transport properties that are controlled by the occurrence of different deformation mechanisms related to different protolites.

In situ Vp profiles match well the laboratory measurements demonstrating that laboratory data are valuable for implications at larger scale. Combining the experimental values of elastic moduli and frictional properties it results that at shallow crustal levels, M 1 earthquakes are less favored, in agreement with earthquake-depth distribution during the L'Aquila 2009 seismic sequence that occurred on carbonates.

8.3 TECHOLOGY

Audio amplifier

G. Romeo, G. Spinelli
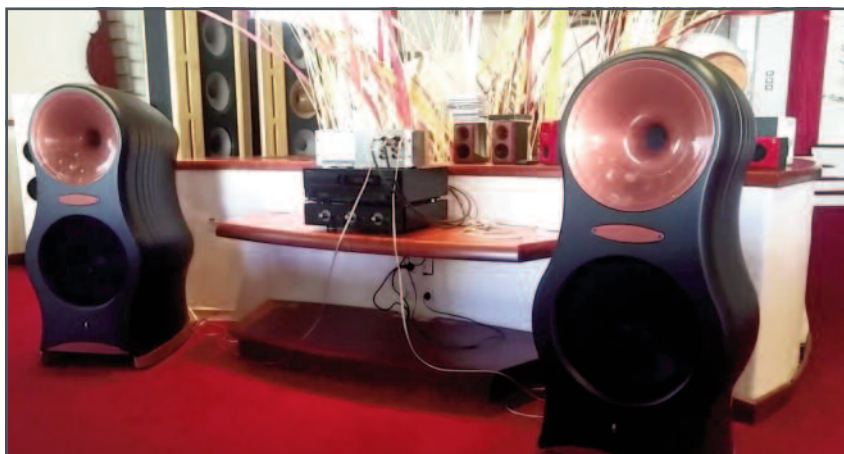
Fig. 1 I The INGV's amplifier at Zingali Acoustics S.p.A.
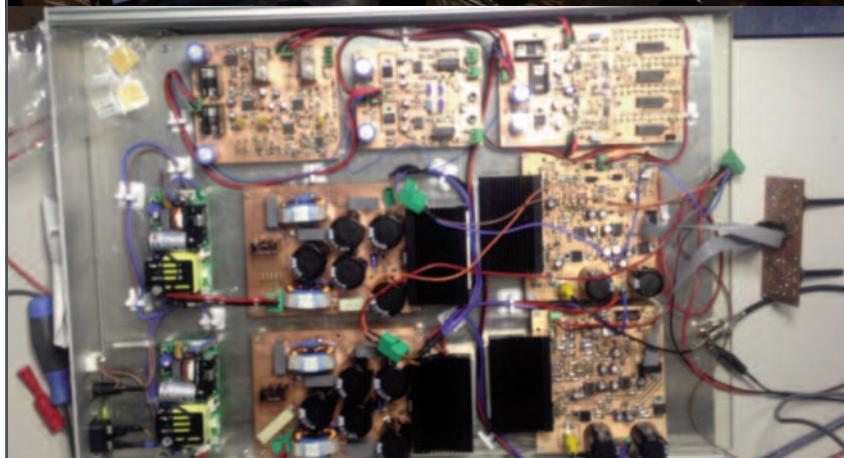
Fig. 2 I Two prototypes of the INGV's amplifier. The results got from the first one (on the top) allowed to better define the requirements of the last prototype (on the bottom), actually under construction.

A couple of years ago LNTS built and patented (Italian patent application n. 102015000071865) an audio amplifier.

Derived by the same recipes used to control the frequency response of the single-coil feedback seismometers, this amplifier showed an excellent performance even if compared with expensive high end amplifiers (Fig. 1). The idea behind this amplifier is to consider the loudspeaker like a part of the power amplifier, instead like a simple transducer. It is the same idea that allow building lp seismometers starting from short period geophones. A couple of prototypes have been built in 2017 (Fig. 2) to allow evaluating the quality of the instrument.

Deep mud sampler

G. Romeo, M. Mari

The deep mud sampler, introduced in the 2016 report is now completed. The sampler, designed in the LusiLab frame work, allows sampling fluids in high pressure (250 bars) and can operate at 250°C.

The working principle is shown in figure. 1. A hermetic chamber is filled with some inert gas (i.e. nitrogen) and the movable cover is kept in position by the gas pressure. When the external pressure (hydrostatic fluid pressure) exceeds the gas pressure, the cover opens, allowing the mud to enter and the gas (lower density) to exit. The force of the spring is negligible, respect to the forces operating in the device, but is enough to close the movable cover after the reaching of the equilibrium.

The use of the gas allows to simply tuning the operating pressure, just regulating the gas pressure. The pressure of commercially available nitrogen cylinders is about 200 atm., corresponding to (assuming a mud density of 5kg/dm^3) 400 meters deepness.

Figure 1 shows the working principle (left) and the prototype ready for use (right).

Fig. 1 | Left, the deep mud sampler principle (see text). Right, the sampler ready for operations
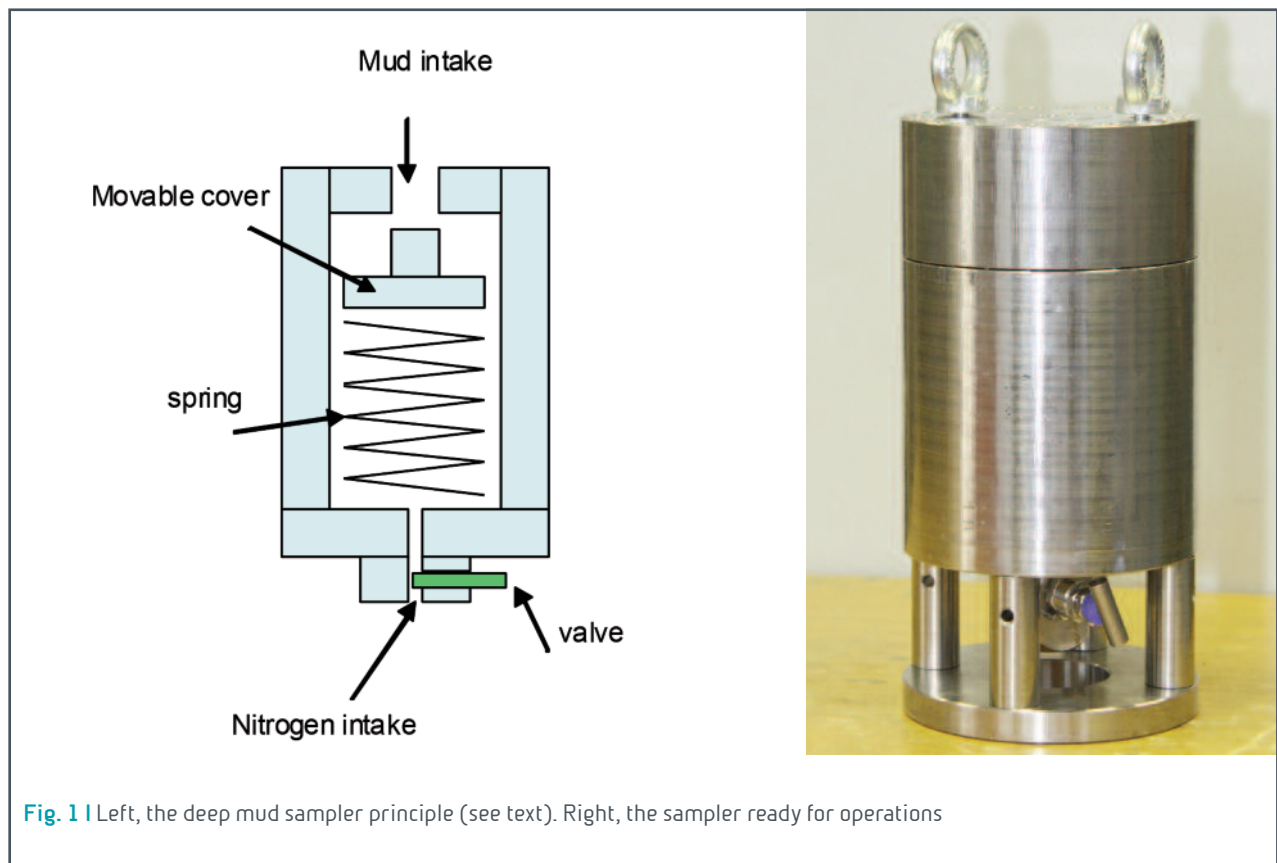
Drone mission in Indonesia

G. Romeo, G. Di Stefano

In the framework of the LusiLab project LNTS participated to the last mission on the site (Indonesia, east Java). The main mission goal was to get samples (soil and gases) from the crater area, gas concentration in the air and near the soil, thermal and visible images, contact temperature measurements.

Since an issue of the previous missions were the exact determination of the battery life and the difficult of the fpv piloting using the gimballed camera, the drone was upgraded with a telemetric energy meter, one more barometric altimeter, and a frontal camera dedicated to piloting. The drone (Fig. 1) has been flown for over 40 hours during the mission, using the LNTS equipment (described in the 2016 annual report) and hosting also gas sensor developed in La Sapienza University. This sensor, equipped with a pump, was used, with a tube and a filter, to get gas samples near the surface, far enough from the propeller's wind.

Fig. 1 | On the left the drone, equipped with the gas sensor developed by La Sapienza, connected with a 5m long pipe and a filter. On the right, up, the drone flies carrying both the INGV's and Sapienza's gases sensors. On the right, bottom, the screen of the fpv monitor during a flight.

Machine shop activity

M. Mari

Although it cannot be counted as research work, the machine shop work is essential to the conduct of all experimental investigations. Moreover the machine shop is the reference facility for the whole INGV Rome site, and performs several machining on request. Usually the machining average is of 1000 machining per year (from consumable for physics rocks experiments to more complex dedicated parts). Figures 1 and 2 show some parts (deep mud sampler and amagnetic sun position detector for magnetometers orientation in polar areas).
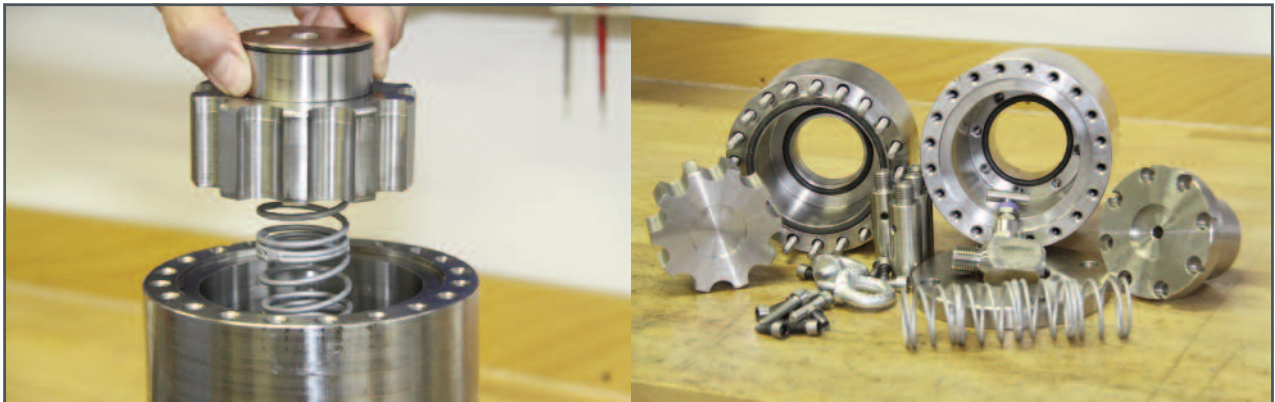
Fig. 1 I On the left, the parts built for the deep mud sampler. On the right, the deep mud sampler during the assembling (stainless steel parts).
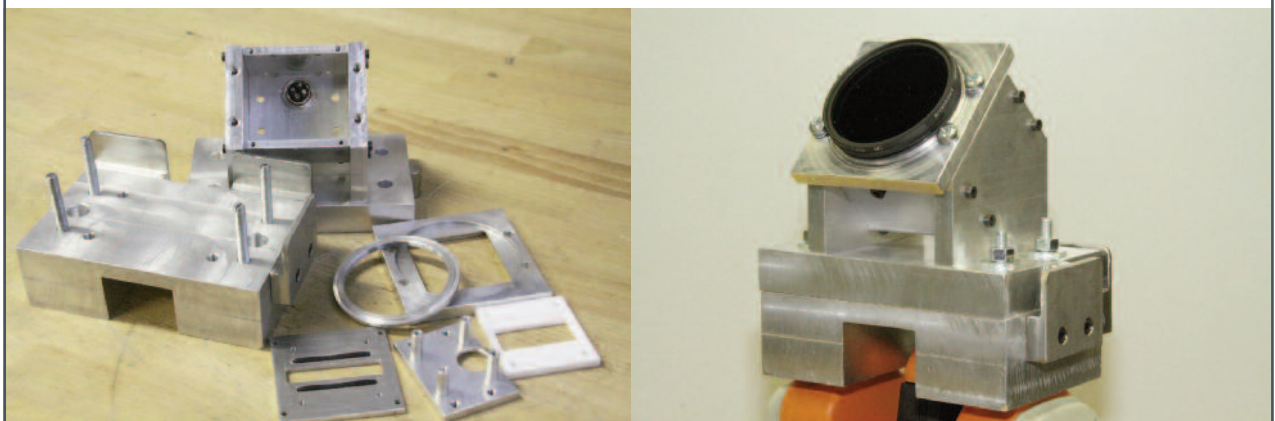
Fig. 2 I On the left the parts built for the sun detector housing, on the right the complete instrument (aluminium parts).

Rotational seismometer

G. Romeo

Fig. 1 I The force transducer on the mass on an existing seismometer measures the angular acceleration when the original mass is balanced by the additional mass
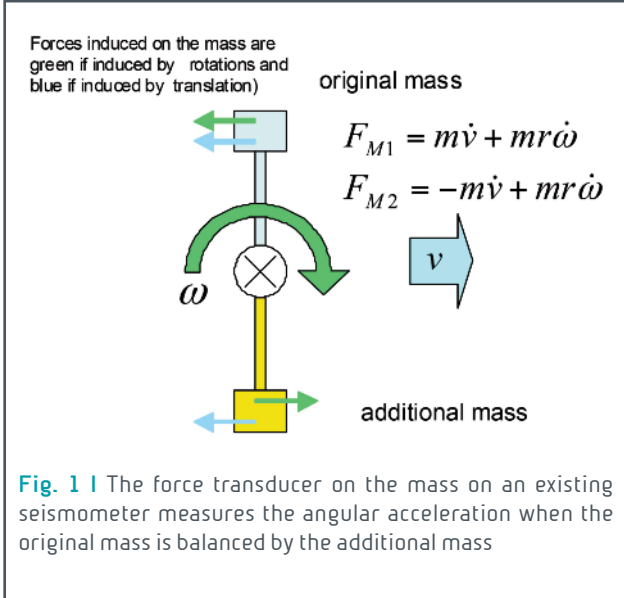
The most part of modern seismometers hold the moving sensing mass by a boom pivoted to the frame with a 0-friction bearings. For horizontal seismometers this is called garden gate suspension. But vertical seismometers use this assembly as well, adding a spring in some clever way to compensate the gravity force (i.e. Lacoste or leaf spring suspensions). This makes seismometers sensitive both to the angular and translational accelerations (Fig. 1). Obtaining a rotational seismometer starting from a horizontal seismometer is quite easy, if we add a second mass, opposite to the first respect to the pivot, to cancel the momentum induced by translations. This operation also doubles the sensitivity to the rotation. The barycentre position is easily tuneable to be on the pivot just moving the sensitive mass over the boom. This modification has been applied to a sts-1 seismometer (Fig. 2), and is actually under test.
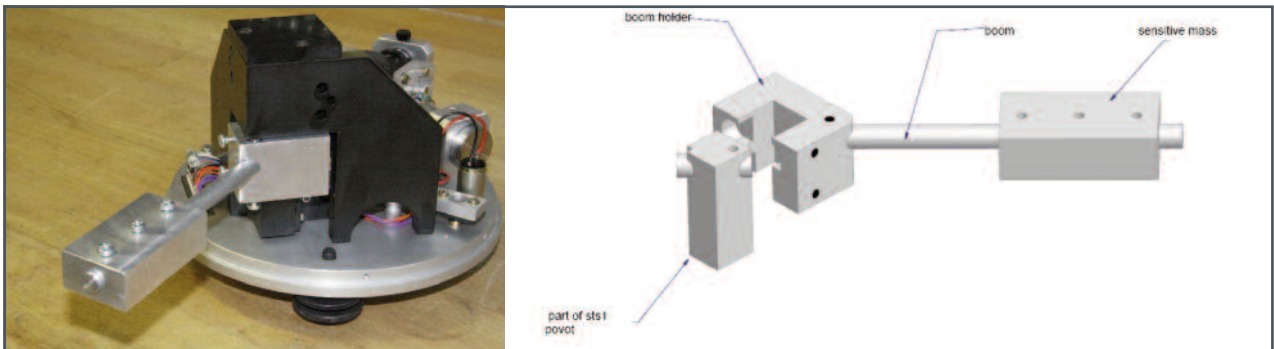
Fig. 2 I On the right, the CAD of the modification. The boom holder clamps on the sts.1 pivot and keeps the boom of the added part in line with the existing sts-1 boom.

Scientific ballooning from North Pole

A. Iarocci, G. Romeo

In December 2017 LNTS took part, together with the Physics Department of La Sapienza University, in the launch campaign for a stratospheric balloon from North Pole (Longyearbyen, Svalbard Islands) in the frame of the PNRA project (Winter long duration stratospheric balloons from Polar regions).The goal of the mission was to test the behaviour of balloon systems during a long duration flight in the cold night of the Artic winter, while the final objective is to develope a long duration flight capacity in the polar night for the benefit of important branches of science such as astronomy, cosmology, physics and atmospheric observations.

In particular LNTS provided the Flight Controller Board of the payload (the CRIUS All In One PRO unit based on Arduino platform) and developed the communication and sensors data acquisition software of the unit.

The payload (total weight of 13,5 kg) consisted of several subsystems (of the future LSPE-Swipe platform) including the power system for winter ballooning (based on Lithium batteries and aerogel insulation for thermal control) and electronics in winter stratospheric condition, in particular:

· Tracking and Termination system;

· Iridium Communication system;

· Attitude Control Sensors and Motion Processor Unit.

As we can see in Figure 1 and 2, the launch (December 17, 2017) was accomplished under arsh conditions with a temperature of -8°C, winds around 2 to 3 m/s and a heavy snow. After launched the balloon ascended nominally and reached a float altitude of 33 km in an hour and half, then moved south entering in the zone ilumina-
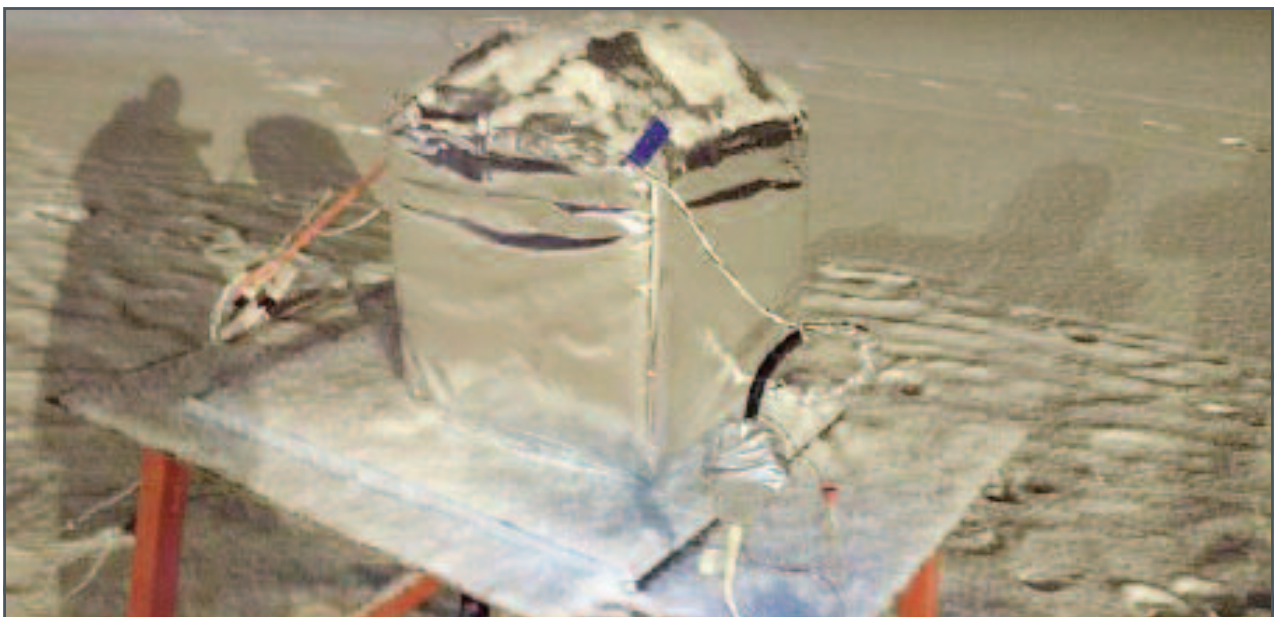

Fig. 1 I The payload before the launch

Fig. 2 | The balloon inflation

Fig. 3 | The trajectory of the flight

ted by the sun and gaining some altitude (overheating). When it returned to shadow the balloon lost altitude and then, on December 18, after 21 hours aloft the flight altitude was down to 16.4 km and so was decided to end the mission (Fig. 3).

The payload landed smoothly in an inhabited area of the north Sweden, and on December 24 a team specialized in the recovery of lost things reached the landing point and recovered the payload undemaged.

During the flight onboard sensors recorded a temperature as low as -91°C.

Temperature measurements on a mud volcano

A. Iarocci, G. Romeo
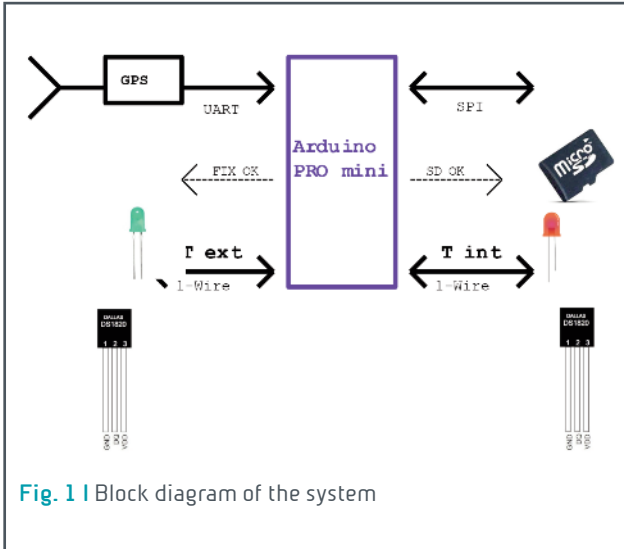
Fig. 1 I Block diagram of the system
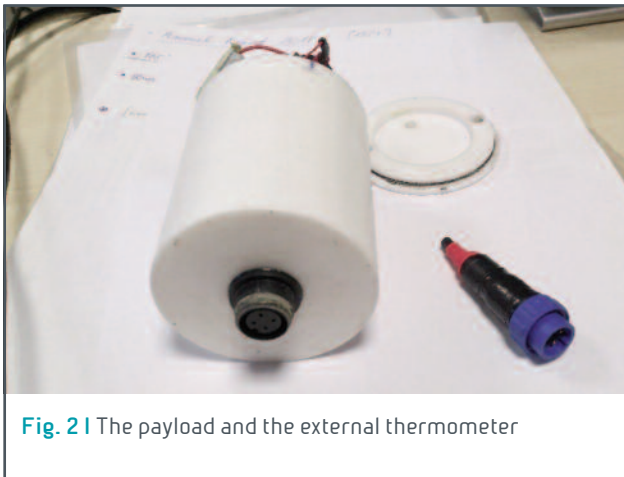
Fig. 2 I The payload and the external thermometer

LNTS designed a payload for temperature measurements in harsh environments. The payload was designed to be operated with a winch onboard of a drone. The target is to carry mud temperature measurements close to the crater of LuSi, a mud volcano in north-east of Java (Indonesia), where temperatures can reach up to 100°C. The system is composed of a microcontroller, a GPS receiver, a SD card and two digital thermometers. It is capable of:

- carry out temperature measurements up to 125°C
- acquire the geographical coordinates of the measurement point
- store data on an external memory (SD card).

The microcontroller interfaces with two digital thermometers (through the communication protocol 1-Wire). One performs the external temperature measurement; the other performs the temperature measurement inside the case containing the electronics. The chosen thermometers (DALLAS DS1820) guarantee measurements in the range -55°C / +125°C. The system is equipped with two signaling LEDs for the operator (Fig. 1). The red LED on indicates that SD card is not properly inserted in the slot or initialization procedure of the SD card did not go well; the green LED flashing indicates the fix of the GPS. The system is housed in a Teflon cylinder (no metal parts are exposed) to withstand high temperature and corrosion (Fig. 2).

The system has two operation modes: Acquisition mode and Download data mode.

The device is equipped with a sealed connector. When the temperature sensor is plugged in, the system enters the data logging mode: it is powered by the built-in rechargeable battery, and continuously records the temperature tagged with the GPS information (time and position). When a PC interface is plugged in, the system enters in the data retrieval mode and uploads the recorded data to the host PC while recharging the battery from the USB power.

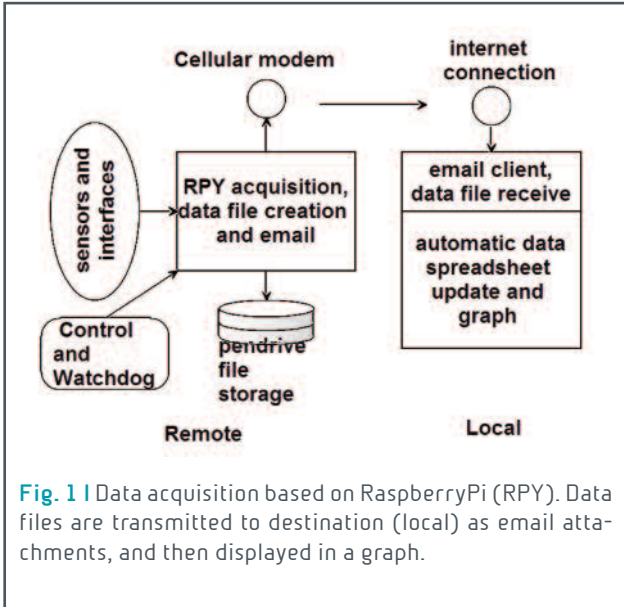# Data acquisition using a RaspberryPi computer

F. Pongetti

Fig. 1 I Data acquisition based on RaspberryPi (RPY). Data files are transmitted to destination (local) as email attachments, and then displayed in a graph.
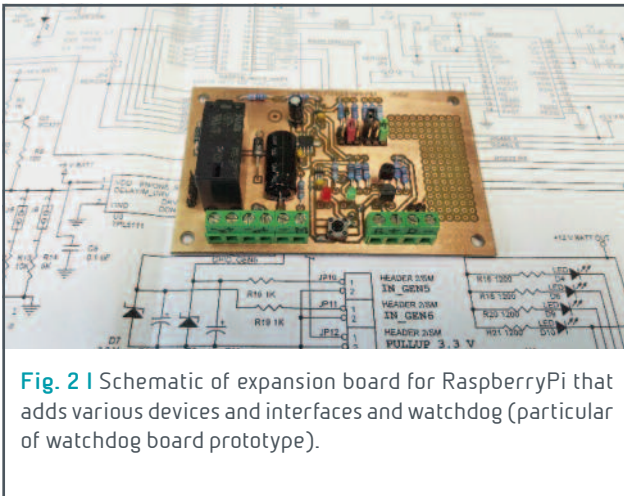

Fig. 2 I Schematic of expansion board for RaspberryPi that adds various devices and interfaces and watchdog (particular of watchdog board prototype).

The RaspberryPi (RPY) is a powerful computer in miniature format that makes available to the user an operating system, software applications, usual devices for human interaction and even some connections points to interact with its internal electronic circuit. This creates the possibility of adding interface cards for data acquisition and control to the minicomputer. In this application, the RPY is used to acquire digital temperature sensors for heat flow monitoring in volcanic area. Part of the system has been previously developed and, as an upgrade, the software for acquisition control and data transmission, via the cellular network, are now implemented (Fig. 1). It has been designed also a new expansion card for the RPY. It adds general interface hardware and some non-implemented devices in the basic RPY, such as real-time clock (RTC) and various input-output types (I/O). The card also performs automatic and independent restart of the system in case of anomalies in hardware or software operation (Watchdog) (Fig. 2).

Seminars

Di Toro G. | I terremoti, un'emergenza (anche) di comunicazione: il caso de L'Aquila | Auditorium Toniolo | Conegliano, Treviso, Italy | 23 Febbraio 2017

Di Toro G. | What is the earthquake fracture energy? | Institute of Geology, Chinese Academy of Geological Sciences | Beijing, China | 9 November 2017

Di Toro G. | What is the earthquake fracture energy? | China Earthquake Administration | Beijing, China | 14 November 2017

Di Toro G. | SHIVA: a rotary shear machine designed to investigate the seismic cycle in the lab. | Institute of Geology, Chinese Academy of Geological Sciences | Beijing, China | 9 November 2017

Di Toro G. | A close at the earthquake engine | Institute of Geology, Chinese Academy of Geological Sciences | Beijing, China | 8 November 2017

Di Toro G. | Fault weakening mechanisms in carbonate-bearing rocks at seismic deformation conditions | Institute of Geology, Chinese Academy of Geological Sciences | Beijing, China | 8 November 2017

Di Toro G. | A close at the earthquake engine | Nanyang Technological University | Singapore | 17 March 2017

Di Toro G. | A close at the earthquake engine | Chinese University of Hong Kong | HK | 15 March 2017

Romeo G. | SAPR i nostri sensi e le nostre mani dal cielo'| ITAS Garibaldi|Roma | 6 April 2017

Romeo G. | To boldly go where no man wants to go | Futuro Remoto | Napoli, Italy | 28 Maggio 2017

Romeo G., Saccorotti G. | Eppur si muove: terremoti e fenomeni geologici (con particolare attenzione alla strumentazione per rilevarli) | Lezione a due voci per Pianeta Galileo | Pisa, Italy | 27 Aprile 2017

Romeo G. | Come osserviamo la Terra | Comune di Duronia, Campobasso, Italy | 18 Ottobre 2017

Romeo G. | Trasduzioni & trasduzioni | Sede INGV | Roma, Italy

Romeo G. | Lezioni per il corso di "Metodi dell'astrofisica spaziale" | Istituto di Fisica della Sapienza | Roma, Italy | 30 Novembre, 5 -7 Dicembre 2017

Scarlato P. | L'Istituto Nazionale di Geofisica e Vulcanologia nel sistema nazionale di Protezione Civile | Università di Perugia, Italy | 22 novembre 2017

Scarlato P. | L'Istituto Nazionale di Geofisica e Vulcanologia nel sistema nazionale di Protezione Civile | Workshop La gestione delle emergenze e il sistema integrato dei soccorsi | Corso Universitario Professionale "Security & Safety Management" | Onna (L'Aquila), Italy | 5 luglio 2017

Spagnuolo E. | Fluid pressure and fault strength: insights from load controlled experiments on Fault rock | EPFL, Lausanne, CH | May 2017

Taddeucci J | Volcanic eruption styles: lights and shadows | Short Course on Melts, Eruptions and Risks | Università di Perugia | Perugia, Italy | 28-31 March 2017

Taddeucci J | Going ballistic on the fly: The in-flight dynamics of volcanic ballistic projectiles | Ludwig Maximillians Universitat of Munich | Munich, Germany | 19 July 2017

Taddeucci J | The fellowship of the synch: multiparametric experiments at active volcanoes | 4th VERTIGO workshop | São Miguel, Azores, Portugal | 26 May 2017

Training

Thesis

1. **Armeni V**. I Graduate Thesis I **Analisi termobarometrica di un sill etneo: stima delle pressioni e temperature di messa in posto del magma I Supervisors:** Mollo S. – Sapienza University of Rome I Nazzari M. - INGV – Roma1

2. **Bonechi B.** I Stage + Percorso d'eccellenza I **Preparation of cell assemblies for experiments using the multi anvil press at P-T conditions of the Earth's transition zone I Supervisors:** Stagno V. – Sapienza University of Rome I Nazzari M.–INGV Roma1

3. **Curzi M.** I Stage I **Influence of bitumen on Seismic waves velocity I Supervisors:** Tesei T. - INGV Roma1

4. **Dominijanni S.** I Stage I **Preparation of cell assemblies for experiments using the multi anvil press at conditions of the Earth's upper mantle I Supervisors:** Stagno V. – Sapienza University of Rome I Nazzari M.– INGV Roma1

5. **Geremia D.** I Master Thesis I **Relazione tra le proprietà petrofisiche e la risposta sismica della formazione di Bolognano. Modellazione ed analisi di AVO (Amplitude vs Offset) sintetici I Supervisors:** Trippetta F., Lipparini L. I Sapienza University of Rome I Tesei T. - INGV Roma1

6. **Loemba T.** I Master Thesis I **Ricostruzione della profondità del livello di magma nel condotto e del diametro di bocche eruttive da video ad alta velocità girati sull'Etna e lo Stromboli I Supervisors:** Taddeucci J., INGV I Palladino D.M. Sapienza University of Rome

7. **Luciani N.** I Stage +Master Thesis I **Ca rich magmas: Molten carbonate plus solid silicate or Molten silicate plusSolid carbonate? The case study of pleistocene Polino volcanic rocks (central Italy) I Supervisors:** Lustrino M., Stagno V. – Sapienza University of Rome I Masotta M. –University of Pisa.

8. **Manzi M.** I Magistrale Thesis I **Caratterizzazione meccanica di un fronte di cava in rocce carbonatiche mediante esperimenti di laboratorio I Supervisors:** Collettini C., Scuderi M.M. I Sapienza University of Rome

9. **Narzisi S.** I Stage + Master Thesis I **Experimental investigation of the chemical interaction between calcite and basic-ultrabasic melts: implications for wall rock-magma interaction and the origin of CO^2-rich magmas I Supervisors:** Lustrino M., Stagno V. – Sapienza University of Rome

10. **Rossi R.** I Stage I **Tracking of volcanic bombs from high-speed video I Sapienza University of Rome I Supervisor:** Taddeucci J. - INGV Roma1

11. **Tersigni C.** I Bachelor Thesis I **Tracking of volcanic bombs from high-speed video I Supervisors:** Taddeucci J., INGV Roma1 I Palladino D.M. Sapienza University of Rome

Mollo S. - Stagno V. I **4 Visits to the HPHT lab by 12 students enrolled in the Experimental Petrology applied to Igneous Processes I** Sapienza University of Rome

PhD

1. **Aretusini S**. | PhD | Frictional processes of clay-rich gouges in megathrust and landslide decollement environments | **Supervisors:** Di Toro G. - University of Manchester, Manchester, UK | Spagnuolo E. - INGV Roma1

2. **Caruso M.** | PhD | The Earth's deep volatile cycle over geological time as function of mantle redox state, pressure and temperature | **Supervisors:** Stagno V. –Sapienza University of Rome | Scarlato P. – INGV Roma1

3. **Demurtas M.** | PhD | Seismogenic carbonate-built normal faults: structure and deformation processes.| **Supervisors:** Di Toro G., Fondriest M.- Manchester University. UK | Smith S.A.F. - Otago University, NZ

4. **Di Stefano F.** | PhD | Olivine-clinopyroxene-plagioclase-melt cation exchange reactions as a tool for understanding magma dynamics | **Supervisors:** Mollo S. - Sapienza University of Rome | Scarlato P. - INGV Roma1

5. **Forni F.** | PhD | Caldera collapses and evolutionary trends: the case of Phlegraean Fields volcanic system | **Supervisors:** Bachman O. – ETH Zurigo | De Astis G. INGV Roma 1

6. **Giacomel P.** | PhD | Laboratory investigation on the frictional properties of basalts interacting with H_2O- and CO^2-rich fluids and implications for CO_2 storage | **Supervisors:** Collettini C. - Sapienza University of Rome | Spagnuolo E. – INGV Roma1 | Di Toro G. – Padua University

7. **Giorgetti C.** | PhD | Caratterizzazione strutturale e meccanica in faglie in misture di carbonati e fillosilicati | **Supervisors:** Collettini C., Scuderi M.M. - Sapienza University of Rome.

8. **Haywards K.** | PhD | Seismic slip processes in crustal and subduction zone settings: laboratory and field study **Supervisors:** Cox S., Hermann J., Kennett B. – ANU, Australia | Di Toro G. – University of Manchester, UK | Pennachioni G. – Padua University, IT | Spagnuolo E. - INGV Roma 1

9. **Mercuri M.** | PhD | Struttura e comportamento meccanico di zone di faglia carbonatiche in presenza di plaghe argillose. | **Supervisors:** Collettini C., Carminati E. – Sapienza University of Rome.

10. **Nazzari M.** | PhD | Unravelling the effect of undercooling on (dis)equilibrium textures and compositions ofbasaltic magmas | **Supervisors:** Mollo S. - Sapienza University of Rome

11. **Ruggieri R.** | PhD | Multidisciplinary approach for a study about the interaction between fluids and rocks in crustal processes | **Supervisors:** Trippetta F., Scuderi M. - Sapienza University of Rome | Di Stefano G. - INGV Roma1

12. **Tecchiato V.** | PhD | Il ruolo dei mush cristallini nei processi di differenziazione dei magmi calcalcalini: caratteri giaciturali, petrografici, geochimici e modellistica sperimentale | **Supervisors:** Gaeta M., Mollo S. - Sapienza University of Rome

13. **Tournigand P.Y.** | PhD | Field-based study of volcanic ash via visible and thermal high-speed imaging of explosive eruptions | **Supervisors:** Palladino D.M. - Sapienza University of Rome | Taddeucci J. - INGV Roma1

14. **Salvatore V.** | PhD | Strombolian explosions: relationships between the conduit system and the resulting explosive activity at the vents | **Supervisors:** Palladino D.M. - Sapienza University of Rome | Taddeucci J. - INGV Roma1

10I VISITING SCIENTISTS

Agliardi F. I Università degli Studi Milano Bicocca, Italy I Milano, Italy

Brenna M. I University of Otago, New Zealand I Otago

Fabbrì O. I University of Franche-Comté I Besancon, France

Marone C. I Penn State University I Pennsylvania, USA

Passelegue F. I University of Manchester I Manchester, UK

Vannucchi P. I Royal Halloway I University of London I London, UK

Veedu D. I Earth Observatory of Singapore I Singapore

Violay M. I Ecole Politechnique Federale de Lausanne I Lausanne, Swiss

Ubide T. I University of Queensland I Brisbane, Australia

11I MEETINGS, WORKSHOP and SYMPOSIA

Tectonics and Structural Geology Annual Meeting | Liverpool, UK | January.

Aretusini S., Plumper O., Spagnuolo E., Di Toro G.
Seismic slip on clay nanofoliation

Demurtas M., Smith S.A.F., Spagnuolo E., Fondriest M., Di Toro G.
Coseismic origin of foliated cataclasites and their preservation in the geological record

Hughes A., Kendrick J., Lavalleè Y., Di Toro, G.
Understanding the role of friction in volcanic environments

Fondriest M., Mitchell T., Vassallo M., Di Giulio G., Balsamo F., Passelegue F., Pischiutta M., Di Toro G.
Multi-scale velocity structure of an active seismogenic normal fault zone

Workshop on Earthquake mechanics: in situ, in lab and through models | La Sapienza University of Rome, Roma, IT | February

Spagnuolo E.
INVITED Fluid pressure and fault strength: insights from load controlled experiments on Fault rocks.

Third DCO International Science Meeting | St Andrews, Scotland | 23–25 March

Stagno V., Kono Y, Stopponi V., Scarlato P., Lustrino M., Irifune T.
An experimental study on the origin and emplacement of carbonate-rich melts through time.

Astarte Final Meeting | Baleares Island | April

Murphy S., Scala A., Romano F., Spagnuolo E., Herrero A., Tonini R., Piatanesi A., Lorito S., Di Toro G., Aretusini S., Festa G., Nielsen S.
Complexity of earthquake rupture dynamics and tsunami hazard applications.

EGU General Assembly | Wien, Austria | 23-28 April

Aretusini S., Plumper O., Spagnuolo E., Di Toro G.
Seismic slip on clay nano-foliation.

Cigala V., Kueppers U., Peña Fernández J.J., Sesterhenn J., Taddeucci J., Dingwell D.B.
The temporal evolution of pyroclast ejection velocity and exit trajectory, a laboratory case study.

Cornelio C., Violay M., Spagnuolo E., Di Toro G.
Effect of fluid viscosity on fault frictional behavior.

Del Bello E., Taddeucci J., Merrison J., Alois S., Iversen J.J., Scarlato P.
Parameterization of volcanic ash remobilization by wind-tunnel erosion experiments.

Demurtas M., Smith S.A.F., Fondriest M., Spagnuolo E., Di Toro G.
Crystallographic control on early stages of cataclasis in carbonate fault gouges.

Fondriest M., Mitchell T., Vassallo M., Di Giulio G., Balsamo F., Passelegue F., Pischiutta M., Di Toro G.
3D multi-scale velocity structure of an active seismogenic normal fault zone (Central Apennines, Italy).

Forni F., Degruyter W., Bachmann O., De Astis G., Mollo S.
Long-term magmatic evolution at the CampiFlegrei caldera (Southern Italy).

Giacomoni P.P., Coltorti M., Mollo S., Ferlito C., Braiato M., Scarlato P.
Petrological study of the products of 2011-2012 paroxysmal eruptions: new insight of the intensive variables of the Mt. Etna magmatic system.

Hughes A., Kendrick J., Yan Lavallée Y., Hornby A., Di Toro G..
Volcanic rock properties control sector collapse events.

Mueller S.B., Kueppers U., Wadsworth F.B., Ayris P.M., Casas A. S., Cimarelli C., Ametsbichler J., Delmelle P., Taddeucci J., Jacob M., Dingwell D.B.
Deposition or not? The fate of volcanic ash after aggregation processes.

Murphy S., Di Toro G., Lorito S., Romano F., Spagnuolo E., Festa G., Aretusini S., Nielsen S., Piatanesi A.
Tsunamigenic earthquake simulations with experimentally derived friction laws.

Passalegue F., Schubnel A., Di Toro G.
Crystal plastic earthquakes in dolostones.

Spagnuolo E., Violay M., Nielsen S., Cornelio C., Di Toro G.
Susceptibility of experimental faults to pore pressure increase: insights from load-controlled experiments on calcite-bearing rocks.

Tisato N., Cordonnier B., De Siena L., Lavier L., Di Toro, G.
Torque controlled rotary-shear experiments reveals pseudotachilites formation-dynamics and precursor events.

Tournigand P.Y., Peña Fernandez J.J., Taddeucci J., Perugini D., Sesterhenn J.
Fractal analysis: A new tool in transient volcanic ash plume characterization.

Traforti A., Massironi, M., Di Toro G., Zampieri D.
Reactivation of pre-existing mechanical anisotropies during polyphase tectonic evolution: slip tendency analysis as a tool to constrain mechanical properties of rocks.

Traforti A., Mari G., Carli C., Demurtas M., Massironi M., Di Toro G.
VNIR reflectance spectroscopy of natural carbonate rocks: implication for remote sensing identification of fault damage zones.

Trippetta F., Ruggieri R., Geremia D., Brandano M.
The influence of hydrocarbons in changing the mechanical and acoustic properties of a carbonate reservoir: implications of laboratory results on larger scale processes.

IAVCEI General Assembly | Portland, Oregon USA | August

Del Bello E., Taddeucci J., Merrison J.P, Alois S., Iversen J. J.
Modelling volcanic ash resuspension by environmental wind tunnel experiments: the effect of grain size and humidity.

Forni F., Degruyter W., Bachmann O., De Astis G., Mollo S.
Long-term magmatic evolution at the CampiFlegrei caldera (Southern Italy).

Houghton B., Orr T., Mintz B., Taddeucci J., Del Bello E., Gaudin D., Kueppers U., Carey R., Edmonds M.
Transitions in style and intensity during Strombolian and Hawaiian eruptions: examples from Kīlauea in 2011-2017.

Laeger K., Andronico D., Petrelli M, Taddeucci J., Misiti V., Scarlato P., Cimarelli C., Del Bello E.
Constraining the magma dynamics during the Eyjafjallajökull 2010 eruption by high-resolution geochemical mapping.

Laeger K., Petrelli M., Andronico D., Misiti V., Scarlato P., Cimarelli C., Taddeucci J., del Bello E., Perugini D.
High-resolution geochemistry of volcanic ash highlights complex magma dynamics during the Eyjafjallajökull 2010 eruption.

Mueller S., Helo C., Keller F., Taddeucci J., Castro J.
The Atmosphere Strikes Back: Rapid Remelting of Ash by Volcanic Lightning in the Laboratory.

Scarlato P., Del Bello E., Spina L., Gaudin, D., Taddeucci J.
Exploring the variability of Strombolian explosions at Batu Tara volcano (Indonesia) using infrasound and high speed imagery.

Taddeucci, J., Alatorre Ibargüengoitia, M. A., Cruz Vázquez, O., Del Bello, E., Scarlato, P., Ricci, T.
The in-flight dynamics of Volcanic Ballistic Projectiles: An high-speed imaging perspective.

Tournigand P., Taddeucci J., Gaudin D., Peña Fernández J., Perugini D., Del Bello E., Scarlato P., Sesterhenn J.
Initial transient ash plume dynamics: new insights from combined highspeed imagery, computer vision techniques and fractal analysis.

Truby J.M., Llewellin E.W., Taddeucci J., Dungan M.A.
Mobilizing a magma mush through bubble growth – rheological triggering of the largest eruptions.

Turner N., Houghton B., Perroy R., Taddeucci J., Bisson M.
Volcanic hazard monitoring with a small unmanned aerial system: structure-from- motion based studies of lava flows and explosive volcanism.

GOLDSCHMIDT 2017 | Paris, France| August

Caruso M., Stagno V.
The Transition from Carbonatitic to Carbonate-Silicate Magmas in Carbonated Eclogite Rocks as Function of Pressure, Temperature and Oxygen Fugacity.

Greaux S., Stagno V., Irifune T.
Melting Temperature of Tagish Lake (CI2) Meteorite from 5 to 30 GPa.

Stagno V., Kono Y., Greaux .S, Kebukawa Y., Stopponi V., Scarlato P., Lustrino M., Irifune T.
From Carbon in Meteorites to Carbonatite Rocks on Earth.

Stagno V., McCammon C.A., Cerantola V., Andreozzi G.B., Carus. M., Arimoto T. Irifune T.
Do Fe-Bearing Minerals Control the Deep Carbon Cycle in the Interior of the Earth?

Geosciences: a tool in a changing world | Pisa, Italy | Settembre

Giuliani L., Iezzi G., Vetere F., Nazzari M., Mollo S., Misiti V., Ventura G., Cavallo A., Behrens H.
Textural evolution of plagioclase, clynopiroxene and spinel from a basaltic melt as a function of cooling rate.

Giuliani L., Iezzi G., Vetere F., Nazzari M., Mollo S., Misiti V., Ventura G., Cavallo A., Behrens H.
Chemical variations of phases grown from a basaltic melt cooled at variable rates.

Nazzari M., Mollo S., Blundy J.D., Giacomoni P., Scarlato P., Coltorti M., Langone A., Andronico D.
Clinopyroxene-melt element partitioning during interaction between trachybasaltic magma and siliceous crust: Clues from quartzite enclaves at Mt. Etna volcano.

Pontesilli A., Masotta M., Nazzari M., Armienti P., Mollo S., Scarlato P., Brenna M.
Experimental observation of extremely rapid clinopyroxene growth in a trachybasaltic melt: Clues on phenocryst crystallization kinetics in naturally cooled magmas.

12th International Symposium on Crystallization in Glasses and Liquids | Segovia, Spain | September

Giuliani L., Vetere F., Iezzi G., Misiti V., Nazzari M., Mollo S., Ventura G., Behrens H., Cavallo A.
GFA of natural silicate melts: a general reappraisal.

SIMP-SGI-AIV-SoGeI "Geosciences: a tool in a changing world" | Pisa, Italy | Settembre

Stagno V., Bonechi B., Greaux S., Caruso M., Scarlato P.
The stability of an eclogitic clinopyroxene in the Earth's mantle: an experimental investigation.

Stagno V., Caruso M., Dominijanni S.
The speciation of carbon within eclogite rocks as function of pressure, temperature and oxygen fugacity.

Carbon forms, paths, and processes in the Earth | Villa del Grumello, Como, Italy | October

Caruso M., Stagno V.
The transition from carbonatitic to carbonate-silicate magmas in carbonated eclogite rocks as function of pressure, temperature, and oxygen fugacity.

Stagno V.
Carbon forms, paths, and processes in the Earth.

Workshop of Great Earthquakes | College du France, Paris | November

Di Toro G.
INVITED. The geology, physics and chemistry of earthquakes hosted in carbonate-built rocks.

Frontiers in Studies of Earthquakes and Faults | SUSTech, Shenzhen, China | November.

Spagnuolo E., Violay M., Passelegue F., Nielsen S., Di Toro G.
An experimental overview of the seismic cycle.

American Geophysical Union Fall Meeting | New Orleans, USA | December

Aretusini S., Plumper O., Passelegue F., Spagnuolo E., Di Toro G.
Seismic slip on clay nano-foliation.

Bistacchi A., Mittempergher S., Di Toro G., Smith S.A.F., Garofalo P.
The hydraulic structure of the Gole Larghe Fault Zone (Italian Southern Alps) through the seismic cycle.

Fabbri O., Passelegue F.X., Leclere H., Spagnuolo E., Magott R., Etienne L., Di Toro G.
Frictional processes of bimaterial interfaces at seismic slip rates.

Fondriest M., Demurtas M., Bistacchi A., Balsamo F., Storti F., Valoroso L., Di Toro.
Anatomy of an active seismic source: the interplay between present-day seismic activity and inherited fault zone architecture (Central Apennines, Italy).

Guerin-Marthe S., Nielsen S.B., Giani S., Bird R., Di Toro G., 2017.
Earthquake Nucleation Size: Evidence of Loading Rate Dependence in Laboratory Faults.

Passelegue F.X., Aubry J., Nicolas A., Fondriest M., Schubnel A., Di Toro G.
INVITED. Crystal plastic earthquakes in dolostones: from slow to fast ruptures.

Passelegue F., Tielke J., Mecklenburgh J., Di Toro G.
Experimental ductile.

1. *Amoroso S., Milana G., Rollins K.M., Comina C., Minarelli L., Manuel M.R., Monaco P., Franceschini M., Anzidei M., Lusvardi C., Cantore L., Carpena A., Casadei S., Cinti F.R., Civico R., Cox B.R., De Martini P.M, Di Giulio G., Di Naccio D., Di Stefano G., Facciorusso J., Famiani D., Fiorelli F., Fontana D., Foti S., Madiai C., Marangoni V., Marchetti D., Marchetti S.L., Martelli L., Mariotti M., Muscolino E., Pancaldi D., Pantosti D., Passer F., Pesci A., Romeo G., Sapia V., Smedile A., Stefani M., Tarabusi G., Teza G., Vassallo M., Villani F.*
The first Italian blast-induced liquefaction test (Mirabello, Emilia-Romagna, Italy): description of the experiment and preliminary results
Annals of Geophysics l ISSN: 2037-416X, 60(5), S0556; doi: 10.4401/ag-7415.

2. *Aretusini S., Spagnuolo E., Mittempergher S., Plumper O., Gualtieri A., Di Toro G.*
Production of nanoparticles during experimental deformation of smectites and implications for seismic slip
Earth and Planetary Science Letters l vol. 463, pp. 221-231.

3. *Del Bello E., Taddeucci J., de' Michieli Vitturi M., Scarlato P., Andronico D., Scollo S., Kueppers U., Ricci T.*
Effect of particle volume fraction on the settling velocity of volcanic ash particles:
insights from joint experimental and numerical simulations
Scientific Reports l l7, 39620.

4. *Di Piazza A., Del Bello E., Mollo S., Vona A., Alvarado G.E, Masotta M.*
Like a cannonball: origin of dense spherical basaltic ejecta
Bulletin of Volcanology l 79:37.

5. *Ferré E.C., Meado A.L., Geissman J., Di Toro G., Spagnuolo E., Ueda T., Ashwal L.D., Deseta N., Andersen T.B., Filiberto J., Conder J.A.*
Earthquakes in the mantle? Insights from rock magnetism of pseudotachylytes
Journal of Geophysical Research l 10.1002/2017JB014618, pp.1-17.

6. *Fondriest M., Doan M.L., Aben F., Fusseis F., Mitchell T., Voorn M., Secco M., Di Toro G.*
Static versus dynamic fracturing in shallow carbonate fault zones
Earth and Planetary Science Letters l vol. 461, pp. 8-19.

7. *Gaudin D., Taddeucci J., Scarlato P., Harris A., Bombrun M., Del Bello E., Ricci T.*
Characteristics of puffing activity revealed by ground-based, thermal infrared imaging: the example of Stromboli Volcano (Italy)
Bulletin of Volcanology l 79(3), 24.

8. *Gaudin D., Taddeucci J., Scarlato P., Del Bello E., Ricci T., Orr T., Houghton B., Harris A., Rao S., Bucci A.*
Integrating puffing and explosions in a general scheme for Strombolian-style activity,
Journal of Geophysical Research l 122, 1860–1875.

9. *Gaudin D., Ricci T., Finizola A., Delcher E., Alparone S., Barde-Cabusson S., Brothelande E., Di Gangi F., Gambino S., Inguaggiato S., Milluzzo V., Peltier A., Vita F.*
Heat flux-based strategies for the thermal monitoring of sub-fumarolic areas: Examples from Vulcano and La Soufrière de Guadeloupe
Journal of Volcanology and Geothermal Research l doi:10.1016/j.jvolgeores.2017.06.021.

10. *Gresse M., Vandemeulebrouck J., Byrdina S., Chiodini G., Revil A., Johnson T.C., Ricci T., Vilardo G., Mangiacapra A., Lebourg T., Grangeon J., Bascou P., Metral L.*
Three-Dimensional Electrical Resistivity Tomography of the Solfatara Crater (Italy):
Implication for the Multiphase Flow Structure of the Shallow Hydrothermal System
Journal of Geophysical Research – Solid Earth l doi:10.1002/2017JB014389.

11. *Iezzi G., Elbrecht A.L., Davis M., Vetere F., Misiti V., Mollo S., Cavallo A.*
Glass stability (GS) of chemically complex (natural) sub-alkaline glasses
Journal of non Crystalline Solids l 477, 21-30.

12. *Kuo L.W., Di Felice F., Spagnuolo E., Di Toro G., Song S.R., Aretusini S., Li H., Suppe J., Si J., Wen C.Y.*
Fault gouge graphitization as evidence of past seismic slip.
Geology l 10.1130/G39295.1.

13. *Laeger K., Petrelli M., Andronico D., Misiti V., Scarlato P., Cimarelli C., Taddeucci J., Del Bello E., Perugini D.*
High-resolution geochemistry of volcanic ash highlights complex magma dynamics during the Eyjafjallajökull 2010 eruption
American Mineralogist I 102(6), 1173-1186.

14. *Lanzafame G., Iezzi G., Mancini L., Lezzi F., Mollo S., Ferlito C.*
Solidification and Turbulence (Non-laminar) during Magma Ascent: Insights from 2D and 3D Analyses of Bubbles and Minerals in an Etnean Dyke
Journal of Petrology I 58, 1511–1533.

15. *Linde N., Ricci T., Baron L., Shakas A., Berrino G.*
The 3-D structure of the Somma-Vesuvius volcanic complex (Italy) inferred from new and historic gravimetric data
Scientific Reports I doi:10.1038/s41598-017-07496-y.

16. *Mollo S., Hammer J.E.*
Dynamic crystallization in magmas
EMU Notes in Mineralogy I 7, 1–46.

17. *Mollo S., Tuccimei P., Galli G., Iezzi G., Scarlato P.*
The imprint of thermally-induced devolatilization phenomena on radon signal: Implications for the geochemical survey and public health in volcanic areas
Geophysical Journal International I 211, 558-571.

18. *Mollo S., Vetere F., Beherens H., Tecchiato V., Langone A., Scarlato P., Perugini D.*
The effect of degassing and volatile exsolution on the composition of a trachybasaltic melt decompressed at slow and fast rates
Periodico di Mineralogia I 86, 185-197.

19. *Mollo S., Blundy, J.D., Giacomoni P., Nazzari M., Scarlato P., Coltorti M., Langone A., Andronico D.*
Clinopyroxene-melt element partitioning during interaction between trachybasaltic magma and siliceous crust: Clues from quartzite enclaves at Mt. Etna volcano
Lithos I 284-285, 447–461.

20. *Montanaro C., Mayer K., Isaia M., Gresse B., Scheu T.I., Yilmaz J., Vandemeulebrouck J., Ricci T., Dingwell D.B.*
Hydrothermal activity and subsoil complexity: implication for degassing processes at Solfatara crater, CampiFlegrei caldera
Bulletin of Volcanology I doi:10.1007/s00445-017-1167-z.

21. *Pischiutta M., Fondriest M., Demurtas M., Magnoni F., Di Toro G., Rovelli A.*
Structural control on the directional amplification of seismic noise (Campo Imperatore, central Italy)
Earth and Planetary Science Letters I vol. 471, pp. 10-18.

22. *Rempe M., Smith S., Mitchell T., Hirose T., Di Toro G.*
The effect of water on strain localization in calcite fault gouge sheared at seismic slip rates
Journal of Structural Geology I vol. 97, pp. 104-117.

23. *Sagy M., Tesei T., Collettini C.*
Fault-surface geometry controlled by faulting mechanisms: Experimental observations in limestone faults
Geology I doi:10.1130/G39076.1 I P.

24. *Scarlato P., Mollo S., Del Bello E., von Quadt A., Richard J.B., Gutierrez E., Martinez-Hackert B., Papale P.*
The 2013 eruption of Chaparrastique volcano (El Salvador): Effects of magma storage, mixing, and decompression
Chemical Geology I 448, 110-122.

25. *Scuderi M.M., Collettini C., Viti C., Tinti E., Marone C.*
Evolution of Shear Fabric in Granular Fault Gouge From Stable Sliding to Stick-Slip and Implications for Fault Slip Mode
Geology I doi 10.1130/G39033.1.

26. *Scuderi M.M., Collettini C., Marone C.*
Frictional stability and earthquake triggering during fluid pressure stimulation of an experimental fault.
Earth and Planetary Science Letters. I 477, 84-96.

27. *Smeraglia L., Bettucci A., Billi A., Carminati E., Cavallo A., Di Toro G., Natali M., Passeri D., Rossi M., Spagnuolo E.*
Microstructural evidence for seismic and aseismic slip along clay bearing, carbonate faults.
Journal of Geophysical Research I 10.1002/2017JB014042, pp. 1-21.

28. *Smeraglia L., Billi A., Carminati E., Cavallo A., Di Toro G., Spagnuolo E., Zorzi F.*
Ultra-thin clay layers facilitate seismic slip in carbonate rocks.
Nature Scientific Reports I pp. 1-10, vol. 7: 664, DOI:10.1038/s41598-017-00717-4.

29. *Smith S.A.F., Tesei T., Scott J.M., Collettini C.*
Reactivation of normal faults as high-angle reverse faults due to low frictional strength: Experimental data from the Moonlight Fault Zone, New Zealand
Journal of Structural Geology I 105, 34-43.

30. *Smith S.A.F., Griffith J.R., Fondriest M., Di Toro G.*
Coseismic foliations" in gouge and cataclasite: experimental observations and consequences for interpreting the fault rock record
In: "Fault-zone Dynamic Processes: Evolution of Fault Properties During Seismic Rupture"
Eds. M. Thomas, T. Mitchell, H. Bath, Geophysical Monograph Series Vol. 227
(American Geophysical Union Special Volume, Washington D.C., USA) I pp. 81-102.

31. *Spina L., Taddeucci J., Cannata A., Sciotto M., Del Bello E., Scarlato P., Kueppers U., Andronico D., Privitera E., Ricci T., Pena-Fernandez J., Sesterhenn J., Dingwell D. B*
Time-seriesanalysis of fissure-fed multi-ventactivity: a snapshot from the July 2014 eruption of Etna volcano (Italy)
Bulletin of Volcanology I 79(7), 51.

32. *Taddeucci J., Alatorre-Ibargüengoitia M. A., Cruz-Vázquez O., Del Bello E., Scarlato P., Ricci T.*
In-flightdynamics of VolcanicBallisticProjectiles
Reviews of Geophysics I 55, 675–718.

33. *Tesei T, Carpenter B.M., Giorgetti C, Scuderi M.M.,SagyA., ScarlatoP., Collettini C*
Friction and scale-dependent deformation processes of large experimental carbonate faults Nature
Journal of Structural Geology I 100, 12-13.

34. *Trippetta F., Carpenter B.M., Mollo S., Scuderi M.M., Scarlato P., Collettini C.*
Physical and Transport Property Variations Within Carbonate- Bearing Fault Zones:
Insights From the Monte Maggio Fault (Central Italy)
G3 I doi10.1002/2017GC007097.

35. *Turner N., Houghton B., Taddeucci J., von der Lieth J., Kueppers U., Gaudin D., Ricci T., Kim K., Scarlato P.*
Drone peers into open volcanic vents
Eos I doi:10.1029/2017EO082751.

36. *Vannucchi P., Spagnuolo E., Ujiie K., Aretusini S., Di Toro G., Nielsen S., Tsutsumi A.*
Past seismic slip-to-the-trench recorded in Central America megathrust
Nature Geoscience I 10.1038/s41561-017-0013-4.

37. *Yao S., Iezzi G., Della Ventura G., Bellatreccia F., Petibois C., Marcelli A., Nazzari M., Lazzarin F., Di Gioacchino M, Petrarca C.*
Mineralogy and textures of riebeckitic asbestos (crocidolite): the role of single versus agglomerated fibres in toxicological experiments
J. Hazard. Mater I 340, 2017 (472–485).

In press

1. *Mollo S., Tuccimei P., Soligo M., Galli G., Scarlato P.*
   Advancements in understanding the radon signal in volcanic areas: A laboratory approach based on rock physico-chemical changes
   In Integrating Disaster Science and Management. Editors: Pijush Samui, Dookie Kim, and Chandan Ghosh.
   Publisher: Elsevier.

2. *Di Stefano G., Romeo G., Mazzini A, Iarocci A., Hadi S., Pelphrey S.*
   The Lusi drone: A multidisciplinary tool to access extreme environments
   Marine and Petroleum Geology I in press, DOI 10.1016/j.marpetgeo.2017.07.006.

3. *Di Felice F., Mazzini A., Di Stefano G., Romeo G.*
   The Lusi drone: A multidisciplinary tool to access extreme environments
   Marine and Petroleum Geology I in press, DOI 10.1016/j.marpetgeo.2017.10.025.

Patent

Inventors: *Caramelli A.,, Bruno M., Romeo G., Savio G.*
Remittance for multi-rotor vehicles with remote control
Patent application filing No. 812817000098448 of 01/09/2017 entitled.
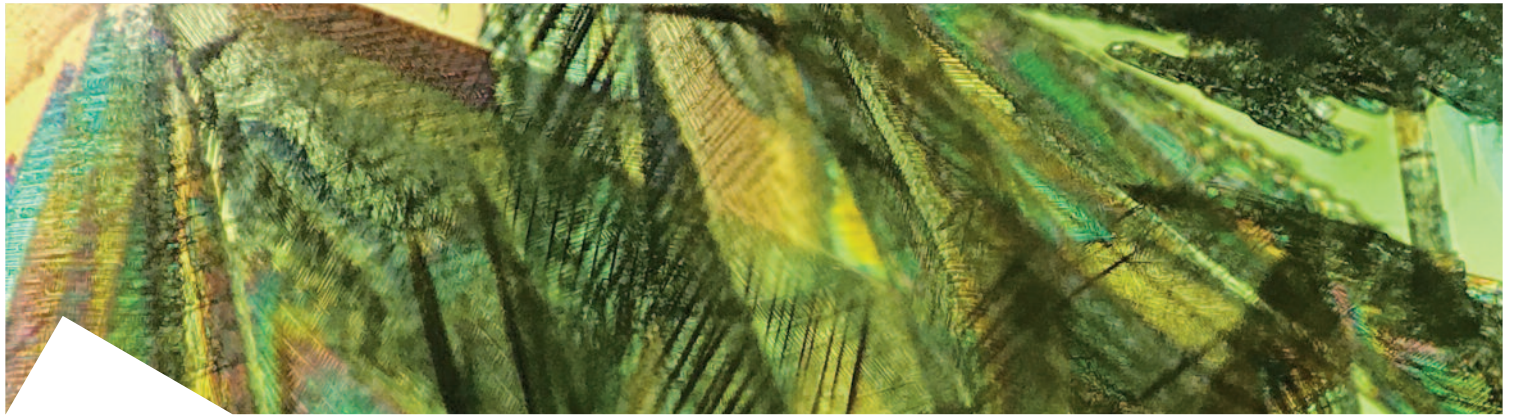
Design by
Laboratorio Grafica e Immagini INGV

Rome, 15 March 2018

Editing by Valeria Misiti and Piergiorgio Scarlato